Department of Mathematics and Statistics

Development of Cloud Removal and Land Cover Change Extraction Algorithms for Remotely-sensed Landsat Imagery

Ahmad Basyiruddin Usman

This thesis is presented for the Degree of
Master of Philosophy of
Curtin University

September 2011

Declaration

To the best of my knowledge and belief, this thesis contains no material previously published by any other person except where due acknowledgement has been made.

This thesis contains no material which has been accepted for the award of any other degree or diploma in any university

Signature:

Date: September 2011

for my late parents who did not have opportunity to watch this work done

for my parents in law who always support me

for my wife and son who always support, assist and encourage me

Acknowledgement

Conducting research and writing a thesis in academic English has been the most challenging experience I had when I enrolled as a Master by Research Student at Curtin University. I am extremely grateful to my supervisors, Professor Louis Caccetta and Professor Peter Caccetta for their guidance, attention and support during candidacy term, conducting research and completion of this thesis.

I express my gratitude to the Australian Agency for International Development (AusAID) that provides me the scholarship through the ADS scheme; to CSIRO Mathematics, Informatics and Statistics that provides me the image data analysis environment; and to Dr. Jeffrey G. Masek of NASA Goddard Space Flight Center that permits me to use the LEDAPS pre processing tools.

I also express my gratitude to Dr. Yetti Rusli, Dr. Hermawan Indrabudi, Dr. Wardoyo, Mr. Saipul Rahman and Ms. Retno Sari, my senior officials within the Indonesian Ministry of Forestry for their support and encouragement to take the opportunity to enrol in a Masters course in Australia.

I am very grateful to Mr. Jeremy Wallace, Ms. Suzanne Furby and Mr. Simon Collings for their support and guidance on image data analysis at the CSIRO facilities at Floreat.

Thanks to the International Officer of Curtin University, Staff of the Mathematics and Statistics Department, Staff of CSIRO facilities at Floreat, and the Indonesian students in Perth for their support and comments.

I will not forget my wife and son that accompany and support me wholeheartedly.

Abstract

Remotely sensed data has been used for land cover change monitoring. Monitoring in the tropical areas has problems such as persistent cloud cover, data availability, and data quality especially for the older data. This research analysis focuses on the elimination of cloud cover in tropical regions. This research is an important step towards addressing the issue of land cover change detection. Our work is briefly summarised hereafter.

Prior to data analysis, atmospheric correction was conducted by using NASA's Landsat Ecosystem Disturbance Adaptive Processing System (LEDAPS) pre processing tools that calibrated the visible and near-infrared bands to surface reflectance and the thermal band to brightness temperature. Subsequently, the atmospherically corrected Landsat data validated with the ground verified surface reflectance of Hymap data and the other Landsat data. Validation between two clear data provides a difference of less than 1% while the cloudy data provides a difference less than 2.5%.

Our cloud screening procedure was conducted with three different methods, the canonical variate analysis, the multiple rules with non-atmospherically corrected image (MRN), and the multiple rules with atmospherically corrected image (MRA). This is followed by the multi-temporal image composition to eliminate clouds. The multiple rules with the atmospherically corrected image provide the best result whereas the persistent cloud cover still remains. The annual composition result provides 1.72% to 11.04% area that is persistently covered by cloud, while biennial composition result provides 1.51% to 3.91%. This condition indicates that longer time frame or more frequent observation is needed to obtain a real clear picture of the Landsat image.

Cloud elimination efforts are also having problems such as the cloud adjacency effect and the missing data. The cloud adjacency effects are the humidified aerosol adjacent to cloud object that makes surface reflectance objects change from its original values. This effect distorts the cloud elimination results. Some experiments have undertaken to eliminate the effects such as calculation of the difference of the surface reflectance of two subsequent observations. The missing data issue can be overcomed by substitution from other clear observations.

Finally, the result of cloud elimination was used for land cover change detection that was undertaken by using bitemporal and post classification methods. Post classification methods provide better performance than bitemporal methods over similar data sources and training areas. Best overall accuracy of post classification is 62.28% and 25.30% for bitemporal. The poor quality of the change detection result is likely caused by the poor quality of the cloud elimination result. The improvement of cloud elimination quality is likely to improve change detection quality.

Contents

List of Figures

List of Tables

Chapter 1

Introduction

1.1 Rationale

Environmental change of the terrestrial ecosystem is driven by a variety of human induced and natural processes. Ecosystems respond to natural processes such as climate variations and long term trends, as well as direct human process such as logging, grazing, and conversions of land from one land use to another. These processes occur globally, leading to changes in forest, rangelands, agricultural, and other land cover extents, as well as changes in the composition of the covers within these categories. A key challenge is to understand these changes, and to identify the components which may be attributable to natural variation and human induced effects. To address this challenge, reliable and quantitative monitoring systems are required to estimate the magnitude, composition and direction of change. Remotely sensed data is providing a synoptic view of the world, and has a significant role to play in such systems (Vitousek et al., 1997; Lepers et al., 2005; Herold, 2009).

Multi-temporal land cover change maps that are produced from remotely sensed, 'ground truth', and other spatial data processing provide a means of quantifying, communicating and understanding the processes of change. In Indonesia for example, land cover maps have been available for a long time and the oldest known land cover map is *Maleische Vegetatieschetsen* published in 1935 by van Steenis. The focus of the effort was mainly on vegetation distribution for Southeast Asia, with the map information obtained

from various sources available at the time. Although incomplete and with limited detail, this was the first overview illustration of Indonesian land cover. In 1958, van Steenis updated this map and issued a *Vegetation Map of Malaysia* presented at the scale of 1:5,000,000. This early work was followed by many publications that covered smaller areas such as one island or part of an island. There was no known map publication that covered the whole of Indonesia until Whitmore (1984) published *A Vegetation Map of Malesia at Scale 1:5 Million* composed of information from various sources including remotely sensed aerial photography and satellite data (Landsat). The term *Maleische or Malaysia* of van Steenis; or *Malesia* of Whitmore refers to the phytogeographical region that stretches from the Southeast Asia Archipelago to the Bismarck Archipelago; or from 95^0 to 153^0 E meridian lines.

The first Indonesian land cover map that was completely generated from remote sensing sources was the Regional Physical Planning Programme for Transmigration (RePPProT) Vegetation Map. This map was produced as part of the project for national transmigration preparation conducted from 1984 to 1990 (Ikawati and Setiawati, 2009). The map was collated from the available remote sensing sources such as Landsat MSS (*Multi Spectral Scanner*), aerial photographs, SPOT (*Systeme Pour l'Observation de la Terre*), SAR (*Synthetic Aperture Radar*), and SLAR *(Side-looking Airborne Radar),* presented at the 1:250,000 scale. The project also produced other maps, such as land system, geology and soil (Poniman et al., 2004; Atmadilaga & Sarbini, 2010).

Subsequent effort which commenced in 2001 was undertaken by the Indonesian Ministry of Forestry (*Departemen Kehutanan – Dephut*) in collaboration with Badan Koordinasi Survey dan Pemetaan Nasional (*Bakosurtanal*) and Lembaga Penerbangan dan Antariksa Nasional (*LAPAN*). The nation-wide land cover mapping was produced at a scale of 1:250,000 from interpretation of 1999/2000 Landsat 7 Enhanced Thematic Mapper Plus (ETM+) data. The map contains 23 land cover classes of which 7 relate to

forested classes and 16 relate to non forested classes. The forested classes comprise three different natural forest types as well as the only human made forest (the timber estate). The natural forest types are the dry land, wetland, and mangrove which each type subdivided into primary and secondary. The secondary forest category in this classification refers to the logged over forest. The non-forested classes comprise of natural objects that are associated with lower vegetation or bare ground, and also the human induced objects associated with agriculture, built up areas and other features (Dephut, 2001; Dephut, 2008a). The complete list of the land cover classes is provided in Appendix 8. The spatial information was updated using 2002/2003, 2005/2006 and 2008/2009 Landsat 7 satellite data (Dephut, 2008a; Purwanto, 2011, pers. comm.). For the 2005/2006, the Landsat 7 data was complemented with Landsat 5 and SPOT 4 data to fill missing data associated with latter Landsat 7 acquisitions (Dephut, 2008c).

Persistent cloud in tropical regions has proven to be a significant impediment of land cover monitoring. Regular land cover updating, say on an annual basis, is difficult to perform. A strategy for dealing with regular and persistent cloud cover is an important issue to consider when reviewing land cover monitoring in tropical areas such as Indonesia. Land areas imaged with the presence of cloud (and smoke for that matter) may be totally obscured (for thick clouds), or partially obscured (by haze). Typically, areas that are considered to be significantly cloud affected are treated as missing data, with the interpretation of what is the most significantly affected parameter in the system or by judgement of an operator. Several options exist such as monitoring interval extension and remote sensing platform substitution.

The first option is to consider extending the monitoring interval, say to a triennial basis to enable preferable image acquisition. Even with this extended period, it is likely that some locations will still be obscured by cloud. The second is to improve the system so as to minimise the proportion of the image which is considered to be significantly affected by cloud (and thus

treated as missing data). Minimisation of rejected data includes making the best use of partially obscure data (haze), and other problematic data such as small gaps (of potentially good observations) between clouds and land cover observation in cloud shadows. While human operators are relatively good at using spatial context to interpret data in such areas, current automated methods are not. Therefore one strategy may be arranged to use manual as opposed to the automated methods. But this imposes significant penalties, including lag time, staff time and consistency in the mapping result. As an indication of staff time, it takes about one full year to process and employ multiple staff from the Ministry, Bakosurtanal and LAPAN (Dephut, 2008c).

Many other strategies for dealing with cloud cover have been considered. One strategy is to use non optical wavelengths that are mostly impervious to cloud cover. Instruments operating at longer wavelengths (radar) can penetrate cloud. Within Indonesia, the experiments with radar data were conducted in Kalimantan Island (*Borneo*) by Hoekman (1999), Nugroho (2006), Prakoso (2006) and Sugardiman (2007). These studies provided appropriate outcomes but due to the complexity of radar processing, the approaches have yet to become operational.

Another strategy is to use optical satellite such as National Oceanic and Atmospheric Administration – Advanced Very High Resolution Radiometer (NOAA-AVHRR) and Moderate Resolution Imaging Spectroradiometer (MODIS) having a higher temporal resolution. This approach improves the chances of obtaining cloud free observations from the many acquisitions. The NOAA-AVHRR and MODIS sensors have a higher temporal resolution but lower spatial resolution. Some studies have been conducted using these instruments. These studies have provided information of annual forest loss (Hansen et al., 2008c) and can be modified to obtain forest gain (Hansen et al., 2010).

The coarser data has limited application for natural resources management.

NOAA-AVHRR or MODIS data (for example) provides course information on disturbance whose form may then be examined with the use of higher resolution information such as the less frequently available Landsat (or similar) imagery (Broich et al., 2011). Given the spatial resolution of the data, limitations in the sensitivity to detect disturbances exist. The strategy of using NOAA-AVHRR and MODIS has some problems such as access to adequate data transmission infrastructure that affect the implementation process.

The investigation of the cloud removal algorithm development and use of the result for change detection is motivated by three conditions: (i) the high prevalence of cloud cover in tropical areas; (ii) the complexity of other remotely sensed data processing methods (either for Radar or MODIS); and (iii) the need of more frequent land cover monitoring (say on an annual basis). This research focuses on Landsat data processing, which is available at the appropriate spatial scale and relevant spectral sensitivity to detect change for the natural resource managers. In particular, we focus on maximising the use of time-series data affected by cloud and haze, with the view to improve the coverage of usable observations obtained.

1.2 Objectives

The main objective of this research is to examine methods for improving the generation of land cover change information in tropical areas using optical satellite imagery. To that end, we focus on two objectives:

(i). to develop effective algorithms for the generation of 'clear-sky' or 'cloud-free' composites of the Landsat data; and
(ii). to obtain land cover change information from these cloud-free composites.

1.3 Outline of the thesis

The main outcomes of our work are:

(1) Validation of the atmospheric calibration result of Landsat data using the ground verified Hymap data.

(2) Development of a simple algorithm for cloud removal. The algorithm needs the calibrated Landsat data and contains four rule sets for cloud screening and three rule sets for multi-temporal image composition.

(3) Application of the cloud removal result for land cover change monitoring.

(4) Propose the possible modification of the calibration, algorithm and change monitoring to enhance the quality of the land cover product.

This thesis is organised into five chapters, for which we now provide an overview.

Chapter 1 provides some introductory remarks, the rationale and objectives of this research.

Chapter 2 reviews the relevant literatures on land cover change monitoring. This also elaborates on the problems associated with monitoring in tropical areas, such as data availability and cloud cover.

Chapter 3 describes the proposed methods for data analysis as well as specification of the algorithms. The analysis is comprised of two parts, cloud removal and land cover change detection. We also describe the data pre-processing such as the calibration of raw digital number to ground reflectance using a recently available procedure (Masek et al., 2006). We describe the computational experiments for the comparison of different algorithms and report on the findings.

Chapter 4 describes the results obtained and provides a discussion on some of the essential issues. We describe an accuracy assessment of the calibration procedure applied by comparing Landsat data with and independently derived estimate of ground reflectance using aerial acquired Hymap data (Cocks et al., 1998; Collings and Caccetta et al., 2011). We next describe the cloud screening results and its complexity on exploration of the generated algorithms. The essential findings are our exploration of some aspects such as cloud spectral characteristics, algorithm portability testing, cloud adjacency effects, and monitoring interval efficiency. Finally, we discuss the change detection procedures and validation of the results.

From this research, we found that the expert derived rules with atmospheric correction for cloud screening provide the best result. We realised that for the analysis of data pertaining to Indonesia, persistent cloud cover still remains even after extending the cloud screening process for biennial time range. Furthermore we discovered the cloud adjacency effect that distorts the composition process to obtain a “cloud free” image is the most challenging phenomenon and its annihilation attempt is very difficult to achieve. We have found that our method to eliminate the cloud adjacency effect using the difference value of consecutive observations succeeded to a certain extent. We also learn that the cloud adjacency effect will diminish the “cloud free” image result quality which subsequently affects the accuracy of the change detection result.

Chapter 5 provides a summary of the overall research and makes some recommendations for future research.

This chapter introduced the rationale and objectives of this research. The following chapter reviews the literature discussing land cover change monitoring and its related issues such as data availability and cloud cover.

Chapter 2

Literature review on land cover change studies

Remote sensing data has now been used for land cover change detection for more than four decades. Much of this work uses optical images obtained through remote sensing platforms, and the global archives of satellite data that have been assembled. Land cover change detection provides us with information on historical changes in land cover including the historical reduction and increase of areas of forest. In tropical areas, efforts to quantify historical land cover change are hampered by the lack of cloud free observations and a limited capability to process partially affected data (Shepard, 1964; Westman et al., 1989; Herold, 2009). In this chapter we provide a review of the literature on this subject.

2.1 Land cover change monitoring

Land cover

DiGregorio (2005) defined that *land cover is the observed (bio)physical cover on the earth's surface*. It may comprise for example, features such as water bodies, crops, bare ground, grasslands, and forested areas. We may also include covers from built environments including concrete, tarmac and buildings. Each represents a feature of the earth's surface, which, depending on how the description of the feature is defined, may be represented categorically or as a continuum. The term *land cover classification* is often

used when referring to categorical definitions. Many land cover classification schemes have been proposed. For example, the United States Geological Survey (USGS) land use and land cover classification was proposed in a hierarchical structure to adapt to the diversity of remote sensing data. This also aimed to answer the needs of standardisation over the various land use and land cover classification systems used by federal, states and local governments (Anderson et al., 1976). Another example is the United Nation's Food and Agriculture Organisation (FAO) Land Cover Classification System (LCCS) that was designed to harmonise the available land cover classification and make it acceptable universally. This system attempted to draft the classification that is independent from the representation scale or data sources such as remotely sensed data, maps, or other spatial data sources (DiGregorio, 2005).

Land cover information is collected through various processes, including observations collected during field surveys, collation of expert knowledge such as farmer surveys of farm paddock usage, and through aerial and space borne platforms. Remotely sensed data may be collected for regions including those that may be inaccessible from the ground, or too expensive to collect by ground based methods on a regular basis. The data may be used to map certain land covers, or if time sequences of remotely sensed data are available, changes in the covers, or *land cover change*.

Land cover change and change detection

Land cover change is the alteration of land cover on the earth from one category to another, for example the conversion of forest to bare ground. Alterations may be sudden, such as the clearing of forest for agricultural production or human settlement, or gradual, such as the establishment of remedial plantings. For sudden alterations, the class may change completely (for example from forest to bare land). For gradual alterations, the class may not change (for example forest), but can be tracked through secondary

attributes (for example forest density). Change detection may include identification of whether an alteration happened or not, and if so, the magnitude of alteration.

With the advent of the Landsat era, the broad-scale satellite observations commencing in 1972 have meant that the use of digital image data for change detection has gained increasing attention. Weismiller et al. (1977) initiated a digital change detection procedure for large area inventory. They proposed the approaches that belong to one of four categories: post classification comparison; delta data change detection; spectral temporal change classification; and layered spectral/temporal change classification. Post classification comparison classifies each image in a sequence independently and then compares class labels for a given location to identify the change. Delta data change calculates the change between two images on a pixel by pixel basis by simply subtracting one image from the other and then considering the magnitude of the difference. This technique is often referred to as image differencing. Spectral/temporal change classification proceeds by firstly concatenating two four-bands Landsat MSS (*Multispectral Scanner*) to obtain eight bands Landsat data and then using statistical analysis of the data to summarise significant change. In the following, the concatenated data is referred as bitemporal space. The final procedure which is referred to as the layered spectral/temporal approach is a multi stage classification having different decision functions applied at each stage. The classification strategy is easier to illustrate by a tree diagram and more readily identified in recent times as a decision tree classifier.

Some satellite platforms used for change detection and their properties

Early researchers made use of the MSS (*Multispectral Scanner*) series of Landsat satellites as a change detection platform (see for example Weismiller et al., 1977, Malila, 1980). Landsat MSS was designed to have a spectral range and spatial resolution (~60m to 80m) appropriate for land

resources analysis. Early on, data volumes required to monitor at the relatively fine resolution of Landsat MSS, combined with limited computational resources, lead some researchers to consider other sensors having lesser spatial and spectral resolution. One such option available was the Advanced Very High Resolution Radiometer (AVHRR) data of the National Oceanic and Atmospheric Administration (NOAA) satellite series. These satellites were initially designed for meteorological monitoring purposes, but have became one of the satellite platforms used for terrestrial change detection (see for example Tucker et al., 1984; Justice et al., 1985). Tucker et al. (1984) used the annual data series of NOAA-6 and -7 AVHRR images to detect regional seasonal dynamics of agricultural activities in the Nile Delta, Egypt. Justice et al. (1985) applied data series of NOAA-6, -7, -8 and -9 AVHRR to monitor global or continental vegetation dynamics such as forest clearance in Brazil, grassland productivity in Africa and agricultural cropping season in China.

At more local scales, change detection is also performed for identifying urban areas and their changes. These applications require relatively high resolution such as SPOT (*Systeme Pour l'Observation de la Terre*) which has a 10 to 20m spatial resolution as well as Landsat TM (*Thematic Mapper*) which has a 30m spatial resolution and are often selected (e.g. Quarmby et al., 1988; Stow et al., 1990). Other more recent systems used for change detection include the MODIS of Terra and Aqua satellites having a similar coverage and temporal repetition to AVHRR but higher spectral and spatial resolution (e.g. Strahler et al., 1995).

Tropical countries such as Indonesia have high cloud coverage which hampers monitoring using the electro optical platform due to lack of observations on the ground (Gastellu-Etchegorry, 1988). For this reason, radar platforms that are able to penetrate cloud have been developed and their efficiency evaluated. For example, Hoekman (1999) evaluated the use of the European Remote Sensing Satellite (ERS) Synthetic Aperture Radar

(SAR) data for deriving maps of trees and land cover change. This work was successfully continued by Nugroho (2006), Prakoso (2006) and Sugardiman (2007).

Nugroho (2006) proposed the integration of SPOT-Vegetation along with Interferometric Synthetic Aperture Radar (InSAR) within a multi stage monitoring systems. The SPOT-Vegetation sensor mounted on SPOT-4 and -5 satellites have wide coverage similar to AVHRR data and acquires an image of a location daily. InSAR is the airborne radar system that attempts to obtain higher resolution data using the interferometric method. The intact forest information is obtained from multi-temporal SPOT-Vegetation data and the change is obtained from a combination of optical data where observations exist and InSAR data for completing those areas where ground observations from the optical data is obscured by clouds. Prakoso (2006) evaluated the combination of the National Aeronautics and Space Administration - Jet Propulsion Laboratory (NASA - JPL's) Airborne Synthetic Aperture Radar (AirSAR) that provides multi polarisation of C-, L-, and P-band SAR data to generate biomass estimation with supported correction by InSAR data. Sugardiman (2007) undertook forest damage assessment caused by fire during an El-Niño event. Fire location was obtained by the detection of thermal anomalies using the NOAA-AVHRR satellites, while the level of damage was assessed using data from ERS-1 and -2 SAR sensors.

Change detection in tropical areas with optical data

The high prevalence of clouds in tropical areas has led researchers to explore the use of a different strategy for monitoring. Because a single clear image is difficult to obtain, change detection analysis must be preceded by a cloud screening process of multiple observations. Cloud screening needs a sufficient number of images to make cloud elimination possible using composition of image clear part of different observation into a new image file. Most of the researchers are using coarser resolution remotely sensed data

such as AVHRR with more frequent observations if evaluating regional level and using higher resolution if evaluating narrower regions. Some researchers focused their study in tropical areas such as Malingreau et al. (1989) who use AVHRR to monitor the Brazilian Amazon and Southeastern Asia; Erasmi et al. (2004) who use Landsat satellite data over part of Indonesia; Leimgruber et al. (2005) who use Landsat for their analysis over Myanmar; Hansen et al. (2008a) who use MODIS and PRODES over Brazil; Hansen et al. (2008b) use MODIS only over Congo Basin; also Perera and Tsuchiya (2009) who use MODIS for their analysis over Sri Lanka.

2.2 Problems on land cover change monitoring

Land cover change monitoring for tropical areas such as Indonesia confronts problems such as data availability, data quality, and enormous cloud coverage. These problems make the excellent monitoring effort very difficult to achieve. This section elaborates in general on data quality, cloud cover and the effort to eliminate cloud.

Data availability and quality

Nowadays, remote sensing data is available in various kinds, from low resolution data such as AVHRR mounted on the NOAA satellite series to very detailed pictures such as digital aerial photographs and aerial hyperspectral data. Remote sensing data types also can be grouped by operational platform; the airborne and space borne data. Airborne data covers a narrow area but acquires more detailed pictures. This is usually available for specific projects or campaigns only, and rarely available for the whole country. Space borne platforms cover a broader area such as from satellites that are stationed in a specific orbit which makes it possible to cover designated areas regularly. Space borne data is usually available for the whole country, except for high-resolution data that is collected by request. The Thematic

Mapper (TM) and Enhanced Thematic Mapper Plus (ETM+) mounted on Landsat satellite series and also MODIS mounted on Terra and Aqua satellites are examples of space borne data that is available for free (Woodcock et al., 2008). If the data is not available for free, the price is relatively expensive (Eurimage, 2010).

Cloud cover

Cloud cover is one of the natural phenomena that always appears on passive remotely sensed data. Enormous cloud cover in tropical regions happens for the whole year. Sometimes, it forces the image quality requirement of clarity to be diminished. Permissible cloud cover amount in remotely sensed data usually is set to 10% (Laumonier, 1996). Acceptable cloud cover amount in such applications is raised up to 30% to make the data available for the whole country, for example the land cover monitoring in Brazil (Asner, 2001).

As a tropical country, Indonesia has considerable cloud cover issues. Table 2.1 shows that cloud cover over Indonesian territory (represented by four major cities) over a significant period averaged is in excess of 50%. This is a serious condition to handle with regular land cover monitoring, and it makes the task of achieving 10% cloud cover or less with regular remotely sensed data acquisition very difficult.

Table 2.1: *Averaged monthly daylight cloud amount from 1983 to 2005 of four major cities of Indonesia. The data are obtained from* http://indonesia-meteo.ru/en/ *and expressed in cloud cover percentage (МЕТЕОДАННЫЕ, 2011)*

Cities	Jan	Feb	Mar	Apr	May	Jun	Jul	Aug	Sep	Oct	Nov	Dec	Annual avg.
Medan	75.4	72.6	74.8	77.2	78.6	76.0	78.2	83.9	86.7	85.3	86.0	80.3	79.6
Jakarta	83.3	83.3	74.9	68.7	59.2	56.0	50.2	48.9	56.8	71.3	82.7	82.3	68.0
Surabaya	75.6	76.2	68.5	61.0	45.8	41.8	36.3	34.9	41.1	57.6	72.0	75.3	57.1
Makassar	81.2	78.8	66.1	55.6	41.7	39.2	32.0	22.8	22.5	40.0	64.4	79.4	51.8

2.3 Cloud cover removal

Cloud cover is a problem in land cover monitoring in that it conceals land that ought to be observed. For the image analysis purpose, clouds can be differentiated into three groups, namely the cloud itself which is opaque, thick and compact, thin cloud, sometimes called haze, which is transmissive, and cloud shadow. Cloud analysis using digital image processing was started as early as digital image data was available. Malberg (1973) tried to identify cloud from digital images from the ESSA-8 (*Environmental Science Service Administration*) satellite (the predecessor of NOAA-AVHRR) by using the short wavelength infrared spectrum. This research was followed by an effort to eliminate transmissive cloud using homomorphic filtering of Landsat MSS (Mitchel and Chen, 1976). The subsequent research then differentiated which pixels are clear and which contain cloud. Differentiation uses a feature space of visual and infrared spectrum of Advanced Very High Resolution Radiometer (AVHRR) Global Area Coverage (GAC) data (Coakley and Bretherton, 1982).

Some other researchers analysed cloud by using different remote sensing data. Tokuno and Tsuchiya (1994) used the combination of visible, water vapour and thermal channels of The Japanese Marine Observation Satellite (MOS-1) to identify various types of clouds. Ackerman et al. (1998) used a combination of 14 channels of MODIS to differentiate various clouds as well as shadow, snow, and the high moisture contained in the atmosphere. Warner et al. (2001) exploited the Measurement of Pollution in the Troposphere sensor of the Terra satellite (MOPITT) that was initially designed for CO and CH_4 detection to identify which pixels contain cloud. Li et al. (2002) generated the “cloud free” image using expert derived rules over 30 observations of the panchromatic channel of a SPOT satellite. Li et al. (2003) evaluated another experiment using more than 50 IKONOS satellite images to produce a multi-scene “cloud free” mosaic of Singapore. Ma et al. (2005)

applied the homomorphism filter to eliminate hazy pixels over 9 observations of The China-Brazil Earth Resources Satellite (CBERS-02).

Beside the various platforms used, various methods have been developed to identify cloud and differentiate it from other image features. Goodman and Henderson-Sellers (1988) argue that most of the cloud analysis and elimination in remote sensing can be categorised according to the method used: the statistical analysis (Gaussian histogram, dynamic clustering, and spatial coherence); thresholds; radiative transfer models or its inverse models; and ground-based measurements. These early base methods have been followed by more advanced methods such as texture based analysis (Ariazza et al., 2003); multi scale wavelet based fusion (Tseng, et al., 2008); and bandelet inpainting (Maalouf et al., 2009).

Cloud shadows also have an important role on distorting data analysis. Objects that are covered by shadow become darker. Some effort has been made to eliminate this phenomenon as well as the cloud itself. Shu and Freeman (1990) started the attempt on aerial photographs using thresholds of the defined shadow segments and then applied some rules to compensate for the brightness of the object underneath the shadow. Richter and Müller (2005) developed de-shadowing algorithms that involved at least one visible and one short-wave infrared band. Some calculation is undertaken including covariance matrix, histogram thresholding and region growing for shadow affected area.

Some researchers also have developed algorithms for cloud screening that involving multiple rules and observation. They are for example: Luo et al. (2008) that designed an algorithm for MODIS; Irish et al. (2006) and Huang et al. (2010) that designed an algorithm for Landsat. Luo et al. (2008) and Irish et al. (2006) based their algorithm on multiple thresholds to identify cloud objects. Huang et al. (2010) proposed a different approach that used reflectance-temperature space that put a reflective band on the x-axis and a

thermal band on the y-axis. All of these algorithmic techniques succeeded to eliminate clouds but some haze still remained to be seen.

Apart from the other two problems (cloud and cloud shadow), haze is the most difficult object to handle. The haze appearance is distracting on digital image analysis. Haze spectral signature is very similar to the underneath object and this makes it difficult to identify and remove. Most of the researchers use formula transformations to remove haze. Lavreau (1991) employed the fourth parameter of the Tasseled-Cap (TC4) transformation. Richter (1996) tried to combine Tasseled-Cap transformation, calibration and filtering to remove haze. Dal Moro and Haluonova (2007) applied a Haze Optimised Transform (HOT). He et al. (2010) modified the HOT transform into the Advanced-HOT (AHOT) transform.

This chapter reviewed the literature in land cover change analysis especially in tropical areas as well as the problems associated with. Our discussion is continued by proposing procedures for data calibration, cloud elimination, change detection and the accuracy assessment in the following chapter.

Chapter 3

Land cover change analysis

Land cover change analysis is an important source that may provide an early indication of serious global change. An effective early warning system that is based on remote sensing or ground measurements is an important tool for global climate management (Skole, et al., 1997; Hansen, et al., 1998). The change detection basically analyses the difference between two image observations that are taken at different times and cover the same area. The images and another data source that are delivered in a digital format are the most desirable for land cover change analysis as they facilitate the possibility of more complex computation such as enhancement, composition or differentiation (Shepard, 1964).

This chapter elaborates on the use of remotely sensed data for land cover change monitoring. Our discussion includes a detailed description of remotely sensed data and image processing tools used for this research as well as the methods applied for change analysis. The methods are organised in three stages, the pre-processing, the land cover change analysis and the validation. The pre-processing stage describes the preparation for Landsat data prior to change detection analysis that includes atmospheric correction, cloud screening and multi-temporal image composition. The land cover change analysis conducted with two different procedures, bitemporal and post classification analysis. The validation stage compares the result of change detection analysis with the higher resolution reference data.

3.1 Data, tools and flow chart

Landsat is selected as the data sources for this research because of its availability and familiarity within the scientific research community. Landsat data series are begun by the launching of Landsat 1 in 1972 that equipped with Multispectral Scanner (MSS) sensor (USGS, 2010a). Landsat satellites were originally named Earth Resource Technology Satellite (ERTS) which was used only for Landsat 1 and 2. The subsequent series never carried the name ERTS. The first generation of Landsat carried two types of sensor, the Return Beam Vidicon (RBV) and Multi Spectral Scanner (MSS). These types of sensors were installed on board in Landsat 1, 2 and 3. The RBV sensor has a spatial resolution of 80m, except for Landsat 3 where it was 40m. The MSS sensor has a spatial resolution of 80m and continued to be kept on board in the second generation satellites, Landsat 4 and 5.

Both second generation satellites carried on board previous MSS sensor with 4 channels and the new Thematic Mapper (TM) sensor with 7 channels. The TM sensor consists of 6 channels of visible and near-infrared spectra which has a 30m resolution and a channel of thermal spectrum which has a 120m resolution. The Landsat series was continued by Landsat 6 (which failed to reach orbit) with an ETM sensor and Landsat 7 with the Enhanced Thematic Mapper Plus (ETM+) sensor. The ETM+ sensor on board Landsat 7 has similar composition to the TM sensor, plus one panchromatic band (15m) and a higher resolution of thermal band (60m). Detail of TM and ETM+ are given in Table 3.1 (NASA, 2011). To date, Landsat 5 and 7 are the only operational Landsat series and Landsat 5 still collects data after 27 years in orbit (Hansen, 2009). This is the good reason to select them for this research.

Each Landsat image covers an area approximately 185 x 185km^2 that is usually named as the scene. The scene is registered to a specific grid system called World Reference System (WRS). Coverage of each grid or scene is identified by a number called path (for x – axis) and row (for y –

axis). Path is the projected orbital track on the ground, which are numbered westward from 001 to 233. Row is latitudinal centre line across a frame of each scene which are numbered southward from 001 to 122 (for descending orbit, day time coverage) and numbered northward from 123 to 248 (for ascending orbit, night time coverage). For Indonesia, the daytime path numbers ranges from 100 to 131 and row from 56 to 67 (NASA, 2011). Totally, there are more than 200 Landsat scenes to cover whole Indonesian terrestrial territory. This excludes Landsat scenes that cover water bodies only.

Table 3.1: *Specification of Landsat 5 and 7 spectral bands. Spectral wavelength is expressed in nanometers (nm). Spatial resolution is given in brackets (NASA, 2011)*

Band number	Landsat 5 TM (launched January 1984)	Landsat 7 ETM+ (launched April 1999)
1	450 – 520 (30m)	450 – 520 (30m)
2	520 – 600 (30m)	520 – 600 (30m)
3	630 – 690 (30m)	630 – 690 (30m)
4	760 – 900 (30m)	760 – 900 (30m)
5	1550 – 1750 (30m)	1550 – 1750 (30m)
6	10400 – 12500 (120m)	10400 – 12500 (60m)
7	2080 – 2350 (30m)	2080 – 2350 (30m)
Pan	n.a.	500 – 900 (15m)

Landsat data for this research was downloaded from http://glovis.usgs.gov (free of charge). The data is stored in compressed GeoTIFF format which contains data volumes between 400 – 700MB after extraction. All selected Landsat data have been radiometrically and geometrically corrected (level L1T) to make it ready for atmospheric correction and the following process. Details of correction levels available are mentioned at Table 3.2

Beside Landsat, Hymap's (hyperspectral mapper) aerial data is also selected

to validate Landsat's atmospheric correction quality. Hymap consists of 128 spectral bands ranging from 0.44 to 2.5μm and two thermal bands (one between 3 - 5μm and the other between 8 - 10μm). Hymap is mounted on board an aircraft that flies at elevation 2,000 - 5,000m above ground level. It has an original resolution of 2 - 10m (Cocks, et al., 1998). This research applies the Hymap's spectral bands that similar to Landsat only. The spatial resolution was resampled to 25m. Hymap data is provided as a surface reflectance value which has been calibrated to surface reflectance measurement on the ground (Collings & Caccetta, 2011).

Table 3.2: *Landsat data correction levels (USGS, 2010d)*

Level	Specification	Data availability
Level 0 reformatted (L0R or L0Rp)	Reformatted raw data without radiometric or geometric correction	TM, ETM+, No longer available, Dec and Sep 2008 respectively
Level 1 radiometrically corrected (L1R)	Radiometrically corrected of L0R data	No longer available
Level 1 systematically corrected (L1G)	Radiometrically and geometrically corrected data. Scene will be rotated, aligned and georeferenced using specified map projection	MSS, TM, ETM+
Level 1 Precision corrected (L1P)	Precision radiometric and geometric correction using ground control points (GCP)	MSS, TM, No longer available, Dec 2008
Level 1 Systematically terrain corrected (L1Gt)	Systematic radiometric and geometric correction with digital elevation model (DEM) for topographic accuracy	ETM+
Level 1 Terrain corrected (L1T)	Systematic radiometric and geometric correction with digital elevation model (DEM) and GCPs for topographic accuracy	MSS, TM, ETM+

Validation of the classification result uses higher resolution remotely sensed data. Google Earth provides the high-resolution remote sensing data that come from at least three image providers: SPOT Image; DigitalGlobe; and GeoEye as well as medium and lower resolution data (Mecham, 2008). Google Earth credits for each geospatial data, providers presented in their window, but does not specify from which satellite the data comes from. SPOT Image (2010) provides image data from SPOT satellite series, the SPOT-4

and SPOT-5. SPOT-4 carries on board a *Haute Rèsolution Visible et Infra Rogue* (HRVIR) sensor, while SPOT-5 carries a *Haute Rèsolution Gèomètrique* (HRG) sensor. DigitalGlobe (2011) provides QuickBird, WorldView-1 and WorldView-2 image data. GeoEye (2011) provides IKONOS and GeoEye-1 image data. These imageries have resolution 0.4m to 10m, and provide more detailed information than Landsat (15m to 30m). Specification of each fleet is described in tables 3.3 to 3.5

Table 3.3: *Specification of SPOTImage's satellites fleet. Spectral wavelength is expressed in nanometers (nm). Resolution is given in brackets (SPOT Image, 2010)*

Band number	SPOT 5 (launched 4 May 2002)	SPOT 4 (launched 24 Mar 1998)
1 (green)	500-590 (10m)	500-590 (20m)
2 (red)	610-680 (10m)	610-680 (20m)
3 (near infrared)	780-890 (10m)	780-890 (20m)
4 (short wavelength infrared)	1580-1750 (10m)	1580-1750 (20m)
Pan	480-710 (5m)	480-710 (10m)

Table 3.4: *Specification of GeoEye's satellite fleet. Spectral wavelength is expressed in nanometers (nm). Resolution is given in brackets (GeoEye, 2011)*

Band number	Ikonos (launched 24 Sep 1999)	GeoEye-1 (launched 6 Sep 2008)
1 (blue)	445-516 (4m)	450-800 (1.65m)
2 (green)	506-595 (4m)	510-580 (1.65m)
3 (red)	632-698 (4m)	655-690 (1.65m)
4 (near infrared)	757-853 (4m)	780-920 (1.65m)
Pan	526-929 (0.82m)	450-800 (0.41m)

This research was conducted on two types of location, the first, within Indonesian territory for land cover change analysis purpose (locations 1, 2 and 3) and the second, within Australian territory for atmospheric correction quality validation purposes (locations 4 and 5). The location within Australian territory is selected as a consequence of Hymap's data availability. Each selected location within Indonesian territory comprises a number of

observation dates (to enable cloud removal) and represents land cover variability. Landsat data which covers Australian territory is selected to co-locate with Hymap's data. These selected locations are stated hereafter and depicted on Figure 3.1 (Dephut, 2008a; Dephut, 2008b; Monk, et al., 2000; Collings & Caccetta, 2011)

Table 3.5: *Specification of DigitalGlobe's satellite fleet. Spectral wavelength is expressed in nanometers (nm). Resolution is given in brackets. (DigitalGlobe, 2011)*

Band number	QuickBird (launched 18 Oct 2001)	WorldView-1 (launched 18 Sep 2007)	WorldView-2 (launched 8 Oct 2009)
1 (red)	630-690 (2.4m)	n.a.	630-690 (1.84m)
2 (blue)	450-520 (2.4m)	n.a.	450-510 (1.84m)
3 (green)	520-600 (2.4m)	n.a.	510-580 (1.84m)
4 (near infrared1)	760-900 (2.4m)	n.a.	770-895 (1.84m)
Pan	450-900 (0.6m)	400-900 (0.5m)	450-800 (0.46m)
Red-edge	n.a.	n.a.	705-745 (1.84m)
Coastal	n.a.	n.a.	400-450 (1.84m)
Yellow	n.a.	n.a.	585-625 (1.84m)
Near infrared2	n.a.	n.a.	860-1040 (1.84m)

Location 1: Path 103 row 63 of Papua Island. This represents higher cloud coverage; combination of evergreen lowland forest, mangrove forest, highland forest, bare land and snow; and low level of land cover change.

Location 2: Path 114 row 66 of Sumbawa Island. This represents lower cloud coverage; combination of evergreen and deciduous forest; and low level of land cover change.

Location 3: Path 127 row 59 of Sumatera Island. This represents higher cloud coverage; combination of wetland and lowland forest, along with land clearing; and high level of land cover change.

Location 4: Path 113 row 80 of Western Australia. This is the only Landsat data outside Indonesia. This is selected because of

ground validated surface reflectance image data (Hymap) availability.

Location 5: Hymap's aerial hyperspectral data acquired at 9 February 2010 covers an area near Mullewa, Western Australia. Illustration of Hymap's detail coverage is depicted on Figure 3.2

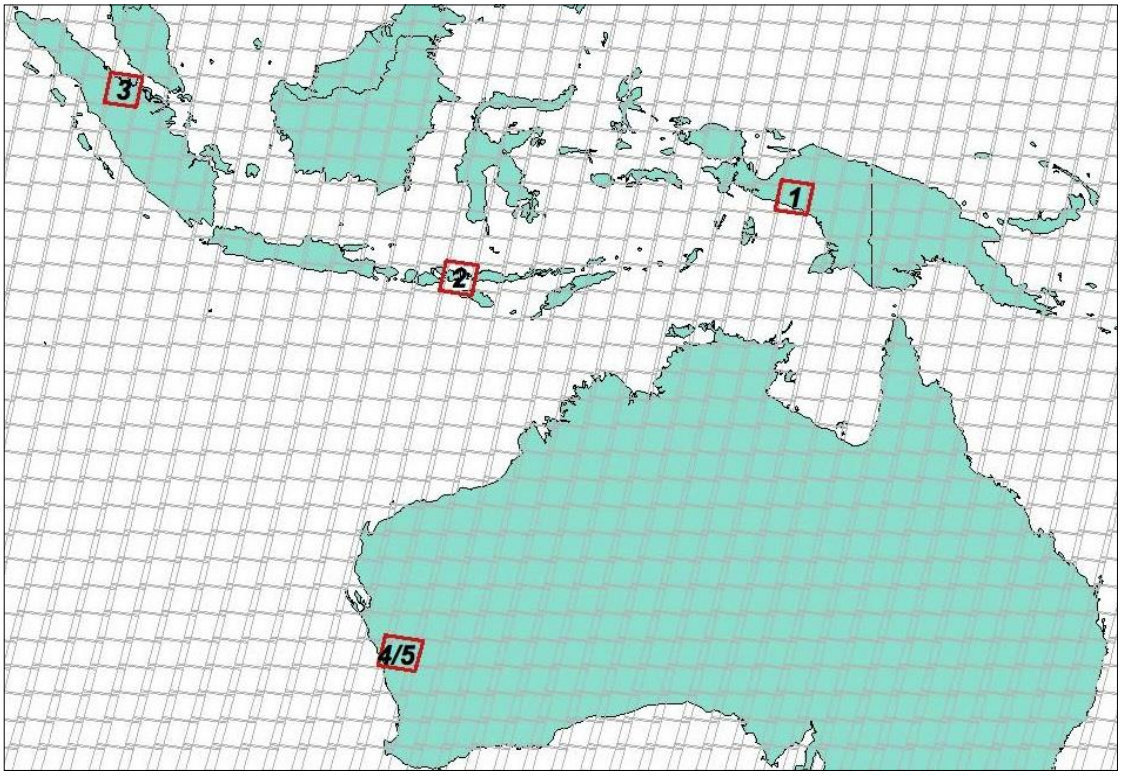

Figure 3.1: *Coverage of Landsat scene (grey grid) and the selected research location (red grid). Location number 5 covers subset area of location number 4 (USGS, 2010b; ESRI, 2006).*

This research is conducted using standard tools for image processing. All computational work is conducted on a PC powered by Intel Core2Duo E6750 2.66GHz processor and 2GB memory, with an additional external storage to save raw, temporary and final results. Most image processing activities are run by ER-Mapper software package (Version 7.1) with support by other Open-source applications, i.e.: QuantumGIS (for spatial data plotting), Inkscape and GIMP (for graphical illustration), as well as R (for statistical analysis). LEDAPS pre-processing tools and CSIRO-MIS proprietary

packages are also included for specific pre-processing and classification procedures.

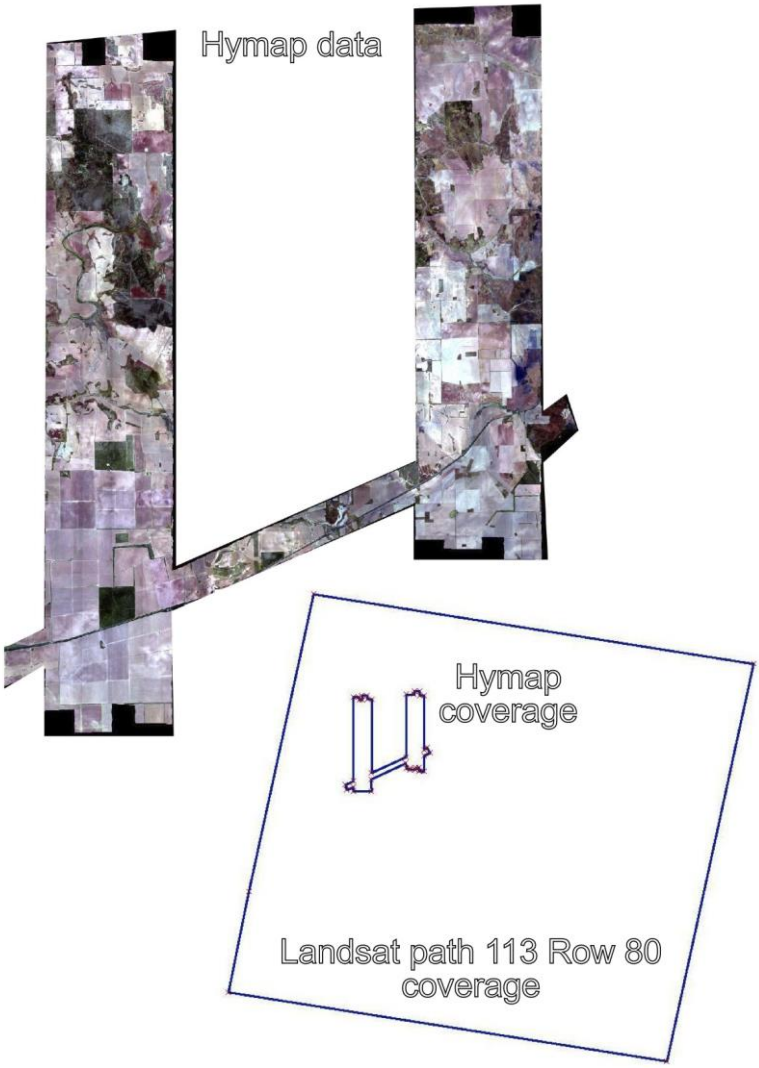

Figure 3.2: *Coverage of Hymap hyperspectral data around Mullewa, Western Australia. The white inset illustrates the Hymap's location within Landsat's path 113 row 80 coverage.*

This research is organised into four stages: remotely sensed data collection; pre processing (atmospheric correction, cloud screening, and cloud elimination); land cover change analysis; and then validation of the land cover change result. The data collection stage is undertaken by downloading Landsat data from the USGS database. The following stage is pre-processing that elaborates the methods for atmospheric correction, cloud screening and multi-temporal composition. Atmospheric correction is the process to correct

atmospheric condition and convert digital numbers to surface reflectance. Cloud screening is the identification of cloud objects and followed by cloud elimination process using the multi-temporal Landsat data to obtain the clearest image possible. The land cover change analysis stage provides the methods to extract the change between two successive image observations. The validation stage explains the procedure to assess the quality of the change analysis result. These stages are conducted in sequence as illustrated in Figure 3.3

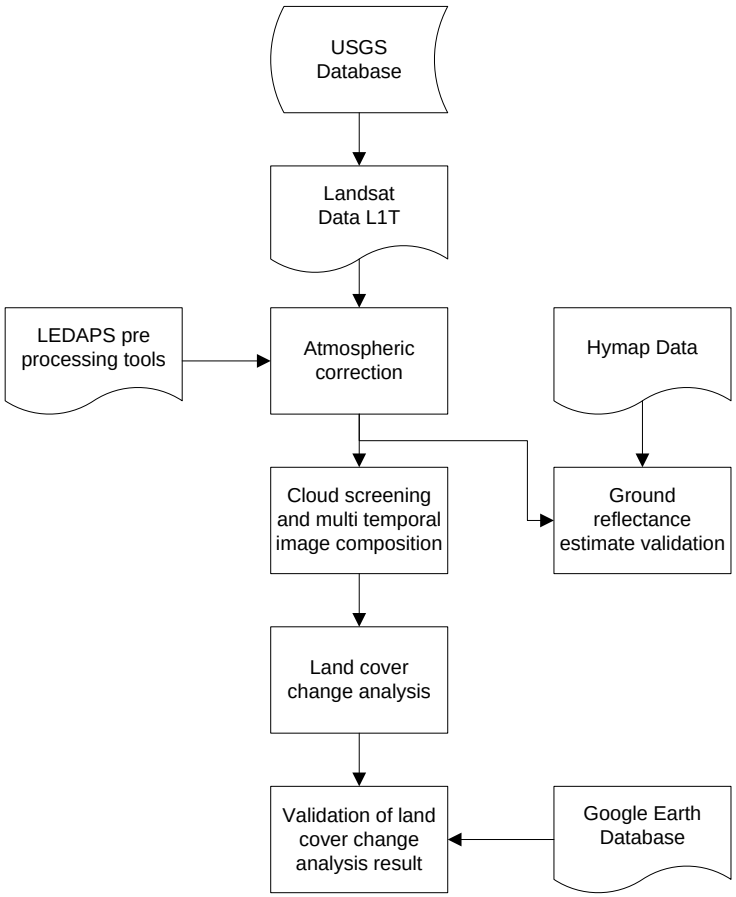

Figure 3.3: *Research flow chart*

3.2 Preprocessing

Landsat data needs correction to allow proper data analysis. Radiometric, geometric, and atmospheric correction procedures involved along with the cloud removal. Radiometric and geometric corrections were conducted by the

USGS as the data was received in Level 1 Terrain corrected (L1T) format (USGS, 2010c). The atmospheric correction and cloud removal procedures conducted in this research are described hereafter.

Atmospheric correction

Atmospheric corrections are carried out in an effort to obtain surface reflectance values from remote sensing imagery (Fallah-Adl, et al., 1995). This is essential for multi-temporal data analysis (Song, et al., 2001). The NASA's Landsat Ecosystem Disturbance Adaptive Processing System (LEDAPS) pre-processing tools running on Linux are selected as the atmospheric correction tool (Masek, et al., 2006). The process itself consists of calibration and atmospheric correction. The calibration process is converting the digital numbers of Landsat data to at-sensor radiance and then calculating the top-of-atmosphere (TOA) reflectance. It needs Landsat orbital information and the band specific gain/bias coefficients (Chander, et al., 2009). The process then continues by applying an atmospheric correction model on the Landsat data to compensate for atmospheric scattering and absorption to obtain surface reflectance. This procedure needs support from other remote sensing data that is sensitive to ozone concentration such as Total Ozone Mapping Spectrometer (TOMS) and water vapour abundance obtained from National Center for Environmental Prediction (NCEP) reanalysis data (Masek, et al., 2006, Vermote, et al., 1997).

Atmospheric correction process is followed by the atmospheric correction result assessment. The assessment compares surface reflectance values of two different image observations. The comparison uses the closest possible observation to reduce the seasonal characteristics influence. The assessment is represented by the following three experiments:

Experiment (i) Landsat surface reflectance data (path 113 row 80 of 23rd February 2010 compared to Hymap's surface reflectance

data which has validated to field measurements (Collings and Caccetta, 2011)

Experiment (ii) Landsat surface reflectance data (path 113 row 80 of 23rd February 2010 compared to different observation of Landsat surface reflectance data with each represents the clear and cloudy conditions.

Experiment (iii) Landsat surface reflectance data covering Indonesian region compared to different observation of Landsat surface reflectance data.

Cloud screening

Cloud removal or cloud elimination is the subsequent process after the image data are atmospherically corrected. The process aims to obtain the clearer land observation of the imagery. The process is designed to apply in two stages, the cloud screening (cloud masking) followed by the multi-temporal image composition.

Cloud screening is the process to identify which object is cloud and then mask it for cloud elimination. Cloud identification is obtained by visual inspection of the interpreter from spectral signature. The identified clouds are proceeded through specific algorithms and then masked the result with the lowest possible value, the digital number Q = 1 (for non-atmospherically corrected data) or the surface reflectance ρ = 0.01% (for atmospherically corrected data). Cloud screening or cloud masking is conducted by two different procedures, the canonical variate analysis (CVA) and the multiple rules. The CVA identifies objects by using maximum spectral separability (Campbell and Kiiveri, 1993).

Multiple rules identify clouds by applying a set of thresholds, ratios, and indices. The applied rules are designed from the spectral signature generated from training samples. Training samples differentiate objects into

five major land cover classes: clouds, vegetations, bare ground, water bodies and snow, and haze (transmissive clouds). Various formulations have been generated to identify the cloud objects and to make them different from the other objects (Appendix 4). Extensive computational effort has conducted to obtain which formulations are effective for cloud differentiation. The potential formulations obtained from the computation are then arranged for the rule set of the experiments using the Landsat images (The rule sets are provided in Appendix 2). The application of the selected rule sets are investigated using the visual inspection the on ER Mapper display. Some rules may have modification such as an adjusting threshold or change of the parameters to enhance its capability to differentiate cloud. The multiple rules experiments are involving two types of Landsat data, the non-atmospherically corrected data (hereafter is termed MRN) and the atmospherically corrected data (hereafter is called MRA). The rule sets for MRN are given in Appendix 2A, while the rule sets of MRA are mentioned in appendix 2B.

The CVA and MRN tried to differentiate clouds by considering the cloud as a single aspect. The MRA considers cloud as a single feature for the early experiments and then as diverse objects for the following experiments. Considering cloud as a single element has proven difficult to obtain a good result. Our strategy that was inspired for the example presented by Irish et al. (2006) is then modified to categorise cloud into several types based on its appearance: the bright top cloud, the cold cloud, the broken cloud and the cloud edge. Cloud differentiation does not use the meteorological cloud classification system that is based on elevation and cloud forms (Reynolds et al., 2008).

The MRN initiated 9 rule sets. Each set may contain threshold of single or a combination of Landsat bands. The best result of MRN experimentation is given in Formula (3.1):

(3.1)

where Q_i stands for digital number of Landsat data of band i, i: 1,2,3,4,5,6,7. Q is provided in 8 bit data representation which has a range 0-255.

The MRA experimentation arranged 5 rule sets of which two consider cloud as a single element and the other three consider cloud as complex features. The MRA analyses the data in surface reflectance for the visible and infrared spectrum (band 1, 2, 3, 4, 5, and 7) and in brightness temperature for the thermal spectrum (band 6). Surface reflectance has a range 0-1. Brightness temperature is presented in Centigrade that has a range (-100) – 100. The best MRA experimentation is the rule sets that is given in formulas (3.2) to (3.6). The bright top cloud is selected by using Formula (3.2):

$$\rho_1 > 0.5 \tag{3.2}$$

where ρ_i stands for surface reflectance value of band i, i = 1, 2, 3, 4, 5, 7; the cold cloud is identified by using Formula (3.3):

$$T < \text{Abs}\left(\frac{\rho_2}{\rho_5}\right) \tag{3.3}$$

where T stands for brightness temperature of band 6. The broken cloud is distinguished by using Formula (3.4):

$$\left(\frac{\rho_1}{\rho_7}\right) \text{Abs}\left(\frac{\rho_1}{\rho_5}\right) \tag{3.4}$$

and the cloud edge is recognised by using Formula (3.5):

$$\text{NDVI} \left(\frac{\rho_4}{\rho_3}\right) \tag{3.5}$$

where NDVI stands for Normalised Difference Vegetation Index that is given in Formula (3.6):

$$\text{NDVI} = \left(\frac{\rho_4 - \rho_3}{\rho_4 + \rho_3}\right) \tag{3.6}.$$

Image composition to obtain clear sky images

The cloud screening stage showed that cloud covered or clear parts of the image are shifted time to time. This creates an opportunity to obtain cloud free coverage by multi-temporal composition. Then, the rules for compositing the clear part of each observation and eliminating the cloud cover are initiated, but must be aware of several conditions e.g.: the existence of the transmissive clouds, land cover change and leaf phenology. These conditions must be treated carefully to avoid a mis-compilation result. For example, the deciduous vegetation cycle that depicted the transformation from the green vegetation reflectance in rainy season to the bare ground reflectance in dry season. Composition for the location that contains seasonal change of deciduous vegetation must be handled for each respective season separately.

Multi-temporal compilation to obtain 'best' image data was conducted by two different procedures: the maximum-value composites; and the multiple rules. The maximum-value composite is a selection process to find the 'best' pixels by using highest available value only (Holben, 1986). The highest value selection process uses Formula (3.7) or (3.8):

(3.7)

(3.8)

where ρ_x and ρ_y are surface reflectance or brightness temperature of 2007 and 2008 observation respectively. The 'best' image data selection can also be undertaken by finding the highest value of designated band and the selected result is used for the whole bands as in Formula (3.9):

(3.9)

where ρ_{4x} and ρ_{4y} are surface reflectance of band 4 of the year x and y respectively; x: 2007 and y: 2008; or, the selection is conducted by using the highest value of designated formula then applied for whole observation as in Formula (3.10):

(3.10)

where $NDVI_x$ and $NDVI_y$ stand for normalised different vegetation index of

2007 and 2008 observation respectively. Calculation of NDVI is based on Formula (3.6). If the highest value for each band is selected (formula (3.7) or (3.8)), the result for each pixel location (same area, any band) may come from a different observation. If the highest value of designated band or formula is selected, data source for each pixel location must come from the same observation, but the source for each adjacent pixel may come from different observation.

When conducting multi-temporal image composition to obtain 'cloud free' images, some clouds may remain to be seen and influence the process. They may appear as haze, cloud edge or cloud adjacency effects. They cannot be identified as cloud because they are transmissive or their spectral characteristics are very similar to the other land cover objects (Koren, et al., 2007, Marshak, et al., 2008). There are two possible ways to exclude them in the compilation effort: create a region growing mask; or compare two consecutive observations. Region growing can be created by expanding some pixels of masked cloud area to make haze or cloud edge objects included in the masked region (Tseng, et al., 2008). The problem is how to define the expansion size? Some locations only need one or two pixels expansion, but the others need more. The comparison of two consecutive observations then becomes a more reasonable procedure. If RMS difference of both observations is high, it signals that one of the observations is hazy (Lyapustin & Kaufman, 2001).

The composition process can be arranged by multiple rules in hierarchical stages, firstly, if one or two observations are dark (cloud mask or shadow) then the highest value of them will be selected as inFormula (3.11):

 (3.11)

where ρ_{4x} and ρ_{4y} are surface reflectance values of band 4 of the year x and y, x: 2007, y: 2008; and the ρ_x and ρ_y are surface reflectance value for each band of 2007 and 2008 observations, respectively. Secondly, if one

observation is identified as hazy then the lowest value will be selected as the higher value is considered hazy as in Formula (3.12):

(3.12)

where RMS stands for root means square difference between two observations; and for the unselected pixels, selection is made for the observation which has the highest band 4 value as in Formula (3.13):

(3.13)

where ρ_{4x}, and ρ_{4y} stand for surface reflectance value of band 4 of the year x and y observation; x: 2007 and y: 2008; ρ_x and ρ_y stand for surface reflectance value of each band of 2007 and 2008 observation respectively. The formulas (3.11) to (3.13) are arranged to construct the decision tree selection as depicted on Figure 3.4.

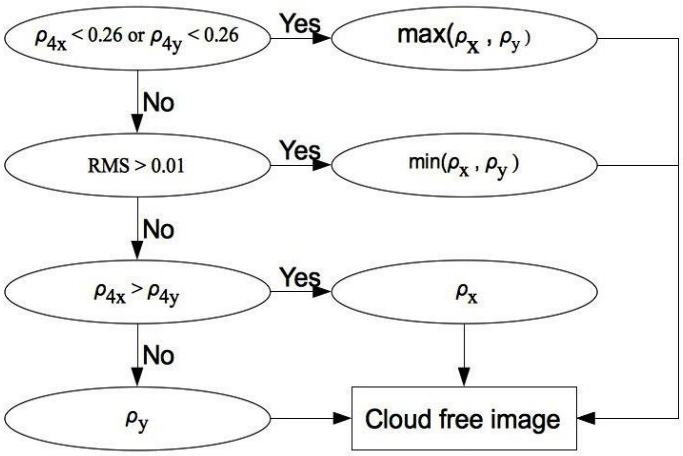

Figure 3.4: *Decision tree designed for obtaining cloud free image.*

3.3 Land cover change analysis

After all observation dates are compiled, the clearest image possible is produced and the process is resumed with land cover change analysis. Land cover change analysis itself requires at least two different observation images to obtain change information (Feranec, et al., 2007). Bogaert, et al. (2004) identified that the change process may appear as various spatial

patterns such as aggregation, attrition, creation, etc. For our experiment, the observation focuses on two spatial patterns, the attrition (decreasing of number or disappearing of feature) and the creation (increasing of number or formation of feature).

Land cover change has influence on various issues (Skole, et al, 1997) that focusses on the unchanged and the changed objects. The unchanged objects will be classified as forest, bush, dwarf vegetation, bare ground, snow, water bodies and persistent cloud. The changed object in the forestry sector will be concerned mainly with decreasing or increasing amount of forested area. Forest degradation and deforestation are familiar terms for the decreasing of forested area (Panta, et al., 2008) as well as reforestation and afforestation for the increasing of forested area (Verchot, et al., 2007).

Land cover change analysis will be conducted in the most intense land cover change location. Path 127 row 59 of Landsat 7 is the location with the highest change rate out of three locations within Indonesian territory (Dephut, 2008b). The change analysis will be carried out for the 2007 to 2008 observation, by using two different techniques, bitemporal and post classification processing. Bitemporal technique is the method to analyse change detection in one stage. Both observations of the year 2007 and 2008 that have 7 bands each are concatenated into one 14-bands file (7 bands from each observation). The changed objects will be obtained from the statistical difference of this composite image. The training area is arranged into three groups, the unchanged group (water, bare land, forest etc.), the degraded group (forest to bush, bush to bare land etc.), and the regrowth group (bush to forest, bare land to estate, etc.).

Post classification processing is a method to analyse change detection in two stages. The first stage conducts classification of each sequence, 2007 and 2008 respectively. Subsequently, this is continued by comparison of results of two different sequences. Both techniques used canonical variate analysis

(CVA) for classification method. Both techniques are then compared to analyse each capability. These methods share the training sample as much as possible, to make the analysis unbiased. The illustration of the hierarchical step of both methods is shown in Figure 3.5.

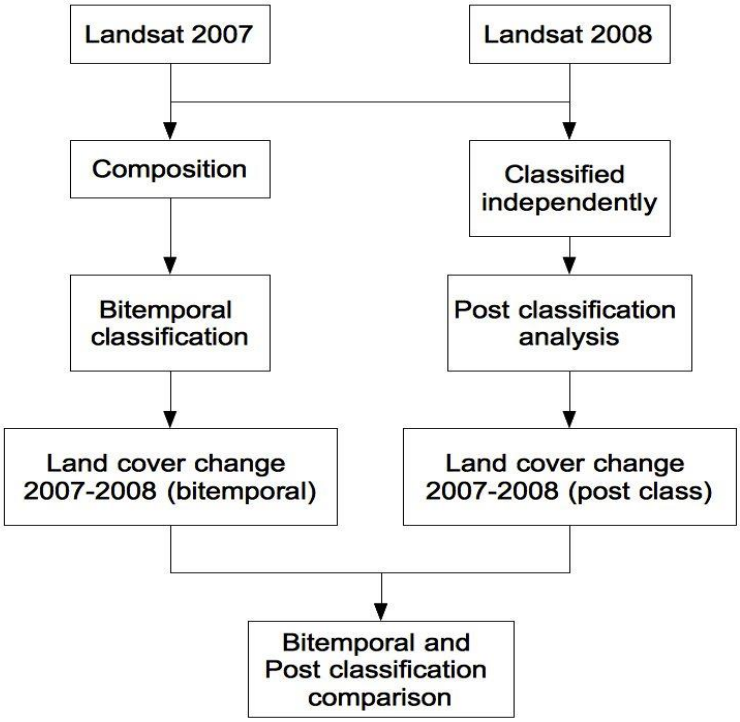

Figure 3.5: *Flow chart for land cover change analysis.*

The change detection methods are running on a pixel basis. It means calculation will be conducted pixel by pixel with disregard to ambient pixels. This method requires a high level of precision of the pre-processing stage. There are two most likely errors that appear if the level of precision is not met, error by image registration or by atmospheric correction. The first type of error appears when image registration of the data is not very good. It will mean that change analysis will not be conducted on exactly the same object and at the end will draw a false conclusion (Townshend, et al., 1992). On the other hand, the non-precisely atmospheric correction can produce error by considering the same object as different because of the difference of digital values (Song, et al., 2001)

3.4 Validation

Validation is conducted to assess quality of change detection classification by using higher resolution remote sensing data as the reference. The assessment will compare the Landsat and reference land cover class and calculate the statistics of true and false classification. Reference data is obtained through Google Earth database (Google, 2011). All available data that co-locates with Landsat 7 path 127 row 59 was used but may cover only partial area of the Landsat scene. The problem with validation is the reference data covers a single observation date only and not multi date compared to the Landsat. The assessment is conducted to compare the reference with the before and after change classes. The connection between the change classes with the before and after classes is mapped in Figure 3.6. The reference data is then grouped into three different time sets, each representing observations prior to, coincident and posterior to Landsat data observation. The list of reference image observation dates and grouping is given in Appendix 1B.

The group that was acquired prior to the Landsat observation date is used to assess prior to change class. The group that was acquired after the Landsat observation date is used to assess after change class. The group that was acquired co-incident to Landsat observation date, because of its date is close to the earliest Landsat data, is then assessed separately.

Classification is undertaken for five classes as depicted in Figure 3.6 for each reference data subset that was obtained from Google Earth. The classes are water, non vegetation, forest, non forest and lower vegetation. The classification result is then resampled to mimic Landsat data at 30m resolution. Each subset is then compared to the Landsat data of the corresponding area to calculate true and false pixels. The result is then summarised into the error matrices to analyse the accuracy of classification (Table 4.10; Table 4.11; and Appendix 7).

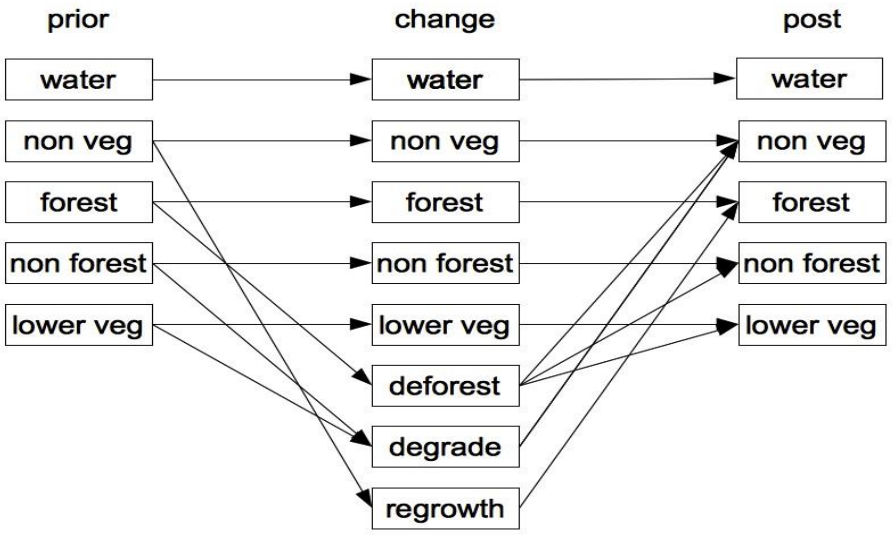

Figure 3.6: *Connection among the land cover change class with its land cover class before and after.*

This chapter described the specification of Landsat, Hymap and high resolution remotely sensed data that is used in this research. Elaboration is also given such as for the applied procedures of pre-processing, land cover change analysis and validation. The following chapter will describe the result of the implemented procedures and discuss the important findings.

Chapter 4

Results and discussion

This chapter has two main components, firstly the important task of normalising the data and identifying data with cloud cover, and secondly the interpretation normalised data for land cover change analysis. Hereafter we refer to the first task as “cloud screening”, where we assemble ground observations, or one clear picture, from numerous images. Typically each image has cloud and land observations which unlike scene by scene, and the idea is to concatenate the land observations into one image. To achieve this, the clouds must be detected in the original images and then treated as missing (land) observations. Later the clear land observations from multiple scenes are composited into a new single image file. Further, as the data acquired from the satellite is not necessarily on the same scale from image to image, the process relies heavily on calibrating the images to a common reference in order that the composited data may be treated as one data source. For calibration, we opt for the algorithm developed by Masek et al. (2006), which we compare with independently calibrated airborne data (Collings and Caccetta, 2011) acquired in Australia. To our knowledge, this is the first such attempt to validate the calibration approach in Australia.

We describe the classification of the “cloud free” images for land cover and change. We use Canonical Variate Analysis (Campbell and Atchley, 1981), a form of linear discriminant analysis, and expert derived rules for this task. The change analysis is conducted using two “cloud free” composites of 2007 and 2008. We provide new results on the change in land cover in this period, and also provide an accuracy assessment using ground truth information.

4.1 Results

Ground reflectance estimates accuracy assessment

Validation of ground reflectance accuracy uses the independently derived ground reflectance estimates. We adopt the approach for Landsat data correction that described by Masek et al. (2006), which incorporates physical modelling of the atmosphere in order to remove its effect. For this reason, such models are commonly referred to as “atmospheric correction” models are applied. A key component of the models is to have information on the light scattering and absorbing elements in the atmosphere at the time of image acquisition.

Direct and absolute observations of these elements are typically not available, and their presence and abundance are inferred either from meteorological information or other satellites data such as the MODIS sensor which has better sensitivity to their presence than the Landsat sensors. The reliance on such information is a major limitation of the approach, especially for calibrating Landsat images acquired prior to the availability of this secondary information. The result of the correction is an affine transformation of each image band, and noting this, some researchers (see for example Furby and Campbell, 2001) have opted for empirical approaches to estimate the correction with the use of image reference samples. A potential pitfall of the empirical approach is that it relies on image reference targets, which may be problematic when trying to calibrate images from different seasons. For example all the reference sites may be damp in the rainy season and have different reflectance characteristics from that of a dry season.

Noting this, and the requirement to work in the tropics, we adopt the physical modelling approach of Masek et al. (2006). Our interest is the accuracy of the method. As good calibration reference sites are few, we make use of results derived by Collings and Caccetta (2011) that using ground reflectance

measurements and an empirical method to calibrate Hymap hyperspectral data to ground reflectance for a site near Mullewa, Western Australia. Although not the tropics, the assessment against these independent sites provides us with some knowledge as to the performance of algorithm, which is still in the research assessment stage.

We compare the Hymap derived estimates to the Landsat derived estimates where the Landsat scene closest in date to the Hymap data was used. The Landsat derived estimates were corrected by LEDAPS pre processing tools that assumed the surface is Lambertian and infinite; and the gaseous absorption and particle scattering are possible to decouple using the TOMS's ozone and NCEP water vapour reanalysis data. The ozone and water vapour data are used to estimate the aerosol optical thickness (AOT) at 1km resolution (Masek et al., 2006).

The Hymap's data was acquired on the 9th February 2010, while the Landsat was acquired at 23rd February 2010. These dates represented the hot dry summer season (of the southern hemisphere) where there was no cropping and land cover changes were minimal. We record the results in tables 4.1 to 4.7, as maximum, minimum value, means, and standard deviation (SD) of the difference in the two estimates. From the tables we observe that the Landsat data (path 113 row 80) and Hymap have a RMS difference of less than 2.25% (Table 4.1). A small number of pixels adjacent to the roads (1500 pixels, 0.13% of total data amount) had a difference up to 20.72% (Table 4.2), which may because of the resolution difference of the original Hymap data (~5m) from that of the Landsat TM data (~30m) as opposed to some deficiency in the Landsat data.

Next we compared the estimates derived from different Landsat scenes acquired relatively close in date over the same area. We chose Landsat (path 113 row 80) 23rd February 2010 (clear) and 22nd January 2010 (clear) for the comparison of clear condition and moreover 23rd February 2010 (clear) and

28th April 2010 (cloudy) for comparison of clear and cloudy condition. To test the performance of the algorithm in the presence of cloud, we purposely compared the results obtained from clear and cloud affected images, and recorded our results in tables 4.3 and 4.4. We observe a maximum difference of 0.87% (clear to clear comparison on Table 4.3) and 1.42% (clear to cloudy comparison on Table 4.4). The results indicate that the performance degrades in the presence of cloud.

We compare the performance of the algorithm for two locations in Indonesia, again using an image pair at each location. Due to the lack of clear scenes, comparison of theLandsat scene identified by path 103 row 63 was performed using two cloud affected images and the result recorded in Table 4.5. In the second location, path 114 row 66, two cloud affected scenes were used, and we also performed a wet and dry season comparison. The results of these tests are recorded in tables 4.6 and 4.7 respectively.

Table 4.1: *Statistics of Landsat and Hymap (expressed in surface reflectance percentage).*

	Band 1	**Band 2**	**Band 3**	**Band 4**	**Band 5**	**Band 7**
Hymap mean	8.66	15.06	21.10	28.48	43.27	33.51
Hymap SD	2.15	3.72	4.73	4.85	6.55	5.85
Landsat mean	7.63	13.17	18.14	25.39	40.40	31.63
Landsat SD	1.58	2.91	3.81	4.09	6.17	5.62
Minimum RMS	0.00	0.00	0.00	0.00	0.00	0.00
Maximum RMS	38.81	20.80	21.20	17.82	88.68	40.06
Mean RMS	0.79	1.41	2.16	2.24	2.25	1.68
SD RMS	0.53	0.82	1.04	1.08	1.37	1.28

Table 4.2: *Extracted statistics of Table 4.1 which has RMS value more than*

10%. Data is expressed in surface reflectance percentage.

	Band 1	Band 2	Band 3	Band 4	Band 5	Band 7
Pixel amount	13.00	13.00	116.00	118.00	1500.00	826.00
Minimum RMS	10.25	10.13	10.02	10.01	10.01	10.01
Maximum RMS	38.81	20.8	21.2	17.82	88.68	40.06
Mean RMS	26.06	12.13	11.07	11.36	11.83	11.76
SD RMS	14.64	6.03	8	5.2	20.73	24.34

Table 4.3: *Statistics of Landsat 5 path 113 row 80 of 23rd February 2010 (clear) and 28 April 2010 (cloudy). Data is expressed in surface reflectance percentage.*

	Band 1	Band 2	Band 3	Band 4	Band 5	Band 7
Minimum RMS	0.00	0.00	0.00	0.00	0.00	0.00
Maximum RMS	30.84	37.77	19.65	21.06	25.05	43.67
Mean RMS	0.77	1.38	1.93	2.34	2.29	1.42
SD RMS	0.61	0.96	1.31	1.69	1.8	1.45

Table 4.4: *Statistics of Landsat 5 path 113 row 80 of 23rd February 2010 (clear) and 22nd January 2010 (clear). Data is expressed in surface reflectance percentage.*

	Band 1	Band 2	Band 3	Band 4	Band 5	Band 7
Minimum RMS	0.00	0.00	0.00	0.00	0.00	0.00
Maximum RMS	21.29	36.9	36.18	9.5	16.79	13.19
Mean RMS	0.34	0.46	0.49	0.52	0.85	0.87
SD RMS	0.3	0.38	0.43	0.48	0.61	0.57

Table 4.5: *Statistics of Landsat 5 path 103 row 63 of 8th January 2007 (cloudy) and 13th March 2007 (cloudy). Data is expressed in surface reflectance percentage.*

	Band 1	Band 2	Band 3	Band 4	Band 5	Band 7
Minimum RMS	0.00	0.00	0.00	0.00	0.00	0.00
Maximum RMS	7.66	8.33	8	13.89	12.53	9.69
Mean RMS	0.34	0.46	0.38	1.6	0.75	0.66
SD RMS	0.4	0.58	0.52	1.5	0.77	0.72

Table 4.6: *Statistics of Landsat 5 path 114 row 66 of 27th April 2007 (cloudy) and 13th May 2007 (cloudy), both represent wet season. Data is expressed in surface reflectance percentage.*

	Band 1	Band 2	Band 3	Band 4	Band 5	Band 7
Minimum RMS	0.00	0.00	0.00	0.00	0.00	0.00
Maximum RMS	4	4.85	7.91	24.91	16.5	13.27
Mean RMS	0.32	0.31	0.65	1.6	0.79	0.88
SD RMS	0.31	0.34	0.7	1.98	1	1.02

Table 4.7: *Statistics of Landsat 5 path 114 row 66 of 17th August 2007 (cloudy) and 2nd September 2007 (cloudy), both represent dry season. Data is expressed in surface reflectance percentage.*

	Band 1	Band 2	Band 3	Band 4	Band 5	Band 7
Minimum RMS	0.00	0.00	0.00	0.00	0.00	0.00
Maximum RMS	8.2	8.85	10.51	20.92	17.66	14.04
Mean RMS	0.45	0.75	0.99	2.12	2.23	1.87
SD RMS	0.44	0.55	0.77	1.66	1.51	1.21

Assessment of the method in Australian territory has the advantage of relatively low cloud cover, and hence many ground reflectance estimates. The comparison for the Australian-site included approximately 1.8 Mega cloud free pixels. This amount is difficult to achieve in Indonesia due to more

cloud cover. In contrast, the assessment in Indonesian-site included 0.1 Mega cloud free pixels only.

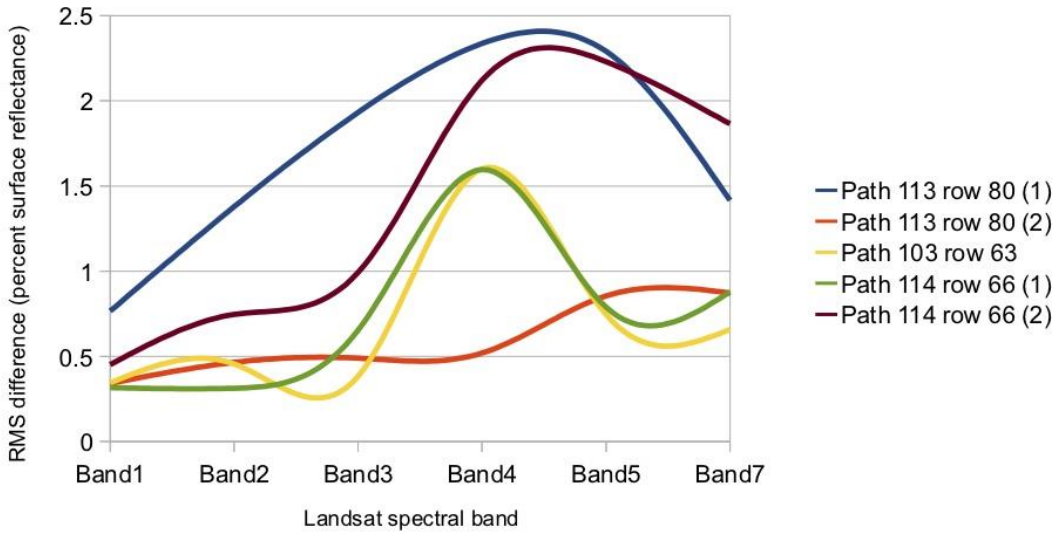

Figure 4.1: *Mean RMS difference of Landsat surface reflectance. Path 113 row 80 dominated by sparse vegetation; (1) compared clear and cloudy; (2) compared clear and clear. Path 103 row 63 dominated by higher vegetation, compared two cloudy observations. Path 114 row 66 dominated by higher vegetation; compared two cloudy observations on rainy season (1) and dry season (2).*

Figure 4.1 illustrates the RMS differences between the Landsat and Hymap derived ground reflectance estimates. We observe a gradual rise in RMS difference from band 1 to band 7 from the graph. The RMS difference is similar for all bands and maximum difference is less than 1% (clear to clear comparison). On the other hand, if comparison is conducted between clear and cloudy or cloudy and cloudy data, variation unveils. Band 4 becomes the peak if location is predominately vegetation (path 103 row 63 and path 114 row 66 in wet season); or band 5 becomes the peak if the location is predominately bare land or lower or sparse vegetation (path 113 row 80 and path 114 row 66 in dry season). For the data where one or both are cloudy, the highest RMS value is mainly less than 2.5%, except for a small number of outliers. We then conclude that the method promises sufficient accuracy for the task of concatenating data from multiple images.

Cloud screening and multi-temporal image composition

In this section the details of the application of the cloud screening methods (for which the procedure details are provided in Chapter 3) are described, the results are recorded and some observations are made.

Cloud identification is initiated by using CVA (Campbell and Atchley, 1981). The approach uses training samples obtained by human interpretation of the imagery. The approach models the various training sites selected via the specification of a sample mean and covariance matrix, and then maximises the ratio of between class distance and within class variance. Each training sample is marked by a specific code so as to make it easier to distinguish it in the analysis. Canonical variates are calculated by using CSIRO-MIS packages and then the results plotted by R software.

Figure 4.2 illustrates the configuration of the training samples of CVA. The figure shows that thick cloud objects (code – h, red dot) are obviously distinct from the other objects while the transmissive clouds or haze (code – m, black dot) are mixed with the objects they cover. The thick cloud is then distinctively grouped into cloud and the transmissive cloud is inevitably included into other respective groups such as higher vegetation or lower vegetation of which its value is closer. The cloud class is then masked out and the digital number (Q) is set to the lowest available value, Q=1. The images are composited into one new image using the maximum value rule (Formula (3.7)).

Next we explored the data for the possibility of using a series of simple rules, which hereafter we refer the term as “multiple rules”. Prior to application of each rule, training samples were collected to produce a spectral signature of each representative object (Figure 4.3). The procedures were comprised of nine rules in combination, each may contain a threshold of specific band, or ratios, or indices, or a combination of these for cloud identification (the list of

the applied rules is provided in Appendix 2A). The identified clouds were masked out and the digital number (Q) was set to the lowest possible, Q=1 and then composited using the maximum value rule (Formula (3.7)) to obtain the cloud free image. The best result was produced from the rules set Number 6 for which the rule formulation is provided in Appendix 2A and the depiction of a cloud free image is shown in Figure 4.5(b). The multiple rules produced better results than the initial attempt using CVA in an overview, but two problems remain: (i) the pixels adjacent to clouds having values different from clouds and from ground pixels that were not adequately handled, and (ii) the “twilight zone” (the transmissive cloud or haze that appeared around the cloud edge) that resulted in dark patches upon multi-temporal compilation (Figure 4.6).

The problems in analysis of multiple rules without atmospheric correction are caused by (i) the digital value of each cell not being normalised, and (ii) “twilight zone” that could not be identified properly. Noting these, we next undertook the multiple rules with atmospherically corrected data that took into account these conditions: (i) cloud objects must be identified separately, each type having a specific formula; (ii) image data must be normalised first (by using atmospheric correction) before the masking and compositing process is started; (iii) characteristics of “twilight zone” or cloud adjacency effect must be identified to find the formula to solve.

At the beginning, cloud is considered as one single object and one average value is expected to be enough to define the threshold (Rules number 1 and 2 of Appendix 2B). The rules defined its thresholds from the spectral signature generated from the average value of the cloud. Several attempts have been done without good results being obtained. Figure 4.4 depicts a typical condition of cloud's spectral signature that obtained from various visible feature of cloud and not from the average value only. This complicated spectral signature lead to apply extra rules to identify cloud and make it difference to other objects. The rules are designed to deal with a variety of

cloud's feature types (Formulas (3.2) to (3.5)). These procedures were developed from the experiment of various rules as given in Appendix 4. The masked out cloud images are then composited hierarchically using Formulas (3.11) to (3.13). The composition stage is elaborated by the diagram in Figure (3.4).

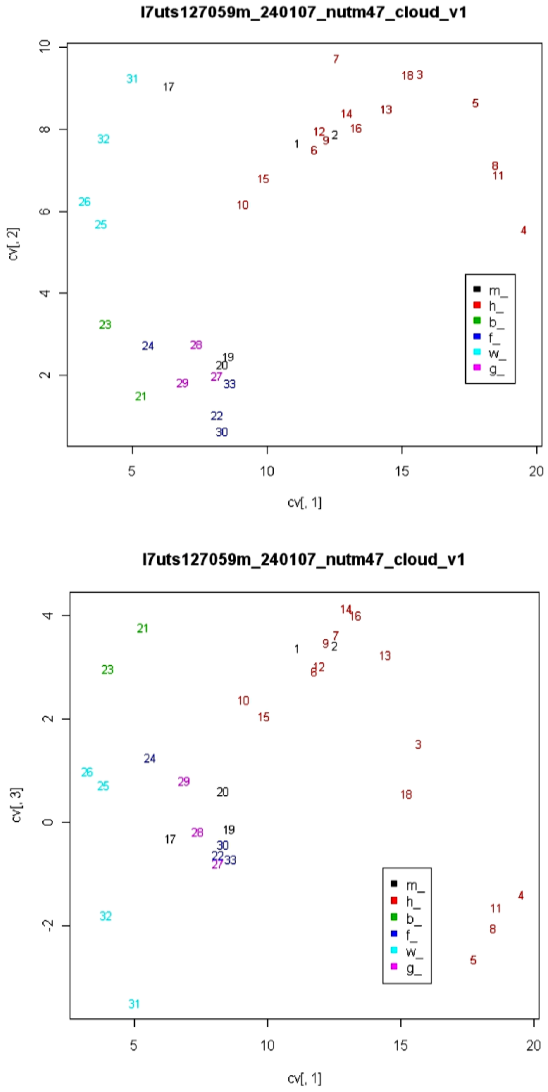

Figure 4.2: *Canonical variate analysis (CVA) of Landsat training samples. The upper diagram depicts canonical variates 1 (cv1) vs cv3, while the lower diagram depicts cv1 vs cv3. The training samples are obtained from Landsat 7 path 127 row 59 of 24th January 2007. Code stands for its respective meaning: (m-black) for transmissive cloud, (h-red) for thick cloud, (b-green) for wetland vegetation, (f-blue) for higher vegetation, (w-light blue) for water bodies, (g-purple) for lower vegetation.*

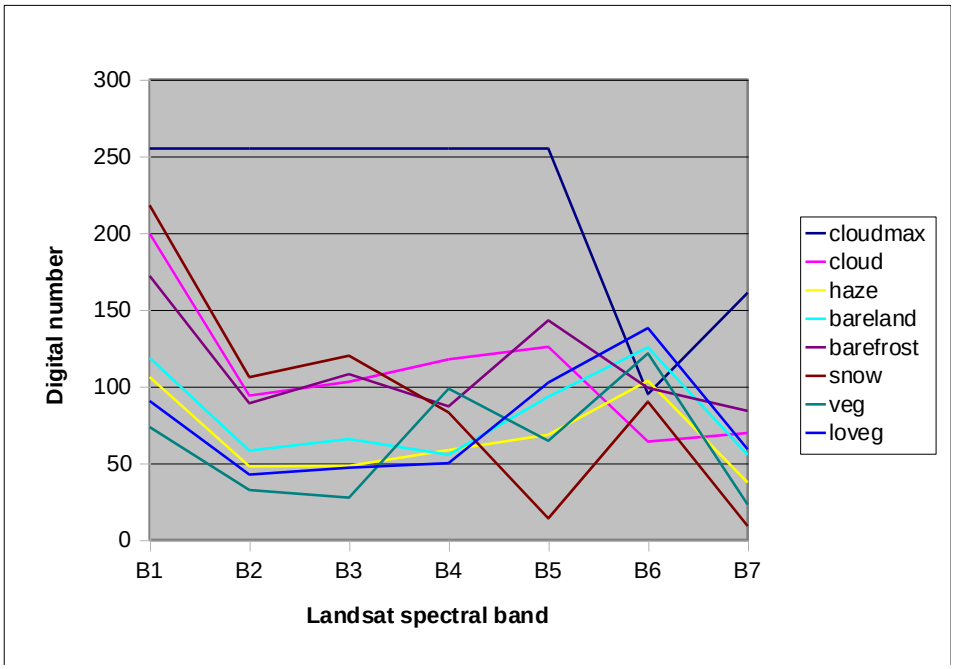

Figure 4.3: *Spectral signature of Landsat 5 path 103 row 63 of 8th January 2007. Graph depicts average value of the selected objects plus one cloud maximum value possible (Cloudmax)*

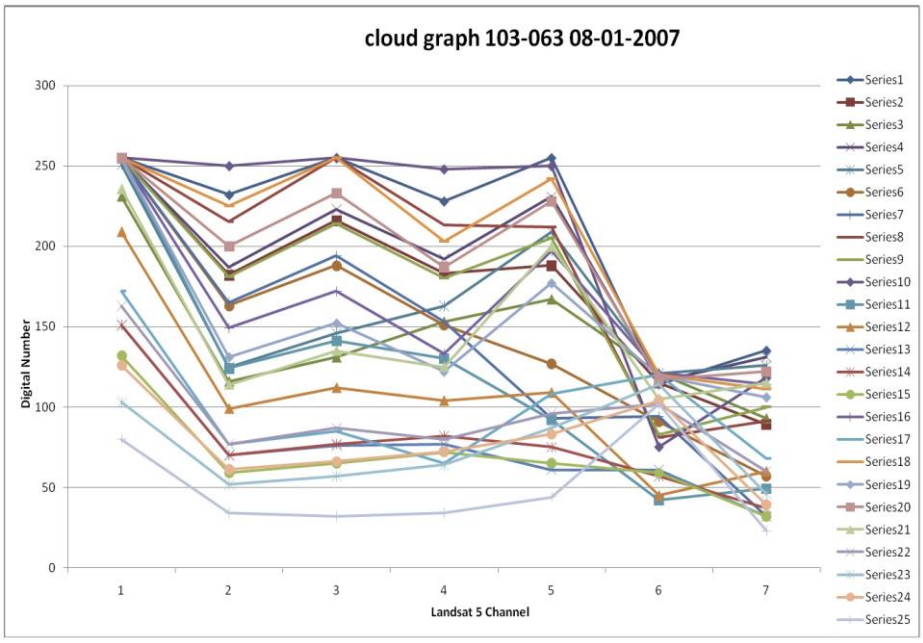

Figure 4.4: *Cloud's spectral signature of Landsat 5 path 103 row 63 of 8th January 2007. The graph depicts variability of clouds. Transmissive clouds are also included. Spectral signature of the other objects is given in Appendix 5.*

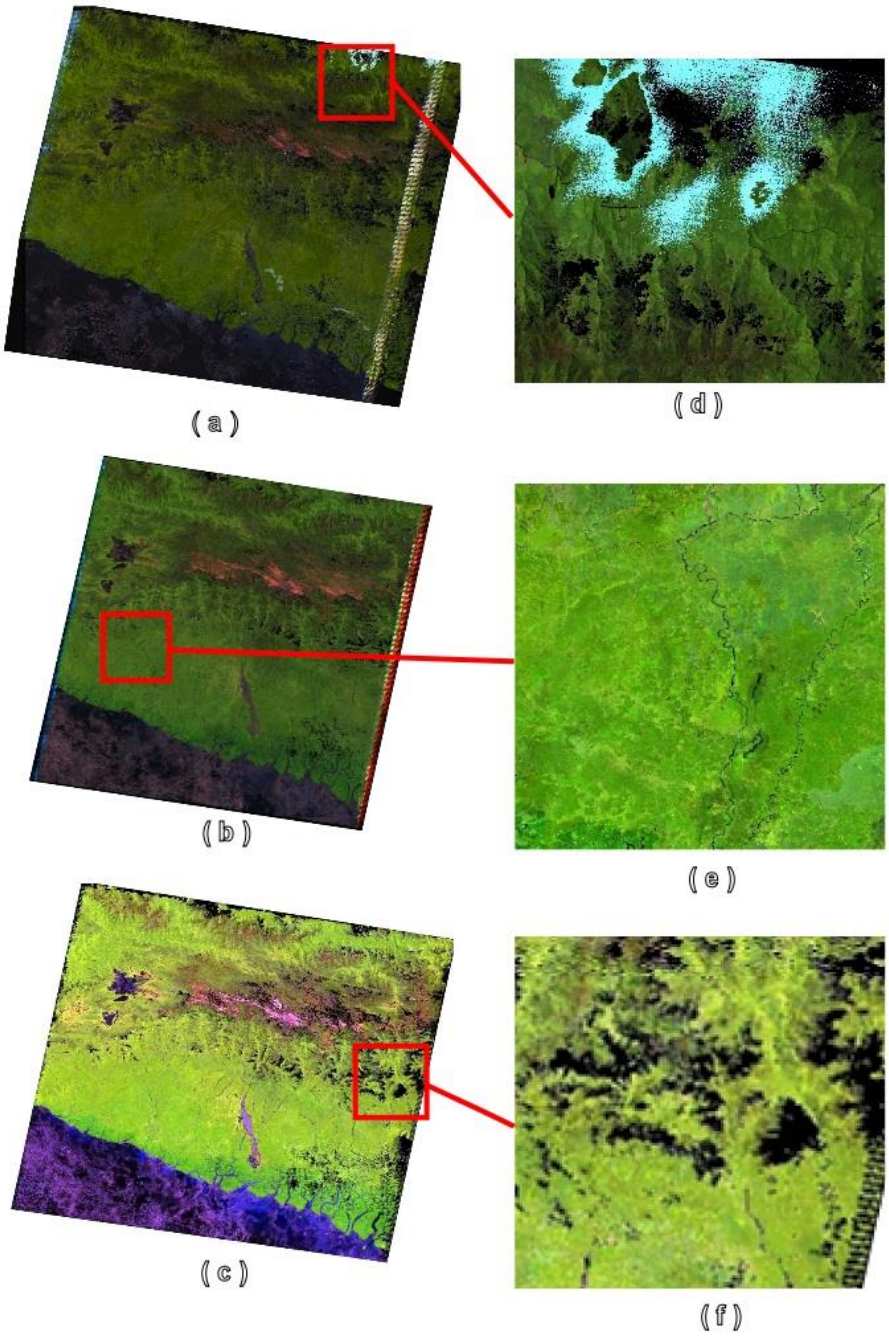

Figure 4.5: *Cloud elimination result of 2007 Landsat 5 path 103 row 063 by using (a) canonical variate analysis (CVA); (b) multiple rules without atmospheric correction (MRN); (c) multiple rules with atmospheric correction (MRA). Persistent clouds still exist as the black patches (f) in all methods; cloud adjacency effects (e) occur at (a) and (b); and saturated values (d) prevail as the blueish white patches at (a). Please note that red insets of (a), (b), and (c) are portrayed in larger picture at (d), (e), and (f) respectively.*

Further on, we compare the result of three experiments to eliminate clouds. The result of each experiment is depicted for the entire image (Figure 4.5) as well as in subset (Figure 4.6) to illustrate some of the finer scale effects. The results of the CVA analysis, multiple rules without atmospheric correction, and multiple rules with atmospheric correction are provided in Figures 4.5(a), (b), and (c) respectively. The illustration uses 2007 Landsat 5 path 103 row 063 as an example.

On first inspection, multiple rules without atmospheric correction appear promising with Figure (4.5(b)) having the least area of visible cloud remnant (black patches) compared to Figures 4.5(a) and (c). On closer inspection, we find dissimilar characteristics. We can perceive a number of amorphous bright cloud patches in Figure 4.6(a) and (b), in contrast to Figure 4.6(c) that succeed to remove this problem. Visual presentation of Figure 4.6(c) demonstrates the importance of data calibration to a common reference for this task, typically for the closer inspection.

Figure 4.5(c) illustrates the result of multiple rules with atmospheric correction application. Errors remain to be seen such as cloud remnant. They appear in, perhaps, as a consequence of no sufficient clear observation available within annual timeframe of the designated scenery. This condition indicates that longer timeframe or more frequent data acquisition may need to consider. Next we discuss the implication of cloud screening methods such as the rules portability, the cloud adjacency effect and the timeframe.

Cloud removal rules portability

The successful cloud removing rules applied for 2007 Landsat 5 path 103 row 63 then be used for portability test. The test implemented for 2007 Landsat 5 path 114 row 66 and Landsat 7 path 127 row 59. The test inferred that modification is needed (Formula (4.1) and (4.2)) for path 114 row 66 to cope with phenological cycle of deciduous vegetation found in this area.

Green vegetation covering forested area in the rainy season will transform into reddish feature comparable to bare ground in the dry season. These contrasting features are unfeasible to compose in the same category for the whole year. The image composition was undertaken for each respective season, dry and wet (rainy), instead of full year composition. The composition effort comprises of 15 observations, of which 8 observation on wet season and 7 observations on dry season.

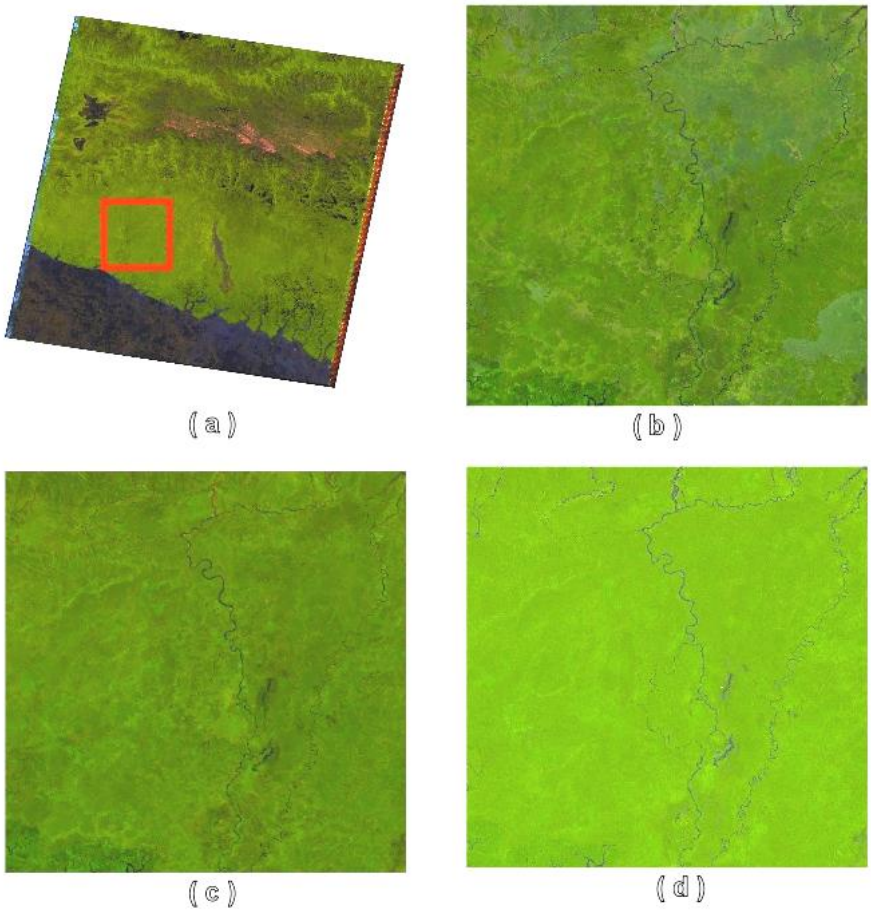

Figure 4.6: *Subsets of cloud elimination result in Figure 4.5. Subset location is marked by red inset (a). Each subset represents their respective processing method, CVA (b), multiple rules without atmospheric correction (c), and multiple rules with atmospheric correction (d). Amorphous bright patches in (a) and (b) illustrate the existence of cloud adjacency effect. The effect is indicated by a slightly higher reflectance than the clear observations that make the effect selected for annual composition. The effect was successfully eliminated in (c).*

Cloud elimination of path 114 row 66 also used a two stage approach; cloud masking and then multi-temporal composition. Three different procedures: CVA, multiple rules without atmospheric correction (MRN) and multiple rules with atmospheric correction (MRA) were performed.

The rules derived using the CVA procedures produced the lowest quality results on cloud elimination for the wet season, largely due to over classification resulting in missing data in the composite for the southern part of the island.

MRN provided adequate results in terms of cloud elimination and maintaining the image details. It produced better quality on cloud elimination but had a lower quality on maintaining tonal details.

MRA provided the best results on cloud elimination both for wet and dry seasons. The nature of vegetation in path 114 row 66, the evergreen and deciduous vegetation resulted in different colour illustration for different seasons. It meant that the composition stage required modification, for example the bright top cloud (Formula 3.1). The modification was implemented by changing the threshold values and including band 5 to adapt specific needs of path 114 row 66 (Formula 4.1). On the other hand Formula (3.4) also needs modification that is given in Formula (4.2):

(4.1)

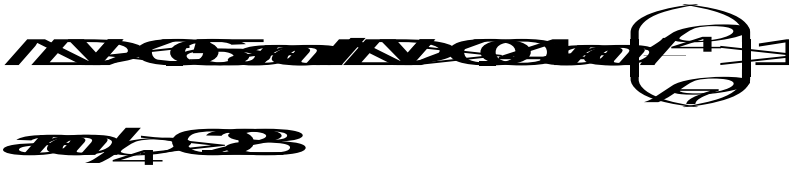

(4.2)

where ρ_i is the surface reflectance value of band i, i: 1, 2, 3, 4, 5 and 7.

Cloud adjacency effect

The "cloud adjacency effect" or "twilight zone" is induced by the humidified aerosols or undetected thin cloud that is mainly found around the broken cloud. The effect will make pixel value around the cloud having localised atmospheric effect (Koren, et al., 2007; Marshak, et al.: 2008). The existence of this effect will distract the composition of cloud-free pixel selection. The effect tend to produce the higher value and make the applied rules are going to select the affected pixels rather than the clear pixels as those being cloud-free. Koren et al. (2007) tried to justify the existence of the cloud adjacency effect by comparing the surface reflectance of water that was identified as clear of clouds, at 3kms and 20kms from the cloud edges. The average reflectance of the site closer to the cloud was 5.6 to 13% higher than the remote site, leading to errors in the identification of cloud/non-cloud pixels and subsequent image compositing process.

Figure 4.7 illustrates how the cloud adjacency effect has an impact on cloud free image composition. This picture was generated using two observations, the clear one (13th March 2007) and the cloudy one (8th January 2007). Both observations were atmospherically calibrated and processed by cloud masking and multi-temporal image composition. The rules on composition are focused on using maximum value of band 4 only. The result is expected, by using the rule, the clear observation (13th March) will dominate the picture and make the scenery clear. But in reality, the clear observation is taking place for the location that definitely identified as cloud and has been masked only. For the location adjacent to cloud masked area, the cloudy observation (8th January) takes place instead of the clear one. This condition happens because the cloudy observation has a slightly higher value of band 4.

Figure 4.7 (d) shows how the cloud adjacency effect becomes visible. The effect comes from the undetected cloud that appeared adjacent to the broken cloud and is hard to identify visually as cloud or cloud affected area (Figure

4.7 (a) and (b)). Their value that is just slightly higher than the clear one made them still identified as clear area and selected for cloud free composition purposes. Another attempt must be applied to differentiate the cloud affected area from the clear one. The attempt is designed to prevent the appearance of cloud affected pixels accumulated in the annual composition result. The characteristics that must be observed to avoid cloud adjacency effect are:

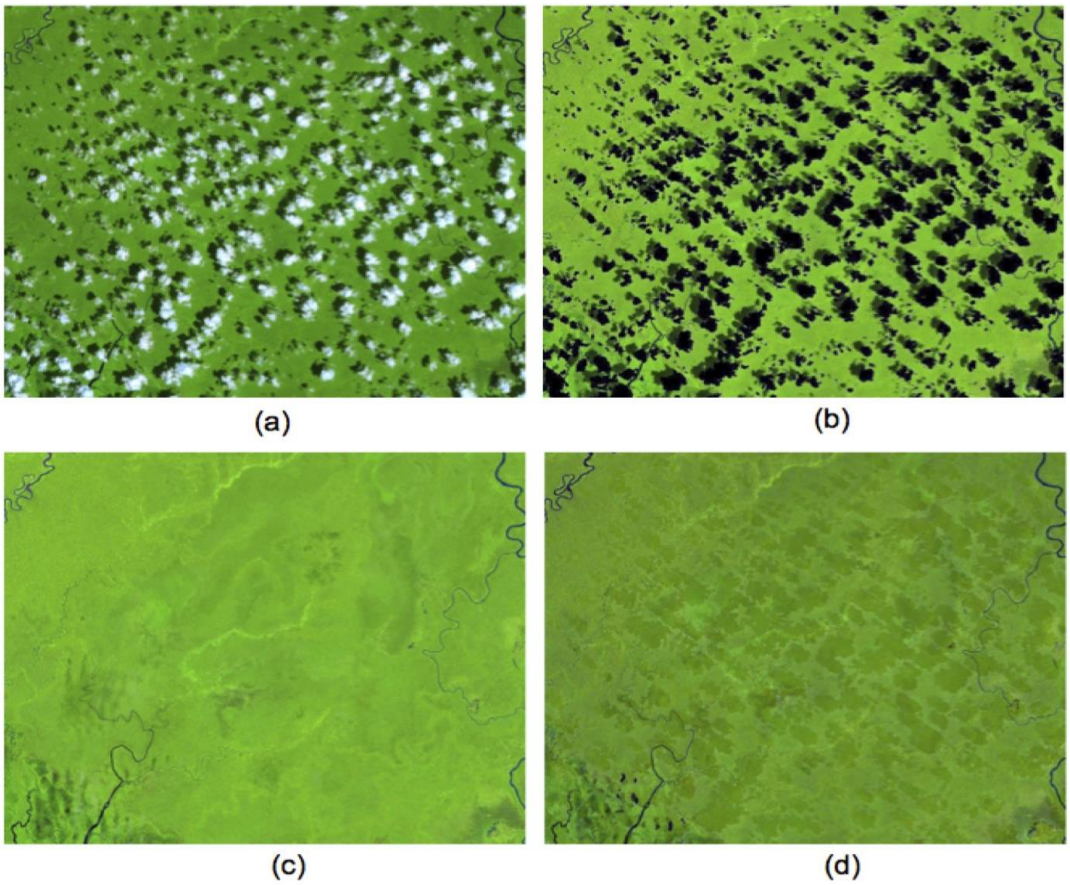

Figure 4.7: *Illustration of the cloud affected pixels that influence cloud-free selection. (a) shows observation of 8th January 2007; (b) shows (a) after cloud masked; (c) shows 13th March 2007 observation (presumed clear); and (d) composition result using maximum band 4 value that produces darker patches.*

(a) Cloud shadow or cloud masked objects appeared on one or both observations. These are associated with very low reflectance. If these conditions are perceived on one or both observations then the maximum value is selected (Formula (3.12)).

(b) Cloud adjacency effect appeared on one or both observations. This is associated with the slightly higher reflectance than the clear object. If this condition detected on at least one observation then the minimum value is selected (Formula (3.13)).

(c) Cloud shadow or cloud masked objects or cloud adjacency effect are not observed on both observations. If this condition noticed then the maximum value of band 4 is used to select which observation as the best cloud-free possible object (Formula (3.11)). Composition flow is illustrated in Figure (3.4).

On the other hand, Figure 4.8 justifies how to solve this problem. This picture illustrates two observations, 13th March 2007 that is presumed clear and 8th January 2007 that is presumed cloudy. For these two observations, band 4 value is selected as an example. The 13th March observation shows a fairly flat graph, in contrast to the 8th January observation that shows a more fluctuated graph. The graph is segregated into several zones: the clear, the shadow, the cloud edge, the cloud, and the cloud adjacency effect zone. The difference value of both graphs at the clear zone is low and the graphs illustrate the similar pattern. The difference raised dramatically in the cloud zone. In cloud adjacency effect / twilight zone in which the image visually appeared as clear, the difference of both graphs is still higher than in the clear zone. Since the left hand side of the cloud zone is confounded with shadow, the twilight zone or cloud adjacency effect is not observed clearly.

Figure 4.9 illustrates the result of cloud adjacency effect elimination using the combination of Formula 3.11, 3.12 and 3.13. These applied rules are only useful if from both observations, at least one observation has really clear data. If there are no really clear data, then the best available value is selected. These rules are not intended to eliminate shadow using de-shadowing algorithm (Richter & Muller, 2005).

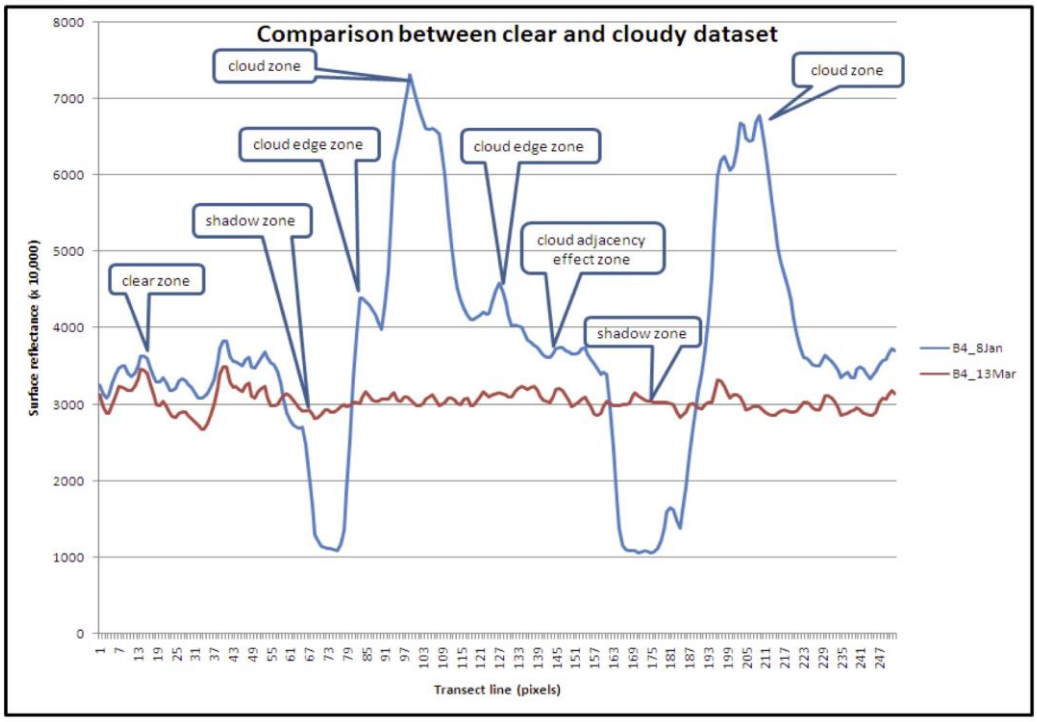

Figure 4.8: *Spectral signature of clear and cloudy Landsat path 103 row 63. The signature is represented by band 4 of 8th January 2007 (cloudy – blue line) and 13th March 2007 (clear – red line). The transect line lied on terrestrially forested area. Value is expressed in surface reflectance times 10,000.*

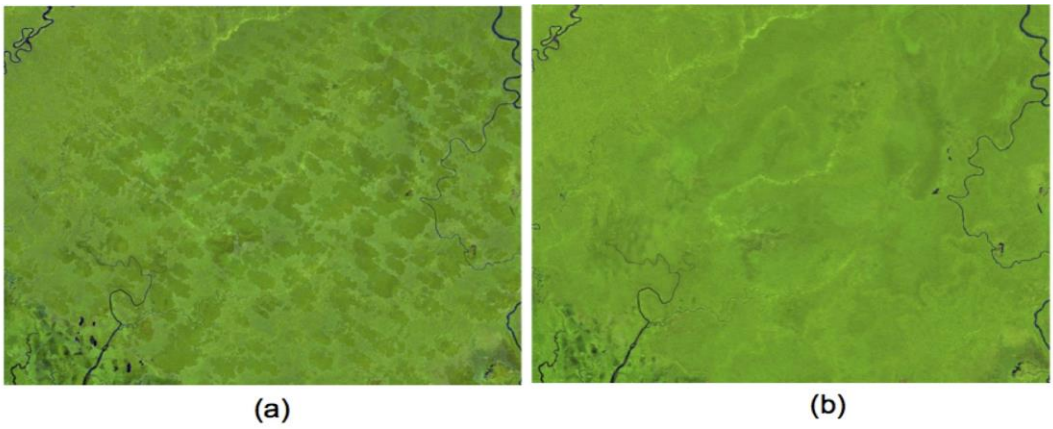

Figure 4.9: *Comparison of two different composition methods that pay attention on cloud adjacency effect (b) and that disregard the effect (a).*

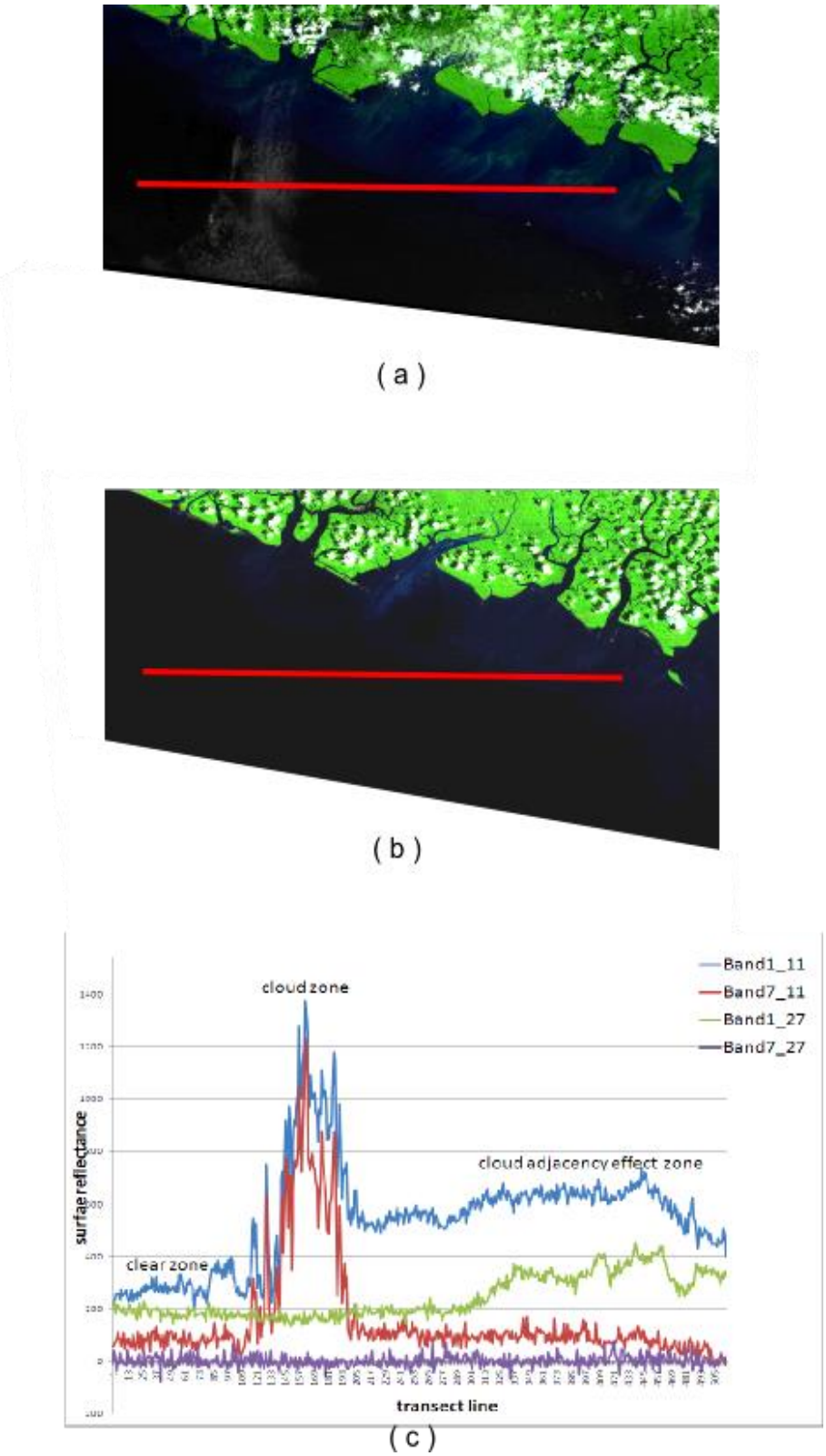

Figure 4.10: *Cloud adjacency effect over water observed on Landsat 5 path 103 row 63 of 11th January 2008 (a) and 27th January 2008 (b). Surface reflectance over the red transect line is plotted in (c) graph.*

Figure 4.8 provides a graph that illustrates cloud adjacency effect on terrestrially forested area. Another example is given by Figure 4.10 that observed the cloud adjacency effect over water bodies. For this condition band 1 and 7 are selected as an example to represent the shortest and the longest spectrum of Landsat. Comparison was conducted between two different observations of Landsat 5 path 103 row 63 of 11th January 2008 that is presumed cloudy (Figure 4.10(a)) and 27th January 2008 observation that is presumed clear (Figure 4.10(b)). The selected region on the image is the ocean of which the transect line is drawn. The left hand side of the transect line covers the area that is presumed as clear water while the right hand side is presumed turbid water. Cloud appeared in Figure 4.10(a), at lower left section of the picture. Band 1 and 7 of 27th January (clear observation) showed the fairly flat graph over the clear water and fluctuated graph of band 1 over the turbid water. In contrast, band 1 and 7 of 11th January (cloudy observation) showed three zones of the graphs, the clear, the cloud and the cloud adjacency effect zones (Figure 4.10(c)). At the clear zone, where visually no observable clouds there, difference of reflectance between the clear and cloudy observation of band 1 is small. At the cloud zone, the difference is exactly high. At the cloud adjacency effect zone, where visually no observable cloud there, difference of reflectance between the clear and cloudy observation of band 1 is still high. Reflectance of band 1 of 11th January (cloudy) at the cloud adjacency effect zone is 18 to 300% higher than band 1 of 27th January (clear). This value is much higher than the Koren et al. (2007) experimentation.

Cloud removal time interval

Cloud removal is conducted by compositing several cloud masked imagery altogether to obtain best cloud free possible. The question becomes what is the most efficient time interval for cloud removal by using Landsat, half year, one year, two year or more? For this research, composition is conducted within one and two year time frame only. If, within one year time range, a cloud free image or clear sky picture is not yet achieved, the time range is

extended to a two year range. If within the two year time range, cloud cover still exists, that will be considered as the optimum cloud free image achieved. On the other hand, in some locations within the image, cloud still permanently covered for the two years range. Technically, it is possible to extent the time range to three, four or five years. But, enforcing cloud elimination for longer than two years is considered too risky because of the possibility of extensive land cover change on such location.

Landsat 5 TM and 7 ETM+ repeat observation for the same location every 16 days (maximum 23 times annually). For path 114 row 66 (relatively lower cloud cover prevalence), we found 15 prospective observations only for the year 2007, while path 103 row 63 (relatively higher cloud cover prevalence) just provided 8 prospective observations. The prospective images are the observations that still have a reasonable portion of clear part to contribute to the composition process. The prospective images are selected to reduce the number of image data that may not give significant contribution to cloud removal. For the location that is presumably a clear area, usually shadow or haze or cloud adjacency effects still exist.

It is hard to obtain a clear sky picture on a half year basis, especially for the location with extreme cloud prevalence. For example, Landsat path 103 row 63 of the year 2007 provided 8 prospective observations only, of which 6 were for January to June, and just 2 images for July to December period. Limited number of imagery suggests that it is more reasonable to process composition on an annual basis rather than a half year basis. Figure 4.11 shows that year 2007 cloud removal attempt is unable to remove the cloud cover completely and so even elimination on an annual basis may not be enough. A similar result is depicted in Figure 4.12 for the year 2008. Both Figures (4.11 and 4.12) show that cloud elimination effort on an annual basis is not sufficient to eliminate entire cloud coverage. The experiment is then extended for a biennial period using the 2007 and 2008 observations. The biennial cloud elimination result is illustrated in Figure 4.13 and there still is

some persistent cloud cover.

Change detection

Land cover change detection analysis was conducted using Landsat 7 path 127 row 59 because it has the highest land cover change than other locations considered in this research (Dephut, 2008b). Change detection used the “cloud free” images of 2007 and 2008 observations as the result of cloud screening and elimination efforts. The 2007 observation resulted from a composition of 9 observation dates, while the 2008 observation was from 7 observation dates. Both observations then analysed for change detection using two different methods, bitemporal and post classification. Both methods shared as much as possible the training area to make the change detection results comparable. Statistics of the classification result is presented in Table 4.9 while the image is in Figure 4.14.

The bitemporal method was initiated by concatenating the 7-layers of each of the 2007 and 2008 observations into one 14-layer image for 2007-2008. The 14-layers 2007-2008 image was then classified using canonical variate analysis. The image result is classified into 7 land cover classes: water, non vegetation (urban and bare ground), forested area, higher vegetation non forest, lower/sparse vegetation, deforested area, and regrowth area. The last two classes (deforested and regrowth) represented the change object. The degraded area class that is available in the post classification method was dropped in the bitemporal method due to a lack of training area.

The post classification analysis is processed in two stages, the land cover classification for each sequence (2007 and 2008) and then land cover change analysis determined from the classification result. For the first stage, the image is classified using canonical variate analysis into 5 land cover classes: water, non vegetation (urban and bare ground), forested area, higher vegetation non forest, and lower/sparse vegetation. Then the

classification result of 2007 and 2008 observations are compared on a pixel by pixel basis. The pixels that perform the same class for both observations are given the same class name, while the pixels that show different class as for 2007 and 2008 are classified as deforested area, degraded area, or regrowth area.

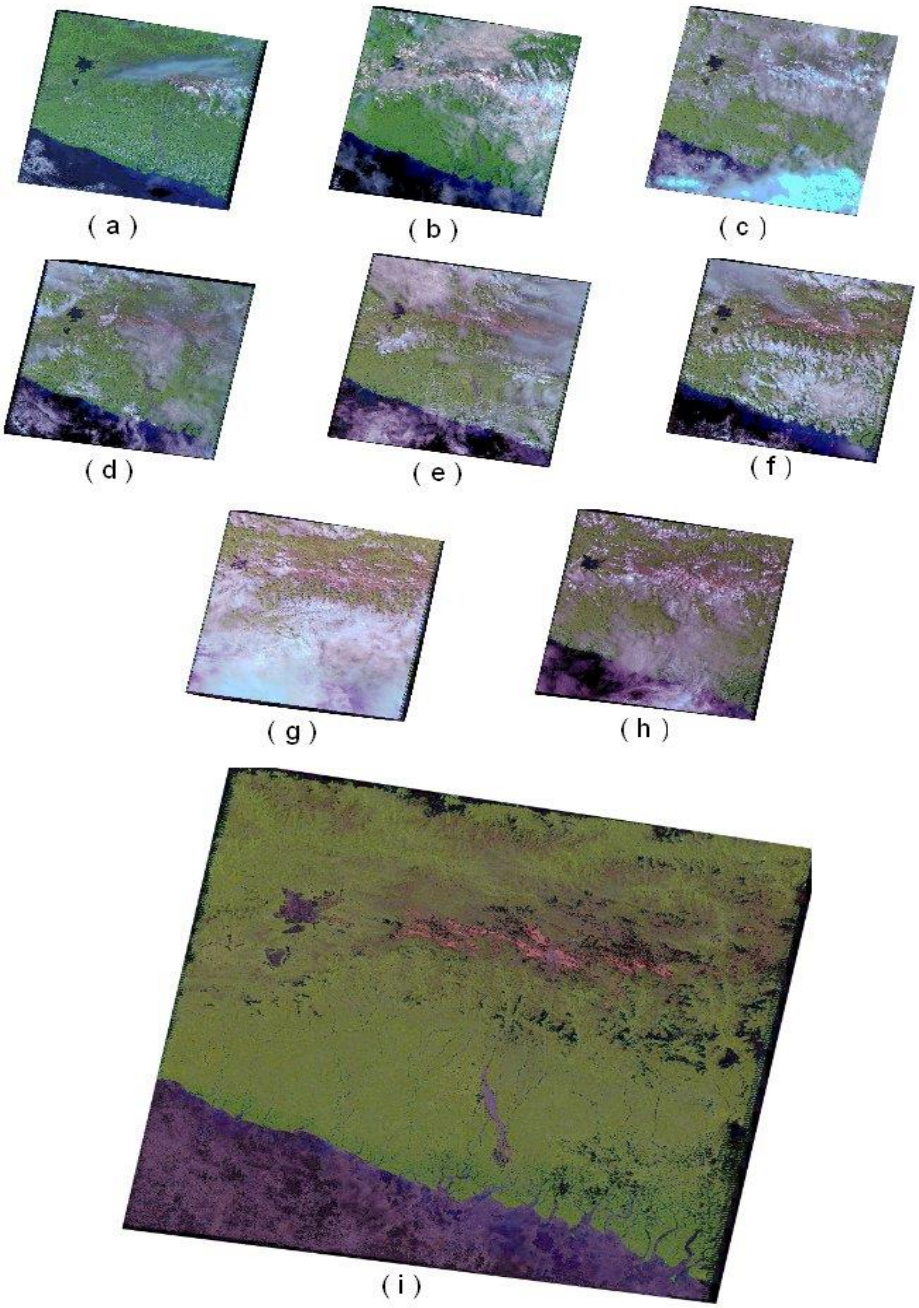

Figure 4.11: *Annual cloud removal result of 2007 Landsat path 103 row 63 (i) that is processed from source image (a) to (h).Cloud on image source appeared as white objects, while on the result is presented as dark patches.*

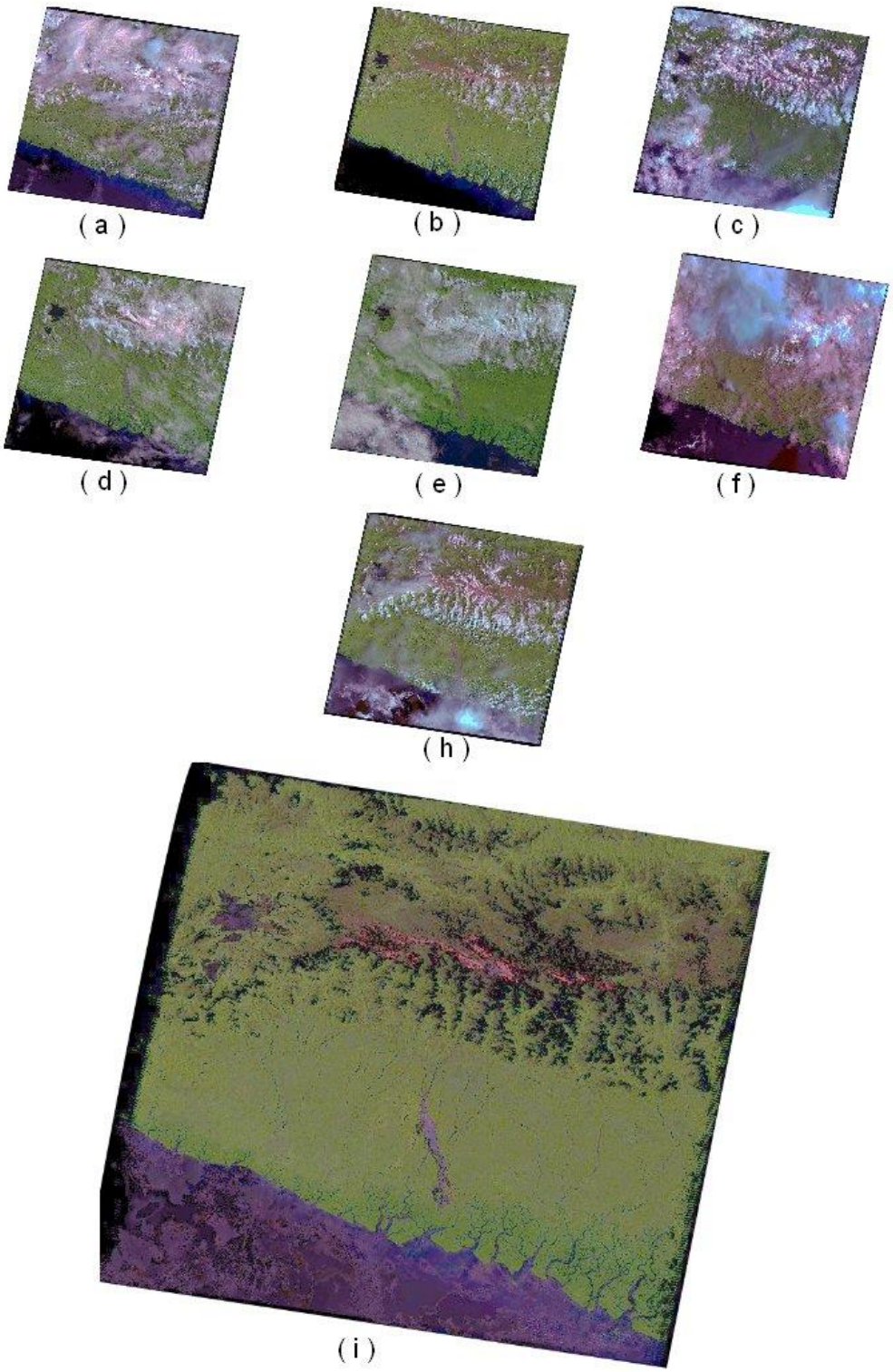

Figure 4.12: *Annual cloud removal result of 2008 Landsat path 103 row 63 (i) that is processed from source image (a) to (h). Cloud on image sources appeared as white objects, while on the result is presented as dark patches.*

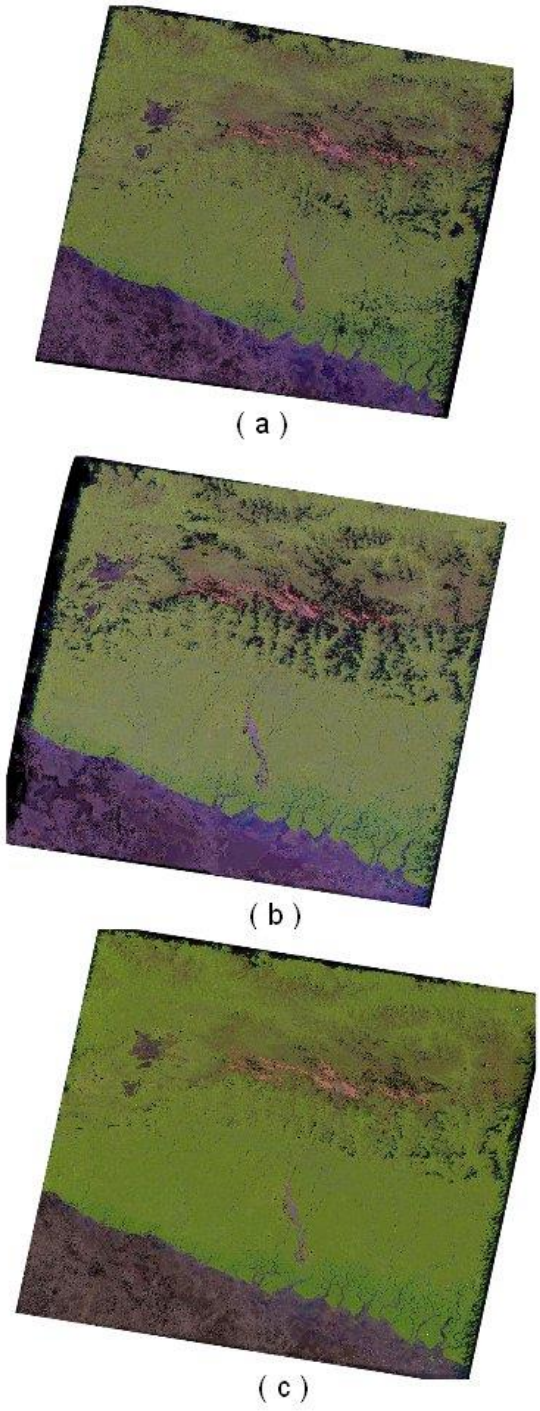

Figure 4.13: *Biennial cloud removal result of 2007-2008 Landsat path 103 row 63 (c), which is composed from annual result of 2007 (a) and 2008 (b). Persistent cloud that is depicted by dark patches still appears in biennial time range. Please note that (a) is the same as Figure 4.11(i) and (b) is the same as Figure 4.12(i)*

Table 4.8: *Classification structure*

Group	Class	Remarks
Unchanged	Water bodies	For sea, river and lake
	Non vegetation	For urban and bare land
	Forest	For natural and human made forest
	Non forest	For estate crops, agroforestry and bush
	Lower vegetation	For shrub and grassland
Changed	Deforested	Change of forest to non forest or non vegetation
	Degraded	Change of non forest or lower vegetation to non vegetation
	Regrowth	Change of non vegetation to forest

Table 4.9: *Statistics of land cover change analysis (expressed in hectares)*

No	Class	Bitemporal	Post classification
1	Unclassified	593,589.15	309,060.45
2	Water bodies	370,638.36	459,673.02
3	Non vegetation	31,688.73	29,138.22
4	Forest	686,866.23	691,978.05
5	Non forest	1,343,382.12	677,358.09
6	Lower vegetation	130,410.90	190,373.04
7	Deforested	120,853.26	241,466.94
8	Regrowth	182,857.86	676,201.23
9	Degraded	0.00	174,303.54
Total		3,460,286.61	3,449,552.58

Table 4.9 shows that land cover change calculation size is similar for the non vegetation and forest class. The highest absolute difference is demonstrated by the regrowth class that attain nearly four times. The other classes illustrate the difference in the range of 1.5 to 2 times. Please note that the difference is accounted from the size and not from the proportion. The degraded is the only class with no comparable size because there are no confident samples found in the bitemporal space.

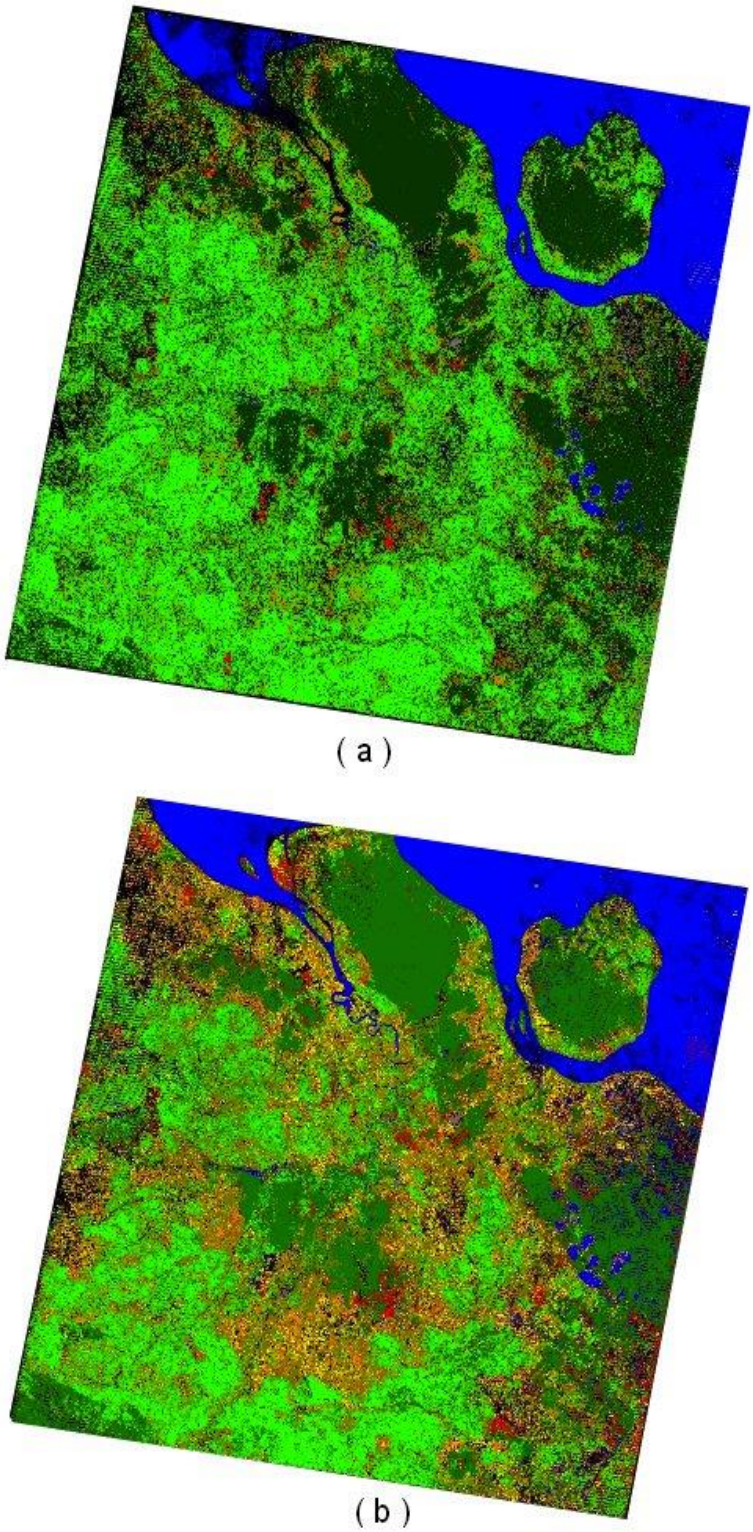

Figure 4.14: *Land cover change detection result of Landsat 7 path 127 row 59 of 2007 and 2008. There are processed using bitemporal analysis (a) and post classification analysis (b). Water bodies is represented by blue, forest - dark green, non forest - bright green, lower vegetation - orange, deforested - red, regrowth - olive, degraded - yellow, and unclassified - black.*

Validation

Validation is conducted using the higher resolution data obtained from the available Google Earth database as a reference. For each available higher resolution data set, some subsets are selected to represent land cover class variability. Each subset location is set to size roughly 1000 by 750 pixels at the highest resolution possible. Before comparison of higher resolution data and Landsat classification, each subset is classified using maximum likelihood methods and then resample to 30m to mimic Landsat resolution. The maximum likelihood classifier is applied since the amount of reference data is insufficient to run a CVA.

The classified reference data is then compared to the land cover change analysis result (bitemporal and post classification) to assess the accuracy location by location. Each location accuracy assessment result is summarised into three subset groups: five subset locations are grouped into the 2001-2005 reference data (the group of reference data that acquired before Landsat acquisition); two subset locations are grouped into the 2007 reference data (the group of reference data that has coincidence with Landsat acquisition); and seven subset locations are grouped into the 2010 reference data (the group of reference data acquired after Landsat acquisition). Details of reference data acquisition is provided in Appendix 1B. The summary of the classification accuracy assessment result is listed in Table 4.10 and 4.11. Details of the error matrices are mentioned in Appendix 7.

Tables 4.10 and 4.11 show in general that post classification result is much better than bitemporal one. The overall accuracy of post classification is more than 50%, compare to less than 30% for bitemporal. Post classification shows increasing overall accuracy from 2001 to 2010 reference, while bitemporal depicts the opposite way. The forest class consistently has the highest accuracy compared to the others for post classification, while forest

and non-forest classes share the position of highest accuracy for bitemporal. For each class accuracy assessment, post classification provides 89.25% for the highest compare to 67.87% of bitemporal.

Table 4.10: *Summary of land cover change classification accuracies for post classification method (expressed in percentage)*

	2001-2005 References		2007 References		2010 References	
Class	**Producer's**	**User's**	**Producer's**	**User's**	**Producer's**	**User's**
Water	11.90	17.30	80.59	63.72	30.22	12.46
Non forest	33.24	38.76	19.63	63.12	26.20	69.00
Forest	65.73	79.01	89.25	62.95	80.61	82.77
Non vegetation	49.06	1.84	10.46	19.66	0.00	0.00
Overall accuracy	54.64		59.54		62.28	
Kappa	16.86		26.44		29.50	

Table 4.11: *Summary of land cover change classification accuracies for bitemporal method (expressed in percentage)*

	2001-2005 References		2007 References		2010 References	
Class	**Producer's**	**User's**	**Producer's**	**User's**	**Producer's**	**User's**
Water	0.71	0.16	1.25	18.37	0.00	0.00
Non forest	16.36	49.57	13.51	58.65	20.26	57.80
Forest	30.44	55.98	5.33	18.18	17.94	41.85
Non vegetation	2.04	0.03	67.87	13.77	0.00	0.00
Overall accuracy	25.30		16.24		18.08	
Kappa	-6.04		-6.41		-5.67	

4.2 Discussion

Cloud screening

The results of the cloud screening process showed that some technical problems appeared during data analysis. The problem in the cloud screening stage is exploring the best procedure to eliminate clouds. Based on this research, the best procedure to eliminate clouds is the multiple rules using the atmospherically corrected Landsat data and considering specific rules to

handle each type of cloud. The problems in multi-temporal image composition are the remotely sensed data quality, the existence of transmissive clouds (haze or cloud adjacency effect), the rules for the clear observations selection, and the efficiency analysis for multi-temporal image composition interval.

The problem for remotely sensed data quality is the missing data caused by the appearance of null values that typically appeared on Landsat 7 data. This condition appeared as a consequence of the SLC-off stripping problem of the Landsat 7 sensor where the scan line corrector (SLC) failed and made the stripped line happen after 2003. On ER Mapper software, the missing data ordinarily represented as a null value, by default is set as the highest digital number (Q = 255 of 8bit data). This problem must be handled with specific precautions to prevent misjudgement in multi-temporal composition. For example, the null value is set to the lowest digital number possible, say Q = 1. This selection of the lowest value possible intends to remove the masked cloud in image composition.

The next problem is the transmissive clouds that appeared adjacent to cloud objects but unable to be identified as cloud and named as the cloud adjacency effects. This value performs a similar trend to the land cover class that they obscured such as vegetation but it has a slightly higher value specifically at bands 1, 2 and 3. This problem is specifically discussed in the following cloud adjacency effect section.

Various rules have been explored to select the clear observation in the composition stage. The example rule that has essential features is the Normalised Difference Vegetation Index (NDVI) maximum-value composite (MVC). NDVI is renowned for differentiating vegetation from other objects such as water, cloud etc. This condition motivated us to apply NDVI as an algorithm for cloud elimination. The example is multiple rules without atmospheric correction (Rules no. 8 of Appendix 2A). The rules are designed

so that objects with highest NDVI values will be selected as the clearest observation (NDVI maximum value composite). Application of this formulation presumed that cloud and water (as well as cloud shadow) objects will have very low indices whereas vegetation objects have very high indices.

Experiments illustrated that this argument is true for cloud and water objects, but not true for the cloud shadow (Figure 4.15). Spectral signature of cloud shadow over vegetation depicts a similar pattern to the vegetation itself. Unfortunately, the NDVI value of vegetation under cloud shadow is higher than vegetation under the clear condition (Table 4.12, note the red highlight). The application of the Rule set no. 8, will select the area under shadow as "the clearest one" and present the shadowy area in the final image result. Figure 4.15 (a) illustrates the example of a cloudy area, (b) the clearer area and (c) the composition result using NDVI as the selection rules. Areas with red circle are the example of shadow region that was selected as the clearest coverage. This condition notices that using NDVI for cloud elimination must be treated with care.

Table 4.12: *Surface reflectance value (in percentage) of image depicts in Figure 4.15. Data shows that NDVI value of the object under cloud shadow is higher than forests (highlighted in red)*

Objects	Band1	Band2	Band3	Band4	Band5	Band6	Band7	NDVI
cloud	100.00	46.51	100.00	60.03	51.13	16.01	42.37	-0.2498
cloud-edge	25.65	27.70	27.89	45.70	36.43	16.55	27.67	0.2420
cloud-shadow	0.94	1.32	0.73	16.62	4.99	19.21	2.27	**0.9159**
forest	1.97	2.80	1.78	29.41	11.27	18.69	3.87	**0.8859**
estate crops	3.88	7.36	5.03	38.62	18.80	17.62	7.85	0.7695
bare land	3.34	4.89	5.09	21.35	23.38	23.86	15.87	0.6150

Cloud adjacency effect

The cloud adjacency effect is the real problem in cloud elimination procedure. The affected objects will have the spectral signature slightly raised above the normal value. For example, this effect appeared as the increasing of

vegetation spectral signature value at a similar intensity for all the bands. It made the differentiation effort more challenging because of spectral signature of the clear land cover is similar to that of the obscured land cover. One strategy that has been implemented is to calculate the difference of two successive observations (Formula 3.12), that presumed the higher difference refers to the possibility of haziness of one observation. This formulation needs some precautions such as the data need to be normalised to assure that the calculation is conducted on the same basis. Visual inspection depicts that Formula (3.12) succeeded to eliminate cloud adjacency effects to a certain extent (Figure 4.16). Some effects still persisted and need another strategy to handle. The failure of this strategy to suppress the whole cloud adjacency effect (Figure 4.16(a)) also influences the change detection result (Figure 4.16(b)).

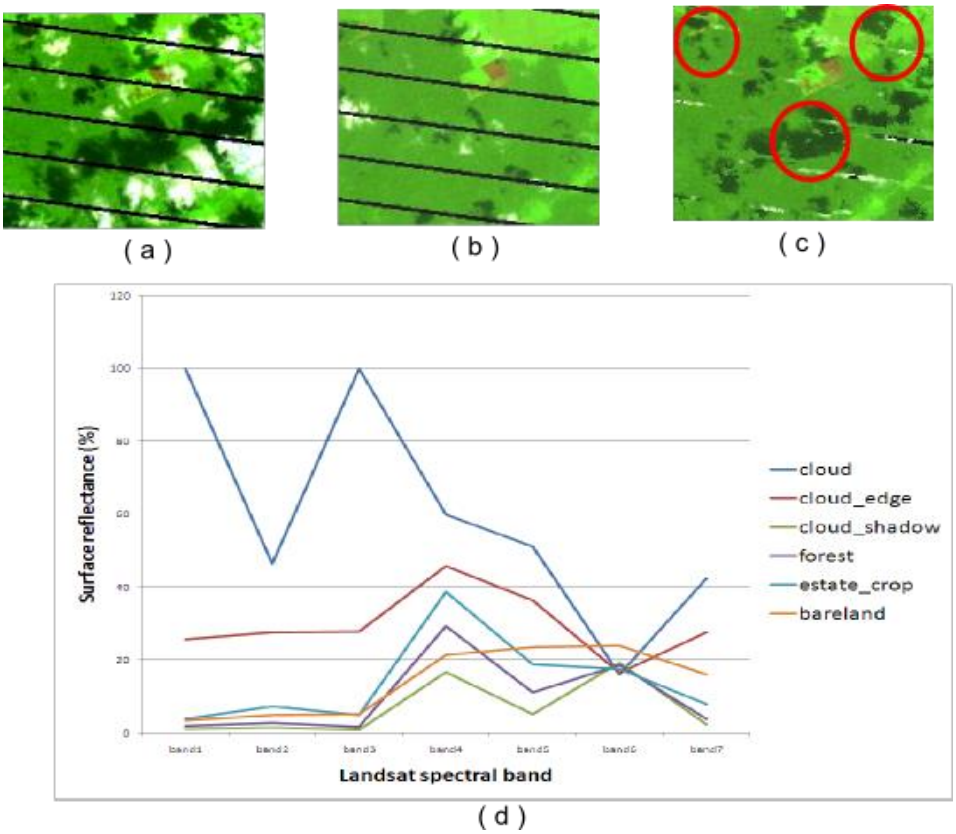

Figure 4.15: *Cloud elimination methods by using maximum value composite (MVC) of NDVI, (a) depicts the cloudy area of Landsat 7 path 127 row 59; (b) the clearer area; (c) the result using MVC of NDVI; (d) spectral graph selected objects includes cloud shadow. (c) illustrates that cloud shadows on (a) failed to be eliminated by (b) highlighted by red circles.*

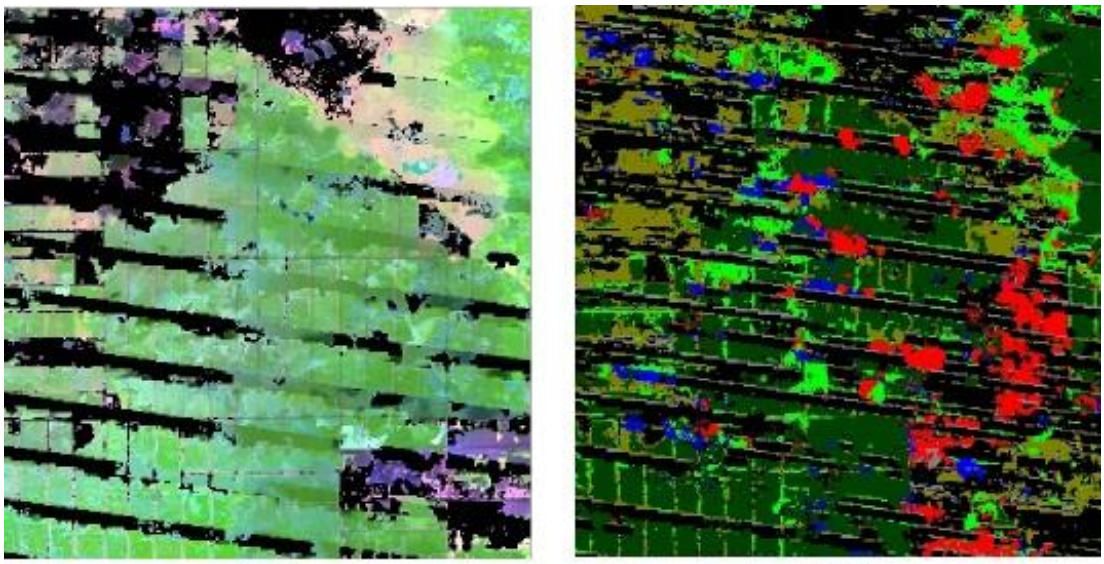

(a) (b)

Figure 4.16: *Cloud adjacency effect on Landsat 7 path 127 row 59 of 2007 (a) and change detection result (b). Although the rules are already modified, some of cloud adjacency effect still appears and disturb change detection analysis.*

Cloud removal efficiency, annually or biennially

The cloud removal method produced the “cloud free” image from compositing enormous image observations. For the location having higher cloud cover prevalence such as Landsat 5 path 103 row 63 and Landsat 7 path 127 row 59, composition of annual time range is not enough. Figure 4.11 and 4.12 justified that the composition for the annual time range still contained the persistent cloud cover remnant. The extension of the observational duration from annual to biennial proved that the amount of persistent cloud cover reduced to the lower intensity (Figure 4.13). The problem for the cloud elimination effort is the efficiency. For example we can examine Table 4.13 that illustrates the annual cloud removal result. Cloud elimination of Landsat 5 path 103 row 63 of 2007 observation provides 6.70% remaining cloud cover, while the 2008 observation provides 9.11% remaining cloud cover. The extension of annual into biennial data analysis gives reduction of the cloud remnant to 3.89%.

The other example in tables 4.14 to 4.16 depicted that the durational

extension gave no significant amelioration of cloud removal. If we focus on efficiency then the acceptable cloud cover threshold become the key. Laumonier (1996) explained that the 10% cloud cover level is still acceptable for land cover mapping purposes. The durational extension can be performed for biennial, triennial, quadrennial or even quinquennial time ranges without any warranty of zero cloud cover results. The durational extension also increasing the risk that the land cover changes is too much to compile into one single multi-temporal layer. The annual composition perhaps is the most efficient time range to date with considering cloud removal and the level of changes. The efficiency is possible to increase by obtaining more frequent observation using various available remotely sensed data.

Table 4.13: *Comparison of cloud covered and total pixels on Landsat data for each cloud removal sequence of path 103 row 063.*

Category	2007 only	2008 only	2007-2008
Total pixels	57,390,801	57,390,801	57,390,801
In image region pixels	42,373,140	39,898,787	43,473,410
Background pixels	15,017,661	17,492,014	13,917,391
Cloud covered pixels	2,839,744	3,633,197	1,693,027
Cloud covered pixels percentage	6.70%	9.11%	3.89%

Table 4.14: *Comparison of cloud covered and total pixels on Landsat data for each cloud removal sequence of path 114 row 066 in wet season.*

Category	2007 only	2008 only	2007-2008
Total pixels	88,154,452	54,859,641	54,859,641
In image region pixels	39,364,697	40,026,215	42,501,845
Background pixels	48,789,755	14,833,426	12,357,796
Cloud covered pixels	707,950	687,963	643,263
Cloud covered pixels percentage	1.80%	1.72%	1.51%

Table 4.15: *Comparison of cloud covered and total pixels on Landsat data for each cloud removal sequence of path 114 row 066 in dry season.*

Category	2007 only	2008 only	2007-2008
Total pixels	77,510,416	54,859,641	85,003,690
In image region pixels	42,194,646	40,415,515	42,501,845
Background pixels	35,315,770	14,444,126	12,357,796
Cloud covered pixels	1,388,006	1,716,666	1,305,016
Cloud covered pixels percentage	3.29%	4.25%	3.07%

Table 4.16: *Comparison of cloud covered and total pixels on Landsat data for each cloud removal sequence of path 127 row 059.*

Category	2007 only	2008 only	2007-2008
Total pixels	57,201,161	55,187,891	57,201,161
In image region pixels	40,493,336	40,460,058	40,492,601
Background pixels	16,707,825	14,727,833	16,708,560
Cloud covered pixels	3,073,751	4,467,230	1,583,775
Cloud covered pixels percentage	7.59%	11.04%	3.91%

Change detection

Post classification methods were applied to the 2007 and 2008 sequences independently. The results of both sequences were then composited and the changes were calculated. In contrast, the bitemporal method classifies the change and unchanged class in one stage. Problems usually occur on objects that show gradual change. There are trends to give this gradual change the different labels for different locations. The complexity on defining the training samples then correlates to a lower accuracy of the bitemporal method. If we compare these two methods, post classification is easier to apply and has a better capability to deal with the cloud adjacency effect. On the other hand, the bitemporal method, due to its complexity, needs a higher quality of imagery to process.

This chapter has elaborated the results of the atmospheric correction quality assessment, the cloud screening process and the change detection. Some problems were found in cloud screening such as the cloud adjacency effects, the need of rules modification over the different location and defining the most efficient interval for cloud screening. These problems made distortion in the clear image product such as the hazy part of image. The distortion then reduced the accuracy of the change detection process. The following chapter will summarise the research and define what future work is needed.

Chapter 5

Conclusions and Future work

This chapter summarises the research and also mentions what conditions have been found in this research that need more experiments in future work.

5.1 Conclusions

Land cover change monitoring has been conducted by using various platforms, methods and area of interests. Diverse types of platform have been used for monitoring, from the coarser resolution satellite such as NOAA-AVHRR or MODIS to the most detailed ones such as IKONOS and QuickBird. Various methods have been proposed by researchers to identify changes, from the simple analysis such as image algebra to the more complex methods such as the biophysical parameter method. The area of interests may cover globally, specific continent only or even some urban location (Skole et al., 1997; Lu et al., 2004; Herold et al., 2005).

Land cover change monitoring in tropical areas such as Indonesia is having problems with data availability, data quality and cloud cover. Data availability and quality are substantial issue for the older period when remote sensing data such as aerial photography is available in limited number and coverage. Nowadays, various remote sensing data has provided regularly and acquired by a number of platform, but cloud cover remains a significant problem. Some strategies have been initiated to cope with the problem, such as using radar data with penetrating cloud capability or using more frequent observations. The system complexity and technical issues of those strategies hamper the implementation process.

This research focussed on two main objectives: (i) to obtain 'clear sky' pictures and (ii) to extract land cover change information for those pictures. The first objective dealt with the cloud cover problem exploring various rules. The second objective focussed on the comparison of the changed detection technique from the 'clear sky' picture obtained.

Most of the available pre processing procedures have been carried out by the United States Geological Survey (USGS) except the atmospheric corrections that are undertaken using NASA's Landsat Ecosystem Disturbance Adaptive Processing System (LEDAPS) pre processing tools. Assessment of the atmospheric correction quality was conducted by comparison of the Landsat data to the Hymap data which has been calibrated by ground based measurement. The root mean square difference between Hymap and Landsat is less than 1% (both image are clear) and still less than 2.5% if one or both image are cloudy. The highest difference is on band 4 then followed by band 5 if the location is predominated by higher vegetation. On the other hand, the highest difference shifts to band 5 followed by band 4 if the location is predominated by lower vegetation or bare ground.

The cloud screening stage aims to eliminate cloud cover using multi-temporal observation. Firstly, land cover is categorised to the clear, cloud obscured, and transmissive cloud obscured land observation using a number of rules. Secondly, the cloud obscured land observation is effectively identified and set as missing data for replacing by other clear observations using various rules for multi-temporal composition. This effort succeeded to reduce the amount of cloud covered area although persistent cloud remains to be seen. The problem occurs when selecting the clear land observation from transmissive cloud obscured land observations (hazy land cover). Transmissive cloud has a similar spectral signature to clear land observation and this makes it difficult to select the real clear one. The rules were developed to deal with the issue. The most successful rule is calculating the difference of both observations.

The surface reflectance difference more than 0.01 is considered hazy and then select the darker one as the clearer observation. This rule succeeded to eliminate most of the issue while some haze remains. The remaining persistent cloud indicates the need to extend the observation time frame or to obtain more frequent acquisition, while the remaining haze indicates the need to modify the rule.

The cloud screening experiment uses Landsat 5 path 103 row 63 as the initial location. The best rule of the initial location is then implemented on two different locations, Landsat 5 path 114 row 66 and Landsat 7 path 127 row 59. Implementation on path 114 row 66 with less cloud prevalence and the existence of deciduous forest requires some modification to the rules, while the implementation on path 127 row 59 requires no modification. Cloud screening on path 114 row 66 must be conducted for the dry and rainy seasons separately.

The cloud screening experiment was conducted on annual and biennial time frames. Annual cloud screening succeeded to reduce cloud cover to the level of 1.72% to 11.04%. The time extension to biennial time frame succeeded to reduce cloud cover to the level 1.51% to 3.91%. This experiment depicts that time frame extension succeeded to reduce cloud cover level without any assurance that cloud the cover level becomes zero.

Land cover change analysis was conducted by two different methods, the bitemporal and post classifications. The bitemporal method based the calculation from statistical difference of two observations that have been concatenated into one file. The post classification method based the analysis on calculating the difference of the class code of two observations on a pixel by pixel basis, where each observation was classified before the comparison. Although, both methods share the same data source and as much as possible used the same training area, the result is different. The post classification method obtained an overall accuracy more than 50% and

positive Kappa, whereas the bitemporal method obtained less than 30% overall accuracy and negative Kappa. Because the bitemporal method conducts change detection in one way, it needs more accuracy in training area selection. The other aspect that contributes to the lower accuracy of both methods is that the image sources are not really clear. It will affect the bitemporal methods calculation more severely because it considers both observations are in the one image whatever the conditions.

5.2 Future work

The conclusion section confirms that cloud identification is relatively successful for cloud screening purposes. But some problems remain such as the selection of hazy land cover over the clear land cover. This condition becomes a problem when the clear images are substituted by the hazy images in the composition process. This condition is still acceptable in the worst scenario, when there is no other option than the hazy one to fill the missing data. But this research found that sometimes the hazy land cover supersedes the clear land cover. The problem happens because the rules for image composition are less sensitive to haze or the cloud adjacency effect. Then the problem is how to modify the rules so that they are more sensitive to the cloud adjacency effects. The modified rules should be better to eliminate the hazy land cover (that is spectrally very difficult to distinguish from the clear land cover) in the multi-temporal composition process, except when it is the only option available. The other problem is persistent cloud that remains to be seen. Cloud screening has been extended to a biennial time frame, but the persistent cloud remains. Experiments using triennial, quadrennial or a longer time frame or more frequent data acquisition could prove the best or the most efficient time frame or time interval for cloud screening.

References

Ackerman, S. A., K. I. Strabala, W. P. Menzel, R. A. Frey, C. C. Moeller, and L. E. Gumley. 1998. Discriminating clear sky from clouds with MODIS. *J. Geophys. Res.* 103 (D24): 32141-32157.

Anderson, J. R., E. E. Hardy, J. T. Roach, and R. E. Witmer. 1976. A land use and land cover classification system for use with remote sensor data, edited by U.S. Geological Survey. Washington DC. US Government Printing Office.

Arriaza, J. A. T., F. G. Rojas, M. P. López, and M. Cantón. 2003. An automatic cloud-masking system using backpro neural nets for AVHRR scenes. *IEEE T. Geosci. Remote Sensing* 41 (4): 826-831.

Asner, G. P. 2001. Cloud cover in Landsat observations of the Brazilian Amazon. *Int. J. Remote Sensing* 22 (18): 3855-3862.

Atmadilaga, A. H., and Sarhini. 2010. Updating Land Resource Map as Response to the Sustainable National Development Issues in Indonesia. In *XXIV FIG Congress*. Sydney, NSW, AU.

Bogaert, J., R. Ceulemans, and D. Salvador-van Eysenrode. 2004. Decision tree algorithm for detection of spatial processes in landscape transformation. *Environ. Manage.* 33 (1): 62-73.

Broich, M., M. C. Hansen, P. Potapov, B. Adusei, E. Lindquist, and S. V. Stehman. 2011. Time-series analysis of multi-resolution optical imagery for quantifying forest cover loss in Sumatra and Kalimantan, Indonesia. *Int. J. Appl. Earth Obs. Geoinf.* 13: 277-291.

Campbell, N.A., and W.R. Atchley. 1981. The Geometry of Canonical Variate Analysis. *Syst. Zool.* 30 (3): 268-280.

Campbell, N., and H. T. Kiiveri. 1993. Canonical Variate Analysis with Spatially-Correlated Data. *Aust. J. Stat.* 35 (3): 333-344.

Chander, G., B. Markham, and D. L. Helder. 2009. Summary of current radiometric calibration coefficients for Landsat MSS, TM, ETM+, and EO-1 ALI sensors. *Remote Sensing Environ.* 113: 893-903.

Coakley, J. A., Jr., and F. P. Bretherton. 1982. Cloud cover from high-

resolution scanner data: Detecting and allowing for partially filled fields of view. *J. Geophys. Res.* 87 (C7): 4917-4932.

Cocks, T. D., R. Jenssen, A. Stewart, I. WIlson, and T. Shields. 1998. The Hymap^{TM} Airborne Hyperspectral Sensor: The System, Calibration and Performance. In *First EARSeL workshop on imaging spectroscopy*. Zurich, Switzerland.

Collings, S., Caccetta, P., 2011, On the Generation of broad-scale hyperspectral ground reflectance mosaics from aerial and ground-based observations. *Int. J. of Image and Data Fusion*. 2 (3): 237-253.

Dal Moro, G., and L. Halounova. 2007. Haze removal for high-resolution satellite data: a case study. *Int. J. Remote Sensing* 28 (10): 2187-2205.

(Dephut), Departemen Kehutanan. 2001. Statistik Kehutanan Indonesia 2001.http://www.dephut.go.id/INFORMASI/STATISTIK/2001/Statistik2001.htm. (accessed 20 Jul 2011)

(Dephut), Departemen Kehutanan 2008a. *Rekalkulasi penutupan lahan Indonesia tahun 2008*. Jakarta: Departemen Kehutanan.

(Dephut), Departemen Kehutanan 2008b. *Peta penghitungan deforestasi Indonesia tahun 2008*. Jakarta: Departemen Kehutanan.

(Dephut), Departemen Kehutanan. 2008c. *Pemantauan sumberdaya hutan*. Jakarta, ID: Departemen Kehutanan.

DigitalGlobe, I. 2011. The DigitalGlobe Constellation. http://www.digitalglobe.com/index.php/82/Content+Collection+Systems. (accessed 4 Jul 2011).

Di Gregorio, A. 2005. *Land cover classification system. Classification concepts and user manual. Software version 2*. Roma: FAO.

Erasmi, S., A. Twele, M. Ardianszah, A. Malik, and M. Kappas. 2004. Mapping Deforestation and Land Cover Conversion at the Rainforest Margin in Central Sulawesi, Indonesia. In *EARSeL eProceedings*. EARSeL.

(ESRI), Environmental Systems Research Institute Inc. 2006. *World Countries*. Redlands, CA, US: ESRI Shapefile.

Eurimage. 2010. Eurimage price list. http://www.eurimage.com/_products/docs/eurimage_price_list.pdf. (accessed 27 Jun 2011).

Fallah-adl, H., J. Jájá, S. Liang, Y. J. Kaufman, and J. R. G. Townshend.

1995. *Efficient Algorithms for Atmospheric Correction of Remotely Sensed Data.* In *1995 ACM/IEEE Conference on Supercomputing*

Feranec, J., G. W. Hazeu, S. Christensen, and G. Jaffrain. 2007. Corine land cover change detection in Europe (case studies of the Netherlands and Slovakia). *Land Use Policy* 24: 234-247.

Furby, S.L., and N. Campbell. 2001. Calibrating images from different dates to 'like-value' digital counts. *Remote Sensing Environ.* 77: 186-196

Gastellu-Etchegorry, J.-P. 1988. Monthly probabilities for acquiring remote sensed data of Indonesia with cloud cover less than 10, 20, and 30 percent. *Indonesian Journal of Geography* 18 (55): 11-28.

GeoEye, I. 2011. Imagery Sources. http://www.geoeye.com/CorpSite/products-and-services/imagery-sources/. (accessed 4 Jul 2011).

Goodman, A. H., and A. Henderson-Sellers. 1988. Cloud detection and analysis: A review of recent progress. *Atmos. Res.* 21: 203-228.

Google, Inc. 2011. Google Earth v.6.0. Available from http://earth.google.com (accessed 5 Jul 2011).

Hansen, K. 2009. Earth-observing Landsat 5 turns 25. *NASA News and Features*, http://www.nasa.gov/topics/earth/features/landsat_bday.html. (accessed 18 Apr 2011).

Hansen, M. C., R. S. DeFries, C. Dimiceli, C. Huang, R. Sohlberg, X. Zhan, and J. R. G. Townshend. 1998. Red and infrared space partitioning for detecting land cover change. In *1998 International Geoscience and Remote Sensing Symposium*. IEEE.

Hansen, M. C., Y. E. Shimabukuro, P. Potapov, and K. Pittman. 2008a. Comparing annual MODIS and PRODES forest cover change data for advancing monitoring of Brazilian forest cover. *Remote Sensing Environ.* 112 (10): 3784-3793.

Hansen, M. C., D. P. Roy, E. Lindquist, B. Adusei, C. O. Justice, and A. Altstatt. 2008b. A method for integrating MODIS and Landsat data for systematic monitoring of forest cover and change in the Congo Basin. *Remote Sensing Environ.* 112 (5): 2495-2513.

Hansen, M. C., S. V. Stehman, P. V. Potapov, T. R. Loveland, J. R. G. Townshend, R. S. DeFries, K. W. Pittman, B. Arunarwati, F. Stolle, M. K. Steininger, M. L. Caroll, and C. Dimiceli. 2008c. Humid tropical forest clearing from 2000 to 2005 quantified by using multitemporal and multiresolution remotely sensed data. *P. Natl. Acad. Sci. USA* 105 (27): 9439-9444.

Hansen, M. C., S. V. Stehman, and P. V. Potapov. 2010. Quantification of global gross forest cover loss. *P. Natl. Acad. Sci. USA* 107 (19): 8651-8656.

He, X. Y., J. B. Hu, W. Chen, and X. Y. Li. 2010. Haze removal based on advanced haze- optimized transformation (AHOT) for multispectral imagery. *Int. J. Remote Sensing* 31 (20): 5331-5348.

Herold, M., H. Couclelis, and K. C. Clarke. 2005. The role of spatial metrics in the analysis and modeling of urban land use change. *Comput. Environ. Urban* 29: 369-399.

Herold, M. 2009. *Assessment of the status of the development of the standards for the terrestrial climate variables. T9. Land*. Roma: GTOS.

Hoekman, D. H. 1999. Monitoring tropical forests using Synthetic Aperture Radar In *International MOFEC-Tropenbos and NWO Workshop. The balance between biodiversity conservation and sustainable use of tropical rain forests*. Balikpapan, ID. Tropenbos.

Holben, B. N. 1986. Characteristics of maximum-value composite images from temporal AVHRR data. *Int. J. Remote Sensing* 7 (11): 1417-1434.

Huang, C., N. Thomas, S. N. Goward, J. G. Masek, Z.-L. Zhu, J. R. G. Townshend, and J. E. Vogelmann. 2010. Automated masking of cloud and cloud shadow for forest change analysis using Landsat images. *Int. J. Remote Sensing* 31 (20): 5449-5464.

Ikawati, Y., and D. R. Setiawati. 2009. *Survei dan Pemetaan Nusantara*. Cibinong, ID: Bakosurtanal.

Irish, R. R., J. L. Barker, S. N. Goward, and T. Arvidson. 2006. Characterization of the Landsat-7 ETM+ Automated Cloud cover Assessment (ACCA) Algorithm. *Photog. Eng. Remote Sensing* 72 (10): 1179-1188.

Justice, C. O., J. R. G. Townshend, B. N. Holben, and C. J. Tucker. 1985. Analysis of the phenology of global vegetation using meteorological satellite data. *Int. J. Remote Sensing* 6 (8): 1271-1318.

Koren, I., L. A. Remer, Y. J. Kaufman, Y. Rudich, and J. V. Martins. 2007. On the twilight zone between clouds and aerosols. *Geophys. Res. Lett.* 34 (L08805): 5p.

Laumonier, Y. 1996. *The vegetation and physiography of Sumatera*. Vol. 22,

Geobotany. Dordrecht, NL: Kluwer Academic Publisher.

Lavreau, J. 1991. De-hazing Landsat Thematic Mapper Images. *Photog. Eng. Remote Sensing* 57 (10): 1297-1302.

Leimgruber, P., D. S. Kelly, M. K. Steininger, J. Brunner, T. Müller, and M. Songer. 2005. Forest cover change patterns in Myanmar (Burma) 1990-2000. *Environ. Conserv.* 32 (4): 356-364.

Lepers, E., E. F. Lambin, A. C. Janetos, R. S. DeFries, F. Achard, N. Ramankutty, and R. J. Scholes. 2005. A Synthesis of Information on Rapid Land-cover Change for the Period 1981–2000. *BioScience* 55 (2): 115-124.

Li, M., S. C. Liew, and L. K. Kwoh. 2002. Generating “cloud free” and “cloud-shadow free” mosaic for SPOT Panchromatic images. In *2002 International Geoscience and Remote Sensing Symposium*. IEEE.

Li, M., S. C. Liew, and L. K. Kwoh. 2003. Producing cloud free and cloud-shadow free mosaic from cloudy IKONOS images. In *2003 International Geoscience and Remote Sensing Symposium*. IEEE.

Lu, D., P. W. Mausel, E. S. Brondízio, and E. F. Moran. 2004. Change detection techniques. *Int. J. Remote Sensing* 25 (12): 2365-2407.

Luo, Y., A. P. Trishchenko, and K. V. Khlopenkov. 2008. Developing clear-sky, cloud and cloud shadow mask for producing clear-sky composites at 250-meter spatial resolution for the seven MODIS land bands over Canada and North America. *Remote Sensing Environ.* 112 (12): 4167-4185.

Lyapustin, A. I., and Y. J. Kaufman. 2001. Role of adjacency effect in the remote sensing of aerosol. *J. Geophys. Res.* 106 (D11): 11909-11916.

Ma, J., X. Gu, C. Feng, and J. Guo. 2005. Study of thin cloud removal method for CBERS-02 image. *Sci. China Ser. E Eng. Mat.* 48 (Supp I): 91-99.

Maalouf, A., P. Carré, B. Augereau, and C. Fernandez-Maloigne. 2009. A bandelet-based inpainting technique for clouds removall from remotely sensed images. *IEEE T. Geosci. Remote Sensing* 47 (7): 2363-2371.

Malberg, H. 1973. Comparison of mean cloud cover obtained By satellite photographs and ground-based observations over Europe and the Atlantic. *Mon. Weather Rev.* 101 (12): 893-900.

Malingreau, J.-P., C. J. Tucker, and N. Laporte. 1989. AVHRR for monitoring global tropical deforestation. *Int. J. Remote Sensing* 10 (4-5): 855-867.

Malila, W. A. 1980. Change Vector Analysis: An Approach for Detecting Forest Changes with Landsat. In *LARS Symposia*. The Laboratory for Applications of Remote Sensing.

Marshak, A. L., G. Wen, J. A. Coakley, Jr., L. A. Remer, N. G. Loeb, and R. F. Cahalan. 2008. A simple model for the cloud adjacency effect and the apparent bluing of aerosols near clouds. *J. Geophys. Res.* 113 (D14S17): 7p.

Masek, J. G., E. F. Vermote, N. E. Saleous, R. E. Wolfe, F. G. Hall, K. F. Huemmrich, F. Gao, J. Kutler, and T.-K. Lim. 2006. A Landsat Surface Reflectance Dataset for North America, 1990–2000. *IEEE Geosci. Remote Sensing Lett.* 3 (1): 68-72.

Mecham, M. 2008. GeoEye-1 Expands NGA Image Base. *Aviat. Week Space Tech.* 169 (10): 36-37.

МЕТЕОДАННЫЕ, Р. Т. 2011. Meteodata of Republic of Indonesia. http://indonesia-meteo.ru/en/. (accessed 1 Jul 2011)

Mitchell, O. R., and P. L. Chen. 1976. Filtering to remove cloud cover in satellite imagery. In *Symposium on Machine Processing of Remotely Sensed Data*. West Lafayette, Indiana, USA. The Institute of Electrical and Electronics Engineers, Inc.

Monk, K. A., Y. De Fretes, and G. R. Lilley. 2000. *Ekologi Nusa Tenggara dan Maluku*. Vol. Buku V, *Seri Ekologi Indonesia*. Jakarta: Prenhallindo.

(NASA), National Aeronautics and Space Administration 2011. Landsat 7 Science Data Users Handbook. http://landsathandbook.gsfc.nasa.gov/ pdfs/Landsat7_Handbook.pdf. (accessed 6 Apr 2011)

Nugroho, M. 2006. Integration of multi remotely sensed data and geodatabases for forestry management in Indonesia. Dissertation, Bodemnatuurkunde, Ecohydrologie en het Grondwaterbeheer, Wageningen Universiteit, Wageningen, NL

Panta, M., K. Kim, and C. Joshi. 2008. Temporal mapping of deforestation and forest degradation in Nepal: Applications to forest conservation. *Forest Ecol. Manag.* 256 (9): 1587-1595.

Perera, K., and K. Tsuchiya. 2009. Experiment for mapping land cover and it's change in southeastern Sri Lanka utilizing 250 m resolution MODIS imageries. *Adv. Space Res.* 43 (9): 1349-1355.

Poniman, A., Nurwadjedi, and P. Lumban-Tobing. 2004. Developing the National Land Resource Database for Supporting Spatial Land Use Planning. In *3rd FIG Regional Conference*. Jakarta, ID.

Prakoso, K. U. 2006. Tropical forest mapping using polarimetric and interferometric SAR data. Dissertation, Bodemnatuurkunde, Ecohydrologie en het Grondwaterbeheer, Wageningen Universiteit, Wageningen, NL.

Purwanto, J. 2011. *personal communication on 23 Aug 2011*

Quarmby, N. A., J. R. G. Townshend, and J. L. Cushnie. 1988. *Monitoring urban land cover changes at the fringe from SPOT HRV imagery in south-east England*. FR: CNES.

Reynolds, R., J. C. Hammond, F. Smith, and S. Tempest. 2008. *Weather*. Edited by D. John, R. S. Colson, K. Simkins and C. Martin, *Eyewitness Companions*. London, UK: Dorling Kindersley.

Richter, R. 1996. Atmospheric correction of satellite data with haze removal including a haze/clear transition region. *Comput. Geosci.* 22 (6): 675-681.

Richter, R., and A. Müller. 2005. De-shadowing of satellite/airborne imagery. *Int. J. Remote Sensing* 26 (15): 3137-3148.

Shepard, J. R. 1964. A concept of change detection. *Photog. Eng.* 30: 648-651.

Shu, J. S.-P., and H. Freeman. 1990. Cloud shadow removal from aerial photographs. *Pattern Recogn.* 23 (6): 647-656.

Skole, D. L., C. O. Justice, J. R. G. Townshend, and A. C. Janetos. 1997. A land cover change monitoring program: Strategy for an international effort. *Mitig. Adapt. Strat. Global Chg.* 2: 157-175.

Song, C., C. E. Woodcock, K. C. Seto, M. Pax-Lenney, and S. A. Macomber. 2001. Classification and Change Detection Using Landsat TM Data: When and How to Correct Atmospheric Effects? *Remote Sensing Environ.* 75: 230-244.

Stow, D. A., D. Collins, and D. McKinsey. 1990. Land use change detection based on multi-date imagery from different satellite sensor systems. *Geocarto Int.* 5 (3): 3-12.

SPOTImage. 2010. SPOT satellite technical data. http://www.spotimage.com/automne_modules_files/standard/public/p229_a48f99c03cb2bc

7f6beb7acc41f29fffSpotSatelliteTechnicalData_EN_Sept2010.pdf. (accessed 4 Jul 2011)

Strahler, A. H., A. Moody, and E. F. Lambin. 1995. Land cover and land-cover change from MODIS. In *1995 International Geoscience and Remote Sensing Symposium. 'Quantitative Remote Sensing for Science and Applications'*.

Sugardiman, R. A. 2007. Spaceborne radar monitoring of forest fires and forest cover change. Dissertation, Wageningen Universiteit, Wageningen, NL

Tokuno, M., and K. Tsuchiya. 1994. Classification of cloud types based on data of multiple satellite sensors. *Adv. Space Res.* 14 (3): 199-206.

Tseng, D.-C., H.-T. Tseng, and C.-L. Chien. 2008. Automatic cloud removal from multi-temporal SPOT images. *Appl. Math. Comput.* 205 (2): 584-600.

Townshend, J. R. G., C. O. Justice, C. M. Gurney, and J. McManus. 1992. The impact of misregistration on change detection. *IEEE T. Geosci. Remote Sensing* 30 (5): 1054-1060.

Tucker, C. J., J. A. Gatlin, and S. R. Schneider. 1984. Monitoring vegetation in the Nile Delta with NOAA-6 and NOAA-7 AVHRR imagery. *Photog. Eng. Remote Sensing* 50 (1): 53-61.

(USGS), United States Geological Survey. 2010a. State of the Archive Web. http://landsat.usgs.gov/documents/StateOfTheArchive_web.pdf. (accessed 10 Mar 2011)

(USGS), United States Geological Survey. 2010b. WRS-2 Path/Row Shapefile. http://landsat.usgs.gov/tools_wrs-2_shapefile.php. (accessed 11 Apr 2011)

(USGS), United States Geological Survey. 2010c. Landsat processing details. http://landsat.usgs.gov/Landsat_Processing_Details.php. (accessed 22 Mar 2011)

(USGS), United States Geological Survey. 2010d. Frequently asked questions about the Landsat Missions. What are the descriptions for the levels of processing?, http://landsat.usgs.gov/descriptions_for_the_levels_of_processing.php. (accessed 18 Apr 2011).

van Steenis, C. G. G. J. 1935. Maleische vegetatieschetsen. Toelichting bij de plantengeographische kaart van Nederlandsch Oost-Indië. *Tijdscr. Kon. Ned. Aardr. Gen.* 52 (2): 25-67.

van Steenis, C. G. G. J. 1958. *Vegetation Map of Malaysia*. UNESCO.

Verchot, L. V., R. Zomer, O. van Straaten, and B. Muys. 2007. Implications of country-level decisions on the specification of crown cover in the definition of forests for land area eligible for afforestation and reforestation activities in the CDM. *Climatic Change* 81: 415-430.

Vermote, E. F., N. Z. El Saleous, C. O. Justice, Y. J. Kaufman, J. L. Privette, L. Remer, J.-C. Roger, and D. Tanré. 1997. Atmospheric correction of visible to middle-infrared EOS-MODIS data over land surfaces: Background, operational algorithm and validation. *J. Geophys. Res.* 102 (D14): 17131-17141.

Vitousek, P. M., H. A. Mooney, J. Lubchenco, and J. M. Melillo. 1997. Human Domination of Earth's Ecosystems. *Science* 277: 494-499

Warner, J. X., J. C. Gille, D. P. Edwards, D. C. Ziskin, M. W. Smith, P. L. Bailey, and L. Rokke. 2001. Cloud detection and clearing for the Earth Observing System Terra satellite Measurement of Pollution in the Troposphere (MOPITT) experiment. *Applied Optics* 40 (8): 1269-1284.

Weismiller, R. A., S. J. Kristof, D. Scholz, P. E. Anuta, and S. A. Momin. 1977. Change Detection in Coastal Zone Environments. *Photog. Eng. Remote Sensing* 43 (12): 1533-1539.

Westman, W. E., L. L. Strong, and B. A. Wilcox. 1989. Tropical deforestation and species endangerment: the role of remote sensing. *Landcape Ecology* 3 (2): 97-109.

Whitmore, T. C. 1984. A vegetation map of Malesia 1:5 million. *J. Biogeogr.* 11 (6): 461-471.

Woodcock, C. E., R. Allen, M. Anderson, A. S. Belward, R. A. Bindschadler, W. B. Cohen, F. Gao, S. N. Goward, D. L. Helder, E. Helmer, R. R. Nemani, L. Oreopoulos, J. Schoot, P. S. Thenkabail, E. F. Vermote, J. Vogelmann, M. A. Wulder, and R. H. Wynne. 2008. Free Access to Landsat Imagery. *Science* 230: 1011.

Every reasonable effort has been made to acknowledge the owners of copyright material. I would be pleased to hear from any copyright owner who has been omitted of incorrectly acknowledged.

Appendix 1

Remote sensing observation dates

A. Landsat observation dates.

For path 114 row 066, (d) represents dry season and (w) represents wet season data.

No	Landsat 5 Path 103 Row 063	Landsat 5 Path 114 Row 066	Landsat 7 Path 127 Row 059
		2007	
1	8 Jan 2007	5 Jan 2007 (d)	24 Jan 2007
2	13 Mar 2007	21 Jan 2007 (w)	9 Feb 2007
3	29 Mar 2007	6 Feb 2007 (w)	13 Mar 2007
4	14 Apr 2007	10 Mar 2007 (w)	14 Apr 2007
5	16 May 2007	26 Mar 2007 (w)	1 Jun 2007
6	17 Jun 2007	11 Apr 2007 (w)	3 Jul 2007
7	19 Jul 2007	27 Apr 2007 (w)	19 Jul 2007
8	21 Sep 2007	13 May 2007 (w)	5 Sep 2007
9	-	14 Jun 2007 (w)	24 Nov 2007
10	-	16 Jul 2007 (d)	-
11	-	1 Aug 2007 (d)	-
12	-	17 Aug 2007 (d)	-
13	-	2 Sep 2007 (d)	-
14	-	18 Sep 2007 (d)	-
15	-	4 Oct 2007 (d)	-

No	Landsat 5 Path 103 Row 063	Landsat 5 Path 114 Row 066	Landsat 7 Path 127 Row 059
		2008	
1	11 Jan 2008	25 Feb 2008 (w)	27 Jan 2008
2	27 Jan 2008	12 Mar 2008 (w)	16 Apr 2008
3	15 Mar 2008	13 Apr 2008 (w)	18 May 2008
4	31 Mar 2008	29 Apr 2008 (w)	19 Jun 2008
5	18 May 2008	15 May 2008 (w)	5 Jul 2008
6	9 Oct 2008	31 May 2008 (w)	25 Oct 2008
7	12 Dec 2008	16 Jun 2008 (d)	28 Dec 2008
8	-	2 Jul 2008 (d)	-
9	-	18 Jul 2008 (d)	-
10	-	3 Aug 2008 (d)	-
11	-	4 Sep 2008 (d)	-
12	-	20 Sep 2008 (d)	-
13	-	6 Oct 2008 (d)	-
14	-	22 Oct 2008 (d)	-
15	-	25 Dec 2008 (w)	-

B. Remote sensing reference data observation dates

Reference data for validation purposes is obtained through Google Earth(R). It consists of selected locations from the available high-resolution data that covers the area within Landsat's path 127 row 59 coverages. The selection is attempted to represent classification result variabilities. The Google Earth itself does not mention the specification of each data set but mentions its provider. Each location can consist of one to four subsets to find the clearest possible and cover various objects but keep its size small. These locations are grouped into three categories: the first, location number 1, 2, 3, and 4 acquired in 2001-2005 (prior to Landsat acquisition), the second, location number 5 acquired in 2007 (coincident to Landsat acquisition) and the third, location number 6 and 7 acquired in 2010 (after Landsat acquisition). Some location numbers are missing in the list because it has a problem on processing and is dropped as a reference. Specification of data of each provider is mentioned in Tables 3.3 to 3.5.

No	Location	Dates	Provider
1	Rokan	24 Jun 2005	DigitalGlobe
2	Kunto	17 Sep 2005	DigitalGlobe
3	Dumai	18 Jul 2001	GeoEye
4	Pasir 4 & 5	2 Des 2001	GeoEye
5	Siak 1 & 2	31 Jan 2007	GeoEye
6	Pasir 1, 2, & 3	9 Feb 2010	GeoEye
7	Rupat 2, 3, 5 & 6	9 Feb 2010	GeoEye

Appendix 2

The applied rules for cloud identification and multi-temporal image composition.

A. The applied rules for Landsat without atmospheric correction

Remarks: Qi represent raw digital number for band i, where i: 1, 2, …, 7 and its value range from 0 - 255; Qa and Qb represent raw digital number for on and after observation respectively; NDVI stands for Normalised Difference Vegetation Index (Formula 3.5); NDVIa and NDVIb represent NDVI value for prior to and posterior to observation respectively; and these rules assume that cloud as a single entity

No	Cloud masking rules	Image composition rules	Drawbacks
1	$\left(\frac{Q_5}{Q_1}\right)<1.3$ and $\left(\frac{Q_5}{Q_4}\right)<2.5$ and $\left(\frac{Q_5}{Q_6}\right)>0.4$ and $Q_1>7$	Formula 3.8	Bare land disappeared
2	$\left(\frac{Q_1+Q_4+Q_5}{Q_6}\right)>1$	Formula 3.8	Snow disappeared
3	$\left(\frac{Q_1+Q_4+Q_5}{Q_6}\right)>1.7$ and $Q_6>35$ and $\left(\frac{Q_5}{Q_4}\right)<1.7$	Formula 3.8	Grey cloud remained
4	$\left(\frac{Q_1+Q_4+Q_5}{Q_6}\right)>1.7$ and $Q_6>35$ and $\left(\frac{Q_5}{Q_4}\right)<1.7$ and $\left(\frac{Q_4}{Q_6}\right)<0.7$	Formula 3.8	Snow disappeared grey cloud remained

No	Cloud masking rules	Image composition rules	Drawbacks
5	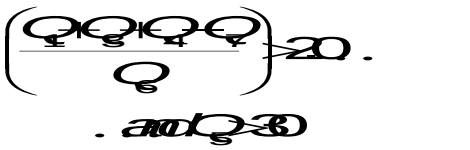	Formula 3.8	Grey cloud remained
6	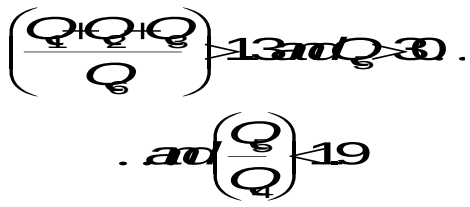	Formula 3.8	Snow & bare land disappeared Grey cloud remained
7	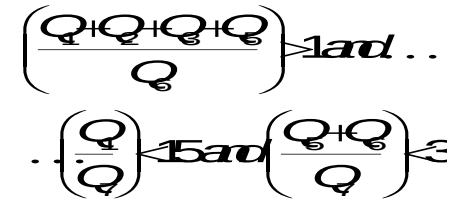	Formula 3.8	Grey cloud remained
8		Iterate formula for other sequence	Snow & bare land disappeared
9	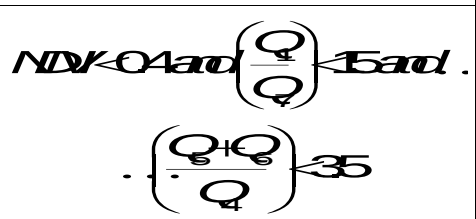	Formula 3.8	Snow & bare land disappeared

B. The applied rules for Landsat data with atmospheric correction

Formula 1 and 2 assume cloud as single feature. Formula 3 to 5 assume cloud as multiple features for which each line of rule represents each type of cloud. (tc) stands for top bright cloud; (cc) stands for cold cloud; (bc) stands for broken cloud; and (ce) stands for cloud edge. Data is presented in surface reflectance (ρ) for band 1, 2, 3, 4, 5, and 7 or in brightness temperature (T) for band 6.

No	Cloud masking rules	Image composition rules	Drawbacks
1		Formula (3.9)	Haze exist
2	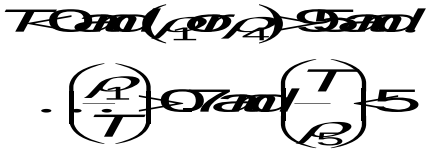	Formula (3.9)	Cloud edge remained
3	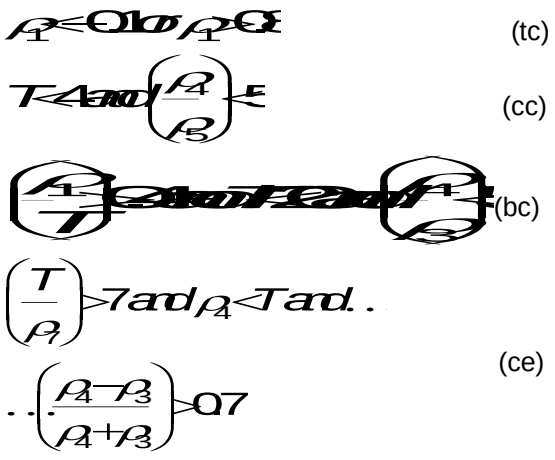 (tc) (cc) (bc) (ce)	Formula (3.9)	Thin cloud remained
4	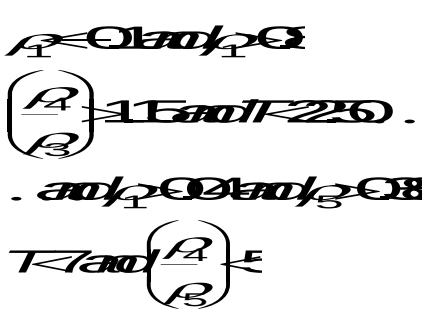 (tc) (cc) (bc)	Formula (3.9)	Haze still exist

No	Cloud masking rules	Image composition rules	Drawbacks
	 (ce)		
5	$\rho_1 > 0.5$ (tc)  (cc)  (bc)   (ce)	Formula (3.11); (3.12); (3.13)	Haze still exist

Appendix 3

Rules syntax

This rules syntax is written for the application in the ER Mapper version 7.1. The ix symbol stands for variable input number x, x: 1, 2, 3,…,n. Bx stands for Landsat band number x, x: 1, 2, 3, 4, 5, 6, and 7.

A. Multiple rules without atmospheric correction

Cloud masking syntax (consider cloud is single object)

1. if (i1 / i2) < 1.3 and (i1/i3) < 2.5 and (i4 / i1) > 0.4 and i2 > 70 then 1 else i5
where i1: B6; i2: B1; i3: B4; i4: B5; i5: Bx

2. if ((i1 + i2 + i3) / i4) > 1.7 then 1 else i5
where i1: B1; i2: B4; i3: B5; i4: B6; i5: Bx

3. if ((i1 + i2 + i3)/i4) > 1.7 and i3 > 35 and (i3/i2) < 1.7 then 1 else i5
where i1: B1; i2: B4; i3: B5; i4: B6; i5: Bx

4. if ((i1 + i2 + i3)/i4) > 1.7 and i3 > 35 and (i3/i2) < 1.7 and (i2/i5) < 0.78 then 1 else i6
where i1: B1; i2: B4; i3: B5; i4: B6; i5: B3; i6: Bx

5. if ((i1 + i2 + i3 - i4)/i5) > 2.0 and i6 > 30 then 1 else i7
where i1: B1; i2: B3; i3: B4; i4: B7; i5: B6; i6: B5; i7: Bx

6. if ((i1 + i2 + i3) / i4) > 2.0 and i5 > 30 and (i5 / i6) < 1.9 then 1 else i7
where i1: B1; i2: B2; i3: B3; i4: B6; i5: B5; i6: B4; i7: Bx

7. if ((i1 + i2 + i3 + i4) / i5) > 1 and (i1/i6) < 15 and ((i4+i5)/i7) < 3 then 1 else i8
where i1: B1; i2: B2; i3: B3; i4: B5; i5: B6; i6: B7; i7: B4; i8: Bx

8. if ((i1 - i2) / (i1 + i2)) > ((i3 - i4) / (i3 + i4)) then i5 else i6
where i1: B4x; i2: B3x; i3: B4y; i4: B3y; i5: Bx; i6: By

9 if ((i1 - i2) / (i1 + i2)) < 0.4 and (i3 / i4) < 15 and ((i5 + i6) / i1) < 3.5 then 1 else i7
where i1: B4; i2: B3; i3 B1; i4: B7; i5: B5; i6: B6; i7: Bx

Cloud elimination (Multi-temporal composition)

"Maximum value composites"
Max (i1, i2)
where: i1: first observation; i2: next observation

B. Multiple rules with atmospheric correction

Cloud masking syntax (consider cloud is single object)

1. if i1 < 0 and (i2 or i3) > 100 and (i2/i1) > 0.75 and (i3/i4) < 5 then 1 else i5
where i1: B6; i2: B1; i3: B4; i4: B5; i5: Bx

2. if i1 < 0 and (i2 or i3) > 95 and (i2/i1) > 0.7 and (i1/i3) < 5 then 1 else i4
where i1: B6; i2: B1; i3: B5; i4: Bx

Cloud masking syntax (consider cloud is not single object)

3. if i1 < -1000 or i1 > 8000 then 1 else (
if i2 < 4 and (i3/i4) < 5 then 1 else (
if (i1/i2) > 0.4 and i6 > 2000 and (i3/i5) < 5 then 1 else (
if (i2 / i6) > 7 and i3 > i2 and ((i3 - i5) /(i3 + i5)) < 1 then 1 else i6)))
where i1: B1; i2: B6; i3 B4; i4: B5; i5: B3; i6: Bx

4. if i1 < -1000 and i1 > 8000 then 1 else (
if (i2 / i3) > 1.15 and i4 < 2250 and i1 > 400 and i5 > 3800 then 1 else (
if i4 < 7 and (i2 / i5) < 5 then 1 else (
if (i1 / i4) > 0.95 and (i2 / i5) < 1 then 1 else i6)))
where i1: B1; i2: B4; i3: B3; i4: B6; i5: B5; i6: Bx

5. if i1 < 400 and i2 / i3 < 5 then 1 else (
if i4 > 5000 then 1 else (
if i4 / i1 > 1 and i4 / i3 > 0.5 and i2 / i3 < 5 then 1 else (
if (i5 - i6) / (i5 + i6) < 0.65 and (i5 - i6) / (i5 + i6) > 0.04
and i5 / i7 > 1 and i5 > 1500 then 1 else i8)))
where: i1: B6; i2: B2; i3: B5; i4: B1; i5: B4; i6: B3; i7: B7; i8: B5 or B4 or B3

Cloud elimination (Multi-temporal composition)

1. if i1 > i2 then i3 else i4

where i1: B4x; i2: B4y; i3: Bx; i4: By

2. if i1 < 2600 or i2 < 2600 then max(i3, i4) else (if SQRT(POW(ABS(I1 - I2), 2) / 2) > 100 then min(i3, i4) else (if i1 > i2 then i3 else i4))

where: i1: B4x; i2: B4y; i3: B5x or B4x or B3x; i4: B5y or B4y or B3y

Appendix 4

Band indices ratio comparison to differentiate cloud and other selected objects.

Group 1

(put on the next page due to its size)

Group 1

Form no	Form	cloudmax	cloud	haze	bareland	barefrost	snow	veg	loveg
1	B2/B1	1.00	0.47	0.45	0.49	0.52	0.49	0.44	0.47
2	B3/B1	1.00	0.52	0.45	0.55	0.63	0.55	0.37	0.52
3	B4/B1	1.00	0.59	0.55	0.47	0.51	0.38	1.34	0.55
4	B5/B1	1.00	0.63	0.65	0.79	0.83	0.06	0.88	1.13
5	B6/B1	0.37	0.32	0.98	1.06	0.58	0.41	1.65	1.52
6	B7/B1	0.63	0.35	0.35	0.47	0.49	0.04	0.31	0.65
7	B1/B2	1.00	2.12	2.22	2.04	1.93	2.06	2.26	2.13
8	B3/B2	1.00	1.10	1.01	1.13	1.21	1.13	0.85	1.11
9	B4/B2	1.00	1.25	1.22	0.95	0.98	0.78	3.03	1.18
10	B5/B2	1.00	1.34	1.43	1.61	1.61	0.13	1.98	2.41
11	B6/B2	0.37	0.68	2.16	2.16	1.11	0.85	3.74	3.25
12	B7/B2	0.63	0.74	0.78	0.95	0.94	0.08	0.71	1.39
13	B1/B3	1.00	1.94	2.20	1.81	1.59	1.82	2.67	1.93
14	B2/B3	1.00	0.91	0.99	0.88	0.82	0.88	1.18	0.90
15	B4/B3	1.00	1.14	1.21	0.84	0.81	0.69	3.58	1.06
16	B5/B3	1.00	1.22	1.42	1.42	1.32	0.12	2.35	2.18
17	B6/B3	0.37	0.62	2.15	1.91	0.92	0.75	4.42	2.94
18	B7/B3	0.63	0.68	0.78	0.84	0.78	0.08	0.84	1.26
19	B1/B4	1.00	1.70	1.81	2.14	1.98	2.63	0.75	1.81
20	B2/B4	1.00	0.80	0.82	1.05	1.02	1.28	0.33	0.85
21	B3/B4	1.00	0.88	0.82	1.19	1.24	1.45	0.28	0.94
22	B5/B4	1.00	1.07	1.17	1.68	1.64	0.17	0.65	2.05
23	B6/B4	0.37	0.54	1.77	2.26	1.14	1.08	1.23	2.76
24	B7/B4	0.63	0.59	0.64	1.00	0.97	0.11	0.23	1.18
25	B1/B5	1.00	1.59	1.55	1.27	1.20	15.57	1.14	0.88
26	B2/B5	1.00	0.75	0.70	0.62	0.62	7.57	0.50	0.41
27	B3/B5	1.00	0.82	0.70	0.70	0.76	8.57	0.43	0.46
28	B4/B5	1.00	0.93	0.85	0.59	0.61	5.93	1.53	0.49
29	B6/B5	0.37	0.51	1.51	1.34	0.69	6.43	1.88	1.35
30	B7/B5	0.63	0.55	0.55	0.59	0.59	0.64	0.36	0.58
31	B1/B6	2.68	3.12	1.02	0.95	1.74	2.42	0.60	0.66
32	B2/B6	2.68	1.47	0.46	0.46	0.90	1.18	0.27	0.31
33	B3/B6	2.68	1.61	0.46	0.52	1.09	1.33	0.23	0.34
34	B4/B6	2.68	1.84	0.56	0.44	0.88	0.92	0.81	0.36
35	B5/B6	2.68	1.97	0.66	0.74	1.44	0.16	0.53	0.74
36	B7/B6	1.69	1.09	0.36	0.44	0.85	0.10	0.19	0.43
37	B1/B7	1.58	2.87	2.84	2.14	2.05	24.22	3.20	1.53
38	B2/B7	1.58	1.35	1.28	1.05	1.06	11.78	1.41	0.72
39	B3/B7	1.58	1.48	1.29	1.19	1.29	13.33	1.20	0.80
40	B4/B7	1.58	1.69	1.56	1.00	1.04	9.22	4.28	0.85
41	B5/B7	1.58	1.81	1.83	1.68	1.70	1.56	2.80	1.74
42	B6/B7	0.59	0.92	2.77	2.26	1.18	10.00	5.28	2.34

Group 2

Form no	Form	cloudmax	cloud	haze	bareland	barefrost	snow	veg	loveg
1	(B1+B2)/B1	2.00	1.47	1.45	1.49	1.52	1.49	1.44	1.47
2	(B2+B3)/B1	2.00	0.99	0.91	1.04	1.15	1.04	0.82	0.99
3	(B3+B4)/B1	2.00	1.11	1.01	1.02	1.13	0.93	1.71	1.07
4	(B4+B5)/B1	2.00	1.22	1.20	1.25	1.34	0.44	2.22	1.69
5	(B5+B6)/B1	1.37	0.95	1.62	1.84	1.41	0.48	2.53	2.66
6	(B6+B7)/B1	1.00	0.67	1.33	1.52	1.06	0.45	1.97	2.18
7	(B1+B2)/B2	2.00	3.12	3.22	3.04	2.93	3.06	3.26	3.13
8	(B2+B3)/B2	2.00	2.10	2.01	2.13	2.21	2.13	1.85	2.11
9	(B3+B4)/B2	2.00	2.35	2.23	2.08	2.19	1.92	3.88	2.28
10	(B4+B5)/B2	2.00	2.59	2.65	2.56	2.58	0.92	5.02	3.59
11	(B5+B6)/B2	1.37	2.02	3.59	3.76	2.72	0.98	5.72	5.66
12	(B6+B7)/B2	1.00	1.42	2.95	3.11	2.06	0.93	4.45	4.64
13	(B1+B2)/B3	2.00	2.85	3.20	2.69	2.42	2.70	3.85	2.83
14	(B2+B3)/B3	2.00	1.91	1.99	1.88	1.82	1.88	2.18	1.90
15	(B3+B4)/B3	2.00	2.14	2.21	1.84	1.81	1.69	4.58	2.06
16	(B4+B5)/B3	2.00	2.36	2.63	2.26	2.13	0.81	5.93	3.24
17	(B5+B6)/B3	1.37	1.84	3.57	3.33	2.24	0.87	6.76	5.12
18	(B6+B7)/B3	1.00	1.30	2.93	2.75	1.69	0.83	5.25	4.19
19	(B1+B2)/B4	2.00	2.50	2.63	3.19	3.00	3.90	1.08	2.66
20	(B2+B3)/B4	2.00	1.68	1.64	2.23	2.26	2.72	0.61	1.79
21	(B3+B4)/B4	2.00	1.88	1.82	2.19	2.24	2.45	1.28	1.94
22	(B4+B5)/B4	2.00	2.07	2.17	2.68	2.64	1.17	1.65	3.05
23	(B5+B6)/B4	1.37	1.61	2.94	3.95	2.78	1.25	1.89	4.81
24	(B6+B7)/B4	1.00	1.14	2.41	3.26	2.10	1.19	1.47	3.94
25	(B1+B2)/B5	2.00	2.33	2.25	1.89	1.83	23.14	1.64	1.30
26	(B2+B3)/B5	2.00	1.57	1.40	1.33	1.38	16.14	0.93	0.87
27	(B3+B4)/B5	2.00	1.75	1.56	1.30	1.36	14.50	1.95	0.95
28	(B4+B5)/B5	2.00	1.93	1.85	1.59	1.61	6.93	2.53	1.49
29	(B5+B6)/B5	1.37	1.51	2.51	2.34	1.69	7.43	2.88	2.35
30	(B6+B7)/B5	1.00	1.06	2.06	1.94	1.28	7.07	2.24	1.92
31	(B1+B2)/B6	5.37	4.59	1.49	1.41	2.64	3.60	0.87	0.96
32	(B2+B3)/B6	5.37	4.59	1.49	1.41	2.64	3.60	0.87	0.96
33	(B3+B4)/B6	5.37	3.45	1.03	0.97	1.97	2.26	1.04	0.70
34	(B4+B5)/B6	5.37	3.80	1.22	1.19	2.32	1.08	1.34	1.11
35	(B5+B6)/B6	3.68	2.97	1.66	1.74	2.44	1.16	1.53	1.74
36	(B6+B7)/B6	2.69	2.09	1.36	1.44	1.85	1.10	1.19	1.43
37	(B1+B2)/B7	3.17	4.22	4.12	3.19	3.11	36.00	4.61	2.25
38	(B2+B3)/B7	3.17	2.83	2.57	2.23	2.35	25.11	2.61	1.52
39	(B3+B4)/B7	3.17	3.17	2.85	2.19	2.32	22.56	5.48	1.64
40	(B4+B5)/B7	3.17	3.50	3.40	2.68	2.74	10.78	7.09	2.58
41	(B5+B6)/B7	2.17	2.73	4.60	3.95	2.88	11.56	8.09	4.08

Group 3

Form no	Form	cloudmax	cloud	haze	bareland	barefrost	snow	veg	loveg
1	(B1+B2+B3)/B1	3.00	1.99	1.91	2.04	2.15	2.04	1.82	1.99
2	(B2+B3+B4)/B1	3.00	1.58	1.46	1.51	1.65	1.42	2.16	1.54
3	(B3+B4+B5)/B1	3.00	1.74	1.65	1.81	1.97	1.00	2.59	2.20
4	(B4+B5+B6)/B1	2.63	1.57	1.55	1.72	1.83	0.49	2.53	2.34
5	(B5+B6+B7)/B1	2.00	1.30	1.98	2.31	1.90	0.52	2.84	3.31
6	(B1+B2+B3)/B2	3.00	4.22	4.22	4.17	4.15	4.19	4.11	4.24
7	(B2+B3+B4)/B2	3.00	3.35	3.23	3.08	3.19	2.92	4.88	3.28
8	(B3+B4+B5)/B2	3.00	3.35	3.23	3.08	3.19	2.92	4.88	3.28
9	(B4+B5+B6)/B2	2.37	3.27	4.82	4.72	3.70	1.76	8.75	6.84
10	(B5+B6+B7)/B2	2.00	2.76	4.38	4.72	3.66	1.07	6.43	7.05
11	(B1+B2+B3)/B3	3.00	3.85	4.20	3.69	3.42	3.70	4.85	3.83
12	(B2+B3+B4)/B3	3.00	3.05	3.21	2.73	2.63	2.58	5.76	2.97
13	(B3+B4+B5)/B3	3.00	3.36	3.63	3.26	3.13	1.81	6.93	4.24
14	(B4+B5+B6)/B3	2.37	2.98	4.79	4.17	3.05	1.56	10.35	6.18
15	(B5+B6+B7)/B3	2.00	2.52	4.35	4.17	3.02	0.94	7.60	6.37
16	(B1+B2+B3)/B4	3.00	3.37	3.46	4.38	4.24	5.35	1.36	3.60
17	(B2+B3+B4)/B4	3.00	2.68	2.64	3.23	3.26	3.72	1.61	2.79
18	(B3+B4+B5)/B4	3.00	2.95	2.99	3.87	3.89	2.61	1.93	3.99
19	(B4+B5+B6)/B4	2.37	2.61	3.94	4.95	3.78	2.25	2.89	5.81
20	(B5+B6+B7)/B4	2.00	2.21	3.58	4.95	3.75	1.36	2.12	5.99
21	(B1+B2+B3)/B5	3.00	3.15	2.95	2.60	2.58	31.71	2.07	1.76
22	(B2+B3+B4)/B5	3.00	2.50	2.26	1.92	1.99	22.07	2.46	1.36
23	(B3+B4+B5)/B5	3.00	2.75	2.56	2.30	2.36	15.50	2.95	1.95
24	(B4+B5+B6)/B5	2.37	2.44	3.37	2.94	2.30	13.36	4.41	2.83
25	(B5+B6+B7)/B5	2.00	2.06	3.06	2.94	2.28	8.07	3.24	2.92
26	(B1+B2+B3)/B6	8.05	6.20	1.95	1.93	3.73	4.93	1.10	1.30
27	(B2+B3+B4)/B6	8.05	4.92	1.49	1.43	2.87	3.43	1.30	1.01
28	(B3+B4+B5)/B6	8.05	5.41	1.69	1.71	3.41	2.41	1.57	1.45
29	(B4+B5+B6)/B6	6.37	4.80	2.22	2.19	3.32	2.08	2.34	2.11
30	(B5+B6+B7)/B6	5.38	4.05	2.02	2.19	3.29	1.26	1.72	2.17
31	(B1+B2+B3)/B7	4.75	5.70	5.41	4.38	4.39	49.33	5.80	3.05
32	(B2+B3+B4)/B7	4.75	4.52	4.13	3.23	3.38	34.33	6.89	2.36
33	(B3+B4+B5)/B7	4.75	4.98	4.68	3.87	4.02	24.11	8.28	3.38
34	(B4+B5+B6)/B7	3.76	4.42	6.17	4.95	3.92	20.78	12.37	4.92
35	(B5+B6+B7)/B7	3.17	3.73	5.60	4.95	3.88	12.56	9.09	5.08
36	(B3+B4+B5)/3	255	115.46667	58.4	71.466667	112.66667	72.333333	63.5	66.5
37	(B2+B3+B4+B5)/B4	255	110.1	55.775	68.125	106.75	80.75	55.75	60.5
38	(B4+B5)/2	255	121.7	63.5	74.35	115	48.5	81.5	76.25
39	(B4-B5)/(B4+B5)	0	-0.033689	-0.07874	-0.254876	-0.243478	0.7113402	0.208589	-0.344262

Group 4

Form no	Form	cloudmax	cloud	haze	bareland	barefrost	snow	veg	loveg
1	(B1/B6)	2.68	3.12	1.02	0.95	1.74	2.42	0.60	0.66
2	(B2/B6)	2.68	1.47	0.46	0.46	0.90	1.18	0.27	0.31
3	(B3/B6)	2.68	1.61	0.46	0.52	1.09	1.33	0.23	0.34
4	(B4/B6)	2.68	1.84	0.56	0.44	0.88	0.92	0.81	0.36
5	(B5/B6)	2.68	1.97	0.66	0.74	1.44	0.16	0.53	0.74
6	(B7/B6)	1.69	1.09	0.36	0.44	0.85	0.10	0.19	0.43
7	(B1+B2)/B6	5.37	4.59	1.49	1.41	2.64	3.60	0.87	0.96
8	(B2+B3)/B6	5.37	3.08	0.93	0.99	1.99	2.51	0.49	0.65
9	(B3+B4)/B6	5.37	3.45	1.03	0.97	1.97	2.26	1.04	0.70
10	(B4+B5)/B6	5.37	3.80	1.22	1.19	2.32	1.08	1.34	1.11
11	(B5+B6)/B6	3.68	2.97	1.66	1.74	2.44	1.16	1.53	1.74
12	(B6+B7)/B6	2.69	2.09	1.36	1.44	1.85	1.10	1.19	1.43
13	(B1+B2+B3)/B6	8.05	6.20	1.95	1.93	3.73	4.93	1.10	1.30
14	(B2+B3+B4)/B6	8.05	4.92	1.49	1.43	2.87	3.43	1.30	1.01
15	(B3+B4+B5)/B6	8.05	5.41	1.69	1.71	3.41	2.41	1.57	1.45
16	(B5+B6+B7)/B6	5.38	4.05	2.02	2.19	3.29	1.26	1.72	2.17
17	(B1+B2+B3+B4)/B6	10.74	8.03	2.51	2.37	4.61	5.86	1.91	1.67
18	(B2+B3+B4+B5)/B6	10.74	6.88	2.15	2.17	4.31	3.59	1.84	1.75
19	(B3+B4+B5+B6)/B6	9.05	6.41	2.69	2.71	4.41	3.41	2.57	2.45
20	(B4+B5+B6+B7)/B6	8.06	5.89	2.59	2.63	4.17	2.18	2.53	2.53
21	(B1+B2+B3-B5)/B6	5.37	4.23	1.29	1.19	2.28	4.78	0.57	0.56
22	(B1+B2-5)/B6	2.68	2.62	0.82	0.67	1.19	3.44	0.34	0.22

Group 5

Form no	Form	cloudmax	cloud	haze	bareland	barefrost	snow	veg	loveg
1	(B1-B2)	0.00	105.60	58.20	60.50	83.00	112.00	41.00	48.00
2	(B1-B3)	0.00	96.60	57.90	52.90	64.00	98.00	46.00	43.50
3	(B1-B4)	0.00	82.00	47.60	63.20	85.00	135.00	-25.00	40.50
4	(B1-B5)	0.00	73.80	37.60	25.30	29.00	204.00	9.00	-12.00
5	(B1-B6)	160.00	135.60	2.40	-6.80	73.00	128.00	-48.00	-47.50
6	(B1-B7)	94.00	130.00	68.70	63.20	88.00	209.00	50.50	31.50
7	(B2-B1)	0.00	-105.60	-58.20	-60.50	-83.00	-112.00	-41.00	-48.00
8	(B2-B3)	0.00	-9.00	-0.30	-7.60	-19.00	-14.00	5.00	-4.50
9	(B2-B4)	0.00	-23.60	-10.60	2.70	2.00	23.00	-66.00	-7.50
10	(B2-B5)	0.00	-31.80	-20.60	-35.20	-54.00	92.00	-32.00	-60.00
11	(B2-B6)	160.00	30.00	-55.80	-67.30	-10.00	16.00	-89.00	-95.50
12	(B2-B7)	94.00	24.40	10.50	2.70	5.00	97.00	9.50	-16.50
13	(B3-B1)	0.00	-96.60	-57.90	-52.90	-64.00	-98.00	-46.00	-43.50
14	(B3-B2)	0.00	9.00	0.30	7.60	19.00	14.00	-5.00	4.50
15	(B3-B4)	0.00	-14.60	-10.30	10.30	21.00	37.00	-71.00	-3.00
16	(B3-B5)	0.00	-22.80	-20.30	-27.60	-35.00	106.00	-37.00	-55.50
17	(B3-B6)	160.00	39.00	-55.50	-59.70	9.00	30.00	-94.00	-91.00
18	(B3-B7)	94.00	33.40	10.80	10.30	24.00	111.00	4.50	-12.00
19	(B4-B1)	0.00	-82.00	-47.60	-63.20	-85.00	-135.00	25.00	-40.50
20	(B4-B2)	0.00	23.60	10.60	-2.70	-2.00	-23.00	66.00	7.50
21	(B4-B3)	0.00	14.60	10.30	-10.30	-21.00	-37.00	71.00	3.00
22	(B4-B5)	0.00	-8.20	-10.00	-37.90	-56.00	69.00	34.00	-52.50
23	(B4-B6)	160.00	53.60	-45.20	-70.00	-12.00	-7.00	-23.00	-88.00
24	(B4-B7)	94.00	48.00	21.10	0.00	3.00	74.00	75.50	-9.00
25	(B5-B1)	0.00	-73.80	-37.60	-25.30	-29.00	-204.00	-9.00	12.00
26	(B5-B2)	0.00	31.80	20.60	35.20	54.00	-92.00	32.00	60.00
27	(B5-B3)	0.00	22.80	20.30	27.60	35.00	-106.00	37.00	55.50
28	(B5-B4)	0.00	8.20	10.00	37.90	56.00	-69.00	-34.00	52.50
29	(B5-B6)	160.00	61.80	-35.20	-32.10	44.00	-76.00	-57.00	-35.50
30	(B5-B7)	94.00	56.20	31.10	37.90	59.00	5.00	41.50	43.50
31	(B6-B1)	-160.00	-135.60	-2.40	6.80	-73.00	-128.00	48.00	47.50
32	(B6-B2)	-160.00	-30.00	55.80	67.30	10.00	-16.00	89.00	95.50
33	(B6-B3)	-160.00	-39.00	55.50	59.70	-9.00	-30.00	94.00	91.00
34	(B6-B4)	-160.00	-53.60	45.20	70.00	12.00	7.00	23.00	88.00
35	(B6-B5)	-160.00	-61.80	35.20	32.10	-44.00	76.00	57.00	35.50
36	(B6-B7)	-66.00	-5.60	66.30	70.00	15.00	81.00	98.50	79.00
37	(B7-B1)	-94.00	-130.00	-68.70	-63.20	-88.00	-209.00	-50.50	-31.50
38	(B7-B2)	-94.00	-24.40	-10.50	-2.70	-5.00	-97.00	-9.50	16.50
39	(B7-B3)	-94.00	-33.40	-10.80	-10.30	-24.00	-111.00	-4.50	12.00
40	(B7-B4)	-94.00	-48.00	-21.10	0.00	-3.00	-74.00	-75.50	9.00
41	(B7-B5)	-94.00	-56.20	-31.10	-37.90	-59.00	-5.00	-41.50	-43.50
42	(B7-B6)	66.00	5.60	-66.30	-70.00	-15.00	-81.00	-98.50	-79.00

Group 6

Form no	Form	cloudmax	cloud	haze	bareland	barefrost	snow	veg	loveg
1	(B1-B2)/B6	0.00	1.65	0.56	0.48	0.84	1.24	0.34	0.35
2	(B1-B3)/B6	0.00	1.51	0.56	0.42	0.65	1.09	0.38	0.32
3	(B1-B4)/B6	0.00	1.28	0.46	0.50	0.86	1.50	-0.21	0.29
4	(B1-B5)/B6	0.00	1.15	0.36	0.20	0.29	2.27	0.07	-0.09
5	(B1-B6)/B6	1.68	2.12	0.02	-0.05	0.74	1.42	-0.40	-0.34
6	(B1-B7)/B6	0.99	2.03	0.66	0.50	0.89	2.32	0.42	0.23
7	(B2-B1)/B6	0.00	-1.65	-0.56	-0.48	-0.84	-1.24	-0.34	-0.35
8	(B2-B3)/B6	0.00	-0.14	0.00	-0.06	-0.19	-0.16	0.04	-0.03
9	(B2-B4)/B6	0.00	-0.37	-0.10	0.02	0.02	0.26	-0.54	-0.05
10	(B2-B5)/B6	0.00	-0.50	-0.20	-0.28	-0.55	1.02	-0.26	-0.43
11	(B2-B6)/B6	1.68	0.47	-0.54	-0.54	-0.10	0.18	-0.73	-0.69
12	(B2-B7)/B6	0.99	0.38	0.10	0.02	0.05	1.08	0.08	-0.12
13	(B3-B1)/B6	0.00	-1.51	-0.56	-0.42	-0.65	-1.09	-0.38	-0.32
14	(B3-B2)/B6	0.00	0.14	0.00	0.06	0.19	0.16	-0.04	0.03
15	(B3-B4)/B6	0.00	-0.23	-0.10	0.08	0.21	0.41	-0.58	-0.02
16	(B3-B5)/B6	0.00	-0.36	-0.20	-0.22	-0.35	1.18	-0.30	-0.40
17	(B3-B6)/B6	1.68	0.61	-0.54	-0.48	0.09	0.33	-0.77	-0.66
18	(B3-B7)/B6	0.99	0.52	0.10	0.08	0.24	1.23	0.04	-0.09
19	(B4-B1)/B6	0.00	-1.28	-0.46	-0.50	-0.86	-1.50	0.21	-0.29
20	(B4-B2)/B6	0.00	0.37	0.10	-0.02	-0.02	-0.26	0.54	0.05
21	(B4-B3)/B6	0.00	0.23	0.10	-0.08	-0.21	-0.41	0.58	0.02
22	(B4-B5)/B6	0.00	-0.13	-0.10	-0.30	-0.57	0.77	0.28	-0.38
23	(B4-B6)/B6	1.68	0.84	-0.44	-0.56	-0.12	-0.08	-0.19	-0.64
24	(B4-B7)/B6	0.99	0.75	0.20	0.00	0.03	0.82	0.62	-0.07
25	(B5-B1)/B6	0.00	-1.15	-0.36	-0.20	-0.29	-2.27	-0.07	0.09
26	(B5-B2)/B6	0.00	0.50	0.20	0.28	0.55	-1.02	0.26	0.43
27	(B5-B3)/B6	0.00	0.36	0.20	0.22	0.35	-1.18	0.30	0.40
28	(B5-B4)/B6	0.00	0.13	0.10	0.30	0.57	-0.77	-0.28	0.38
29	(B5-B6)/B6	1.68	0.97	-0.34	-0.26	0.44	-0.84	-0.47	-0.26
30	(B5-B7)/B6	0.99	0.88	0.30	0.30	0.60	0.06	0.34	0.32
31	(B6-B1)/B6	-1.68	-2.12	-0.02	0.05	-0.74	-1.42	0.40	0.34
32	(B6-B2)/B6	-1.68	-0.47	0.54	0.54	0.10	-0.18	0.73	0.69
33	(B6-B3)/B6	-1.68	-0.61	0.54	0.48	-0.09	-0.33	0.77	0.66
34	(B6-B4)/B6	-1.68	-0.84	0.44	0.56	0.12	0.08	0.19	0.64
35	(B6-B5)/B6	-1.68	-0.97	0.34	0.26	-0.44	0.84	0.47	0.26
36	(B6-B7)/B6	-0.69	-0.09	0.64	0.56	0.15	0.90	0.81	0.57
37	(B7-B1)/B6	-0.99	-2.03	-0.66	-0.50	-0.89	-2.32	-0.42	-0.23
38	(B7-B2)/B6	-0.99	-0.38	-0.10	-0.02	-0.05	-1.08	-0.08	0.12
39	(B7-B3)/B6	-0.99	-0.52	-0.10	-0.08	-0.24	-1.23	-0.04	0.09
40	(B7-B4)/B6	-0.99	-0.75	-0.20	0.00	-0.03	-0.82	-0.62	0.07
41	(B7-B5)/B6	-0.99	-0.88	-0.30	-0.30	-0.60	-0.06	-0.34	-0.32
42	(B7-B6)/B6	0.69	0.09	-0.64	-0.56	-0.15	-0.90	-0.81	-0.57
43	(B1+B7)/B6	4.38	4.21	1.38	1.39	2.59	2.52	0.79	1.08

Group 7

Form no	Form	cloudmax	cloud	haze	bareland	barefrost	snow	veg	loveg
1	(B1+B2)	510.00	293.60	154.00	176.70	261.00	324.00	106.00	133.00
2	(B1+B3)	510.00	302.60	154.30	184.30	280.00	338.00	101.00	137.50
3	(B1+B4)	510.00	317.20	164.60	174.00	259.00	301.00	172.00	140.50
4	(B1+B5)	510.00	325.40	174.60	211.90	315.00	232.00	138.00	193.00
5	(B1+B6)	350.00	263.60	209.80	244.00	271.00	308.00	195.00	228.50
6	(B1+B7)	416.00	269.20	143.50	174.00	256.00	227.00	96.50	149.50
7	(B2+B3)	510.00	197.00	96.10	123.80	197.00	226.00	60.00	89.50
8	(B2+B4)	510.00	211.60	106.40	113.50	176.00	189.00	131.00	92.50
9	(B2+B5)	510.00	219.80	116.40	151.40	232.00	120.00	97.00	145.00
10	(B2+B6)	350.00	158.00	151.60	183.50	188.00	196.00	154.00	180.50
11	(B2+B7)	416.00	163.60	85.30	113.50	173.00	115.00	55.50	101.50
12	(B3+B4)	510.00	220.60	106.70	121.10	195.00	203.00	126.00	97.00
13	(B3+B5)	510.00	228.80	116.70	159.00	251.00	134.00	92.00	149.50
14	(B3+B6)	350.00	167.00	151.90	191.10	207.00	210.00	149.00	185.00
15	(B3+B7)	416.00	172.60	85.60	121.10	192.00	129.00	50.50	106.00
16	(B4+B5)	510.00	243.40	127.00	148.70	230.00	97.00	163.00	152.50
17	(B4+B6)	350.00	181.60	162.20	180.80	186.00	173.00	220.00	188.00
18	(B4+B7)	416.00	187.20	95.90	110.80	171.00	92.00	121.50	109.00
19	(B5+B6)	350.00	189.80	172.20	218.70	242.00	104.00	186.00	240.50
20	(B5+B7)	416.00	195.40	105.90	148.70	227.00	23.00	87.50	161.50
21	(B6+B7)	256.00	133.60	141.10	180.80	183.00	99.00	144.50	197.00

Group 8

Form no	Form	cloudmax	cloud	haze	bareland	barefrost	snow	veg	loveg
1	(B1-B6)/(B1+B2)	0.31	0.46	0.02	-0.04	0.28	0.40	-0.45	-0.36
2	(B2-B6)/(B1+B2)	0.31	0.10	-0.36	-0.38	-0.04	0.05	-0.84	-0.72
3	(B6-B1)/(B1+B2)	-0.31	-0.46	-0.02	0.04	-0.28	-0.40	0.45	0.36
4	(B6-B2)/(B1+B2)	-0.31	-0.10	0.36	0.38	0.04	-0.05	0.84	0.72
5	(B6-B3)/(B1+B2)	-0.31	-0.13	0.36	0.34	-0.03	-0.09	0.89	0.68
6	(B6-B4)/(B1+B2)	-0.31	-0.18	0.29	0.40	0.05	0.02	0.22	0.66
7	(B6-B5)/(B1+B2)	-0.31	-0.21	0.23	0.18	-0.17	0.23	0.54	0.27
8	(B6-B7)/(B1+B2)	-0.13	-0.02	0.43	0.40	0.06	0.25	0.93	0.59
9	(B1-B6)/(B1+B3)	0.31	0.45	0.02	-0.04	0.26	0.38	-0.48	-0.35
10	(B2-B6)/(B1+B3)	0.31	0.10	-0.36	-0.37	-0.04	0.05	-0.88	-0.69
11	(B6-B1)/(B1+B3)	-0.31	-0.45	-0.02	0.04	-0.26	-0.38	0.48	0.35
12	(B6-B2)/(B1+B3)	-0.31	-0.10	0.36	0.37	0.04	-0.05	0.88	0.69
13	(B6-B3)/(B1+B3)	-0.31	-0.13	0.36	0.32	-0.03	-0.09	0.93	0.66
14	(B6-B4)/(B1+B3)	-0.31	-0.18	0.29	0.38	0.04	0.02	0.23	0.64
15	(B6-B5)/(B1+B3)	-0.31	-0.20	0.23	0.17	-0.16	0.22	0.56	0.26
16	(B6-B7)/(B1+B3)	-0.13	-0.02	0.43	0.38	0.05	0.24	0.98	0.57
17	(B1-B6)/'(B2+B3)	0.31	0.69	0.02	-0.05	0.37	0.57	-0.80	-0.53
18	(B2-B6)/(B2+B3)	0.31	0.15	-0.58	-0.54	-0.05	0.07	-1.48	-1.07
19	(B6-B1)/(B2+B3)	-0.31	-0.69	-0.02	0.05	-0.37	-0.57	0.80	0.53
20	(B6-B2)/(B2+B3)	-0.31	-0.15	0.58	0.54	0.05	-0.07	1.48	1.07
21	(B6-B3)/(B2+B3)	-0.31	-0.20	0.58	0.48	-0.05	-0.13	1.57	1.02
22	(B6-B4)/(B2+B3)	-0.31	-0.27	0.47	0.57	0.06	0.03	0.38	0.98
23	(B6-B5)/(B2+B3)	-0.31	-0.31	0.37	0.26	-0.22	0.34	0.95	0.40

Appendix 5

Spectral signature of selected objects

A. Vegetation

(put on the next page due to its size)

A. Vegetation

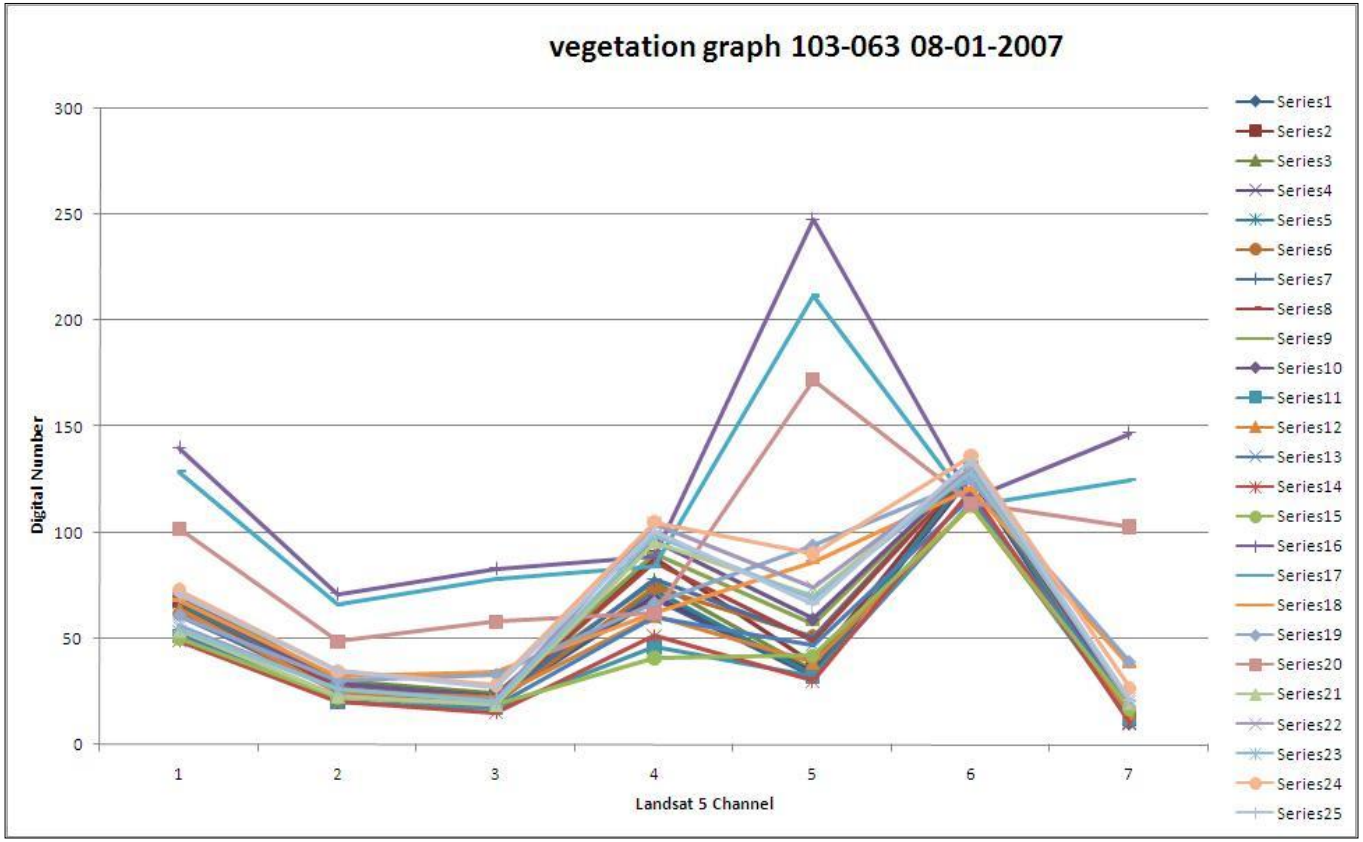

B. Haze

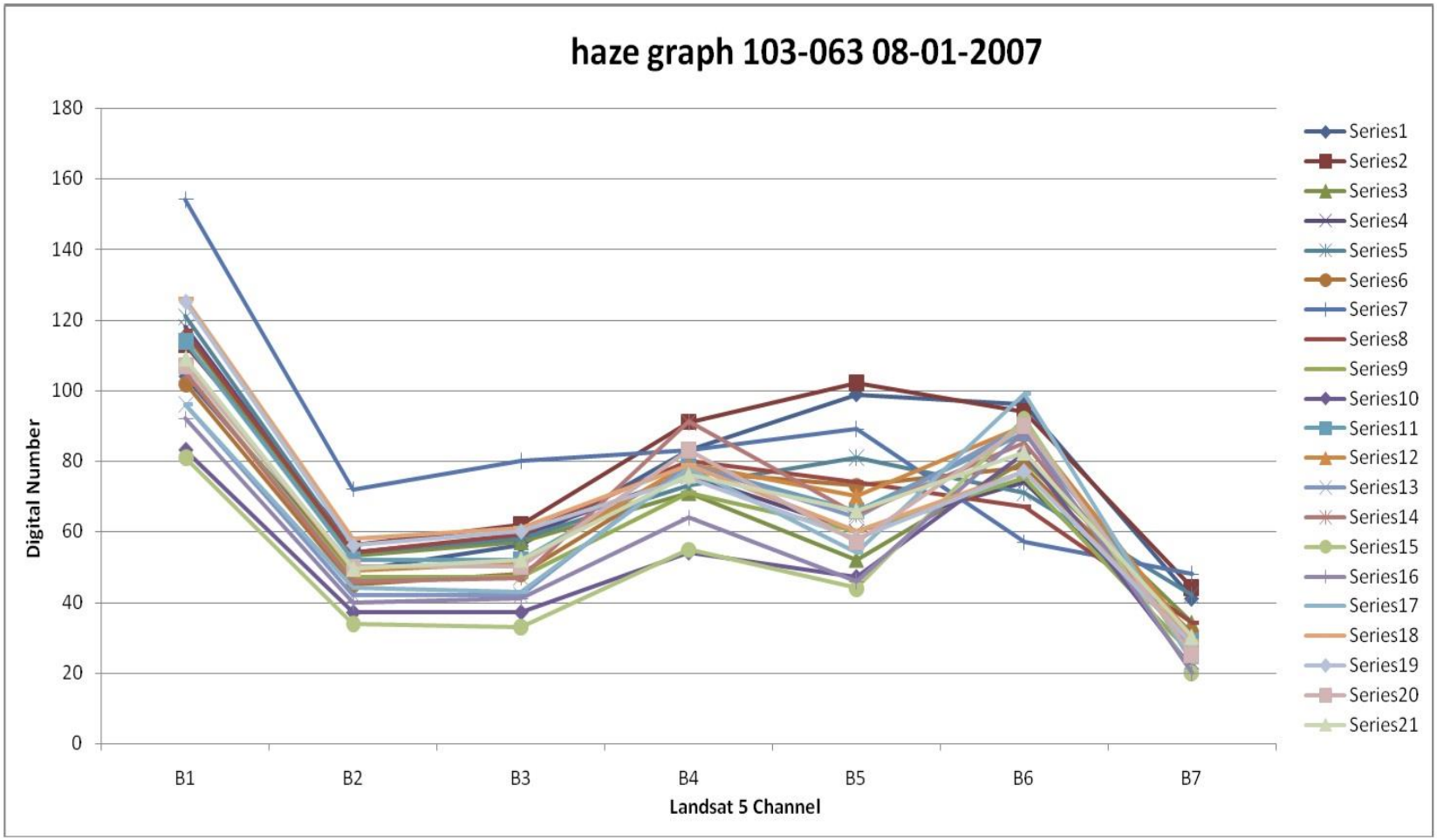
haze graph 103-063 08-01-2007
Digital Number
180
160
140
120
100
80
60
40
20
0
B1
B2
B3
B4
B5
B6
B7
Landsat 5 Channel
Series1
Series2
Series3
Series4
Series5
Series6
Series7
Series8
Series9
Series10
Series11
Series12
Series13
Series14
Series15
Series16
Series17
Series18
Series19
Series20
Series21

C. Bare land

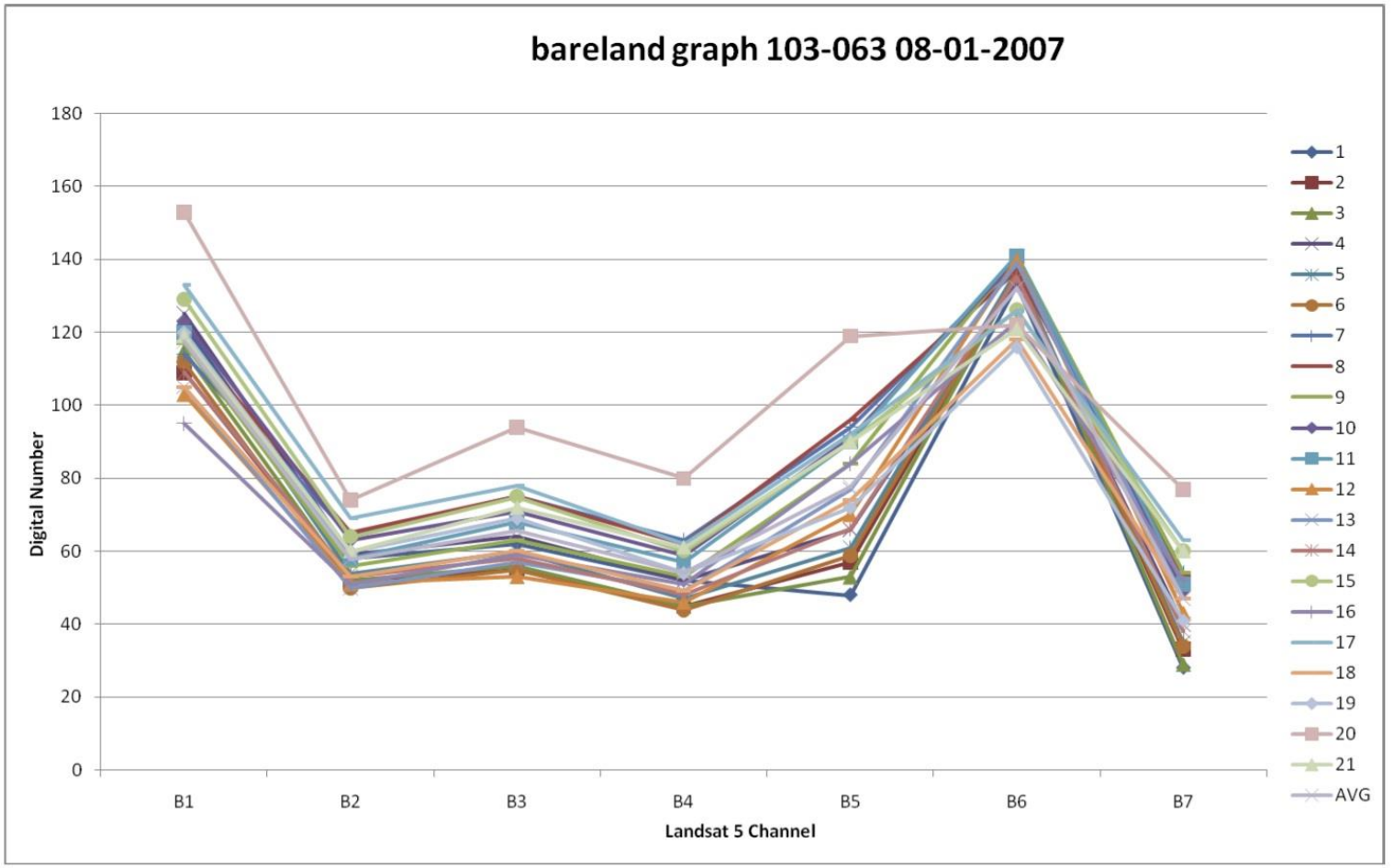
bareland graph 103-063 08-01-2007
Digital Number
180
160
140
120
100
80
60
40
20
0
B1
B2
B3
B4
B5
B6
B7
Landsat 5 Channel
1
2
3
4
5
6
7
8
9
10
11
12
13
14
15
16
17
18
19
20
21
AVG

D. Water and snow

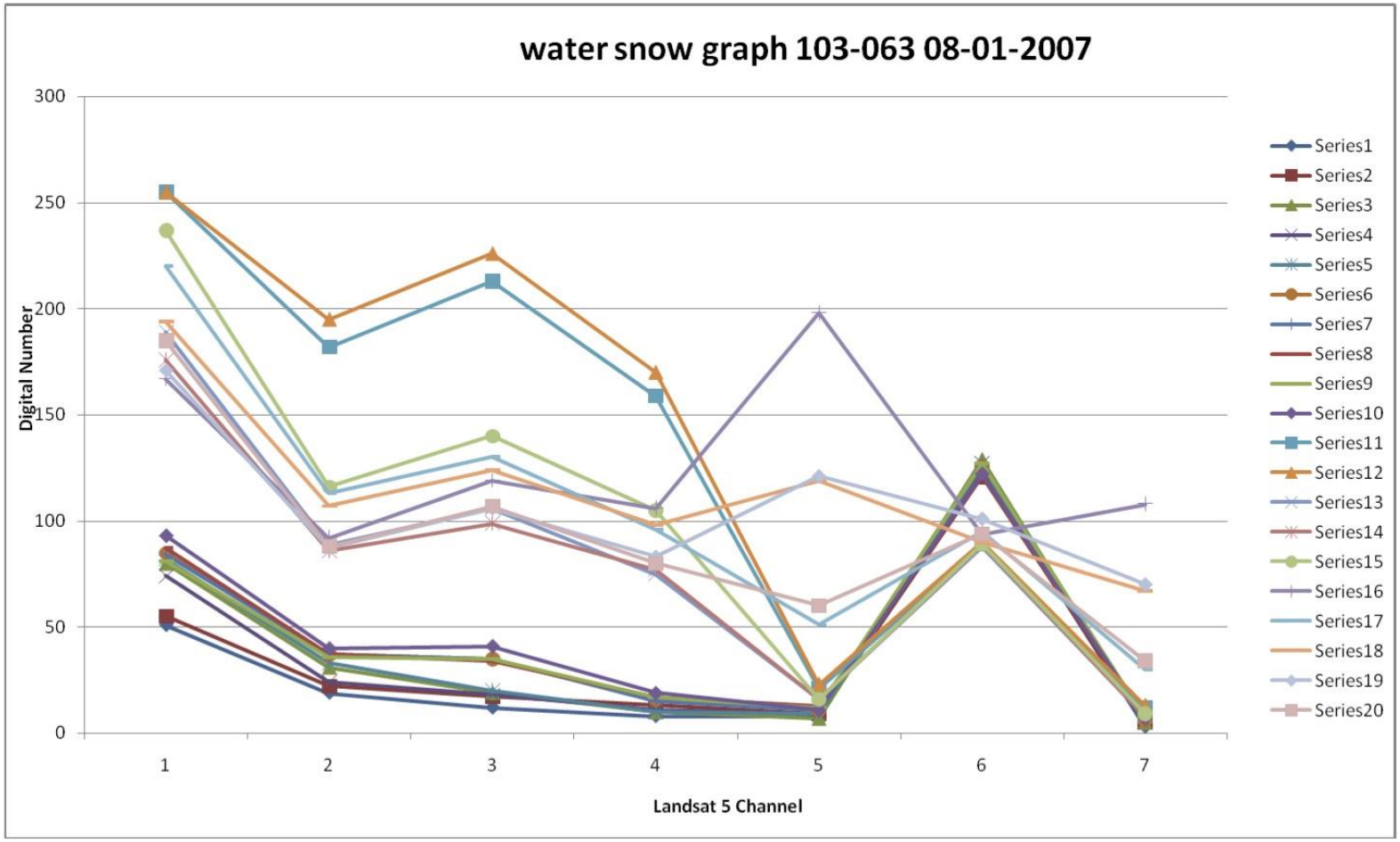

Appendix 6

Abbreviations and terminology

Acronym	Remarks
AHOT	Advanced-Haze Optimised Transform
AirSAR	Airborne Synthetic Aperture Radar. The NASA-JPL's airborne radar remote sensing platform
AVHRR	Advanced Very High Resolution Radiometer. Sensor of the NOAA satellite series
Bakosurtanal	*Badan Koordinasi Survey dan Pemetaan Nasional.* The Indonesian Agency for Survey and Mapping Operation and Coordination
CBERS	China-Brazil Earth Resources Satellite
CSIRO-MIS	Commonwealth Scientific and Industrial Research Organization – Mathematics, Informatics and Statistics Division. A Division of the Australian governmental research agency.
CVA	Canonical variate analysis
Dephut	*Departemen Kehutanan.* The Indonesian Ministry of Forestry
ERS	European Remote Sensing Satellite
ERTS	Earth Resources Technology Satellite
ESSA	Environmental Science Service Administration satellite series. Predecessor of the NOAA satellite series
ETM+	Enhanced Thematic Mapper Plus. Sensor of Landsat 7 satellite
GAC	Global Area Coverage. Product of NOAA AVHRR satellite series
GeoTIFF	Tagged Image Format File Format with georeferencing information embedded. This is fully compliant with TIFF 6.0
GIMP	GNU Image Manipulation Software. Free software for raster graphic editing
HOT	Haze Optimised Transformation

Acronym	Remarks
InSAR	Interferometric Synthetic Aperture Radar. The ERS satellite data product
JPL	Jet Propulsion Laboratory. NASA's division
LAPAN	*Lembaga Penerbangan dan Antariksa Nasional.* The Indonesian Aeronautics and Space Agency
LEDAPS	Landsat Ecosystem Disturbance Adaptive Processing System. NASA's funded project to map North American forest disturbance since 1975 by using Landsat and ASTER satellite data. It produced e.g. preprocessing package for remote sensing data among other tools and products.
MODIS	MODerate resolution Imaging Spectroradiometer. One of Terra and Aqua satellite's sensor.
MOPITT	Measurement of Pollution in the Troposphere. One of Terra satellite's sensor.
MOS	Marine Observation Satellite. Japanese first earth observation satellite.
MRA	Multiple rules applied for the Landsat data with atmospheric correction
MRN	Multiple rules applied for the Landsat data without atmospheric correction
MSS	Multi Spectral Scanner. Sensor carried by Landsat 1 to 5 satellites.
NASA	National Aeronautics and Space Administration. The United States Space Agency
NDR	Normalised Difference Reflectance
NDVI	Normalised Difference Vegetation Index
NOAA	National Oceanic and Atmospheric Administration
PRODES	*Programa de Cálculo Desflorestamento da Amazônia.* Amazon Deforestation Monitoring Project under Brazilian federal government.
RBV	Return Beam Vidicon. Sensor of Landsat 1 to 3 satellite.
RMS	Root means square
SAR	Synthetic Aperture Radar
SPOT	*Système Pour l'Observation de la Terre*. French earth observation satellite series.
TC4	The fourth of Tasseled-Cap transformations.
TM	Thematic Mapper. Sensor of Landsat 4 to 5 satellite.
TOA	Top-of-atmosphere

Acronym	Remarks
USGS	United States Geological Survey. The United States Agency to study landscape, natural resources and natural hazards.
WRS	World Reference System. Landsat satellite's data grid system

Appendix 7

Error matrices of classification result

A. Post classification method

1. 2001 – 2005 reference data

Class	water	Non forest	Forest	Non vegetation	Sum	User's accuracy
Water	59	65	217	0	341	17.30%
Non forest	100	626	862	27	1615	38.76%
Forest	272	701	3662	0	4635	79.01%
Non vegetation	65	491	830	26	1412	1.84%
Sum	496	1883	5571	53	8003	
Producer's accuracy	11.90%	33.24%	65.73%	49.06%		

Overall accuracy: 54.64%
Kappa: 16.86%

2. 2007 reference data

Class	water	Non forest	Forest	Non vegetation	Sum	User's accuracy
Water	42	89	206	0	337	12.46%
Non forest	9	365	143	12	529	69.00%
Forest	26	482	2440	0	2948	82.77%
Non vegetation	62	457	238	0	757	0.00%
Sum	139	1393	3027	12	4571	
Producer's accuracy	30.22%	26.20%	80.61%	0.00%		

Overall accuracy: 62.28%
Kappa: 29.50%

3. 2010 reference data

Class	water	Non forest	Forest	Non vegetation	Sum	User's accuracy
Water	685	106	160	124	1075	63.72%
Non forest	8	688	192	202	1090	63.12%
Forest	125	2299	6806	1582	10812	62.95%
Non vegetation	32	411	468	223	1134	19.66%
Sum	850	3504	7626	2131	14111	
Producer's accuracy	80.59%	19.63%	89.25%	10.46%		

Overall accuracy: 59.54%
Kappa: 26.44%

B. Bitemporal method

1. 2001 – 2005 reference data

Class	water	Non forest	Forest	Non vegetation	Sum	User's accuracy
Water	1	115	520	0	636	0.16%
Non forest	18	291	277	1	587	49,57%
Forest	228	1012	1637	47	2924	55.98%
Non vegetation	141	344	2859	1	3345	0.03%
Sum	424	1779	5377	49	7629	
Producer's accuracy	0.71%	16.36%	30.44%	2.04%		

Overall accuracy: 25.30%
Kappa: -6.04%

2. 2007 reference data

Class	water	Non forest	Forest	Non vegetation	Sum	User's accuracy
Water	0	3	24	0	81	0.00%
Non forest	2	263	190	0	27	57.80%
Forest	70	661	526	0	455	41.85%
Non vegetation	18	356	2170	0	1257	0.00%
Sum	134	1298	2932	0	2544	
Producer's accuracy	0.00%	20.26%	17.94%	0.00%		

Overall accuracy: 18.08%
Kappa: -5.67%

3. 2010 reference data

Class	water	Non forest	Forest	Non vegetation	Sum	User's accuracy
Water	9	15	11	14	49	18.37%
Non forest	2	417	100	192	711	58.65%
Forest	33	1386	395	359	2173	18.18%
Non vegetation	117	1246	6863	1314	9540	13.77%
Sum	720	3087	7407	1936	13150	
Producer's accuracy	1.25%	13.51%	5.33%	67.87%		

Overall accuracy: 16.24%
Kappa: -6.41%

Appendix 8

Indonesian Land Cover Classification Structure

The Indonesian land cover classification structure used for the map series obtained from the interpretation of 1999/2000, 2002/2003, 2005/2006, and 2008/2009 Landsat data (Dephut, 2008c; Purwanto, 2011, pers.comm.).

No	Group	Class
1	Forested	Primary dryland forest
2		Secondary dryland forest
3		Primary wetland forest
4		Secondary wetland forest
5		Primary mangrove forest
6		Secondary mangrove forest
7		Timber estate
8	Non forested	Bushland
9		Wetland bush
10		Grassland
11		Estate crops
12		Dryland agriculture
13		Mixed dryland agriculture and bushland/ Agroforestry
14		Transmigration area
15		Paddy field
16		Fish / salt pond
17		Bare ground
18		Mining / quarry
19		Settlement
20		Swamp
21		Port (Airport / harbour)
22		Cloud
23		No data